

MECHANICAL PERFORMANCES OF CONCRETE BEAMS WITH HYBRID USAGE OF STEEL  
AND FRP REINFORCEMENT



A Dissertation Submitted in Partial Fulfillment of the Requirements  
for the Degree of Doctor of Philosophy in Civil Engineering

Department of Civil Engineering

Faculty of Engineering

Chulalongkorn University

Academic Year 2018

Copyright of Chulalongkorn University

พฤติกรรมเชิงกลของคานคอนกรีตที่เสริมด้วยเหล็กร่วมกับพอลิเมอร์เสริมเส้นใย



วิทยานิพนธ์นี้เป็นส่วนหนึ่งของการศึกษาตามหลักสูตรปริญญาวิศวกรรมศาสตรดุษฎีบัณฑิต  
สาขาวิชาวิศวกรรมโยธา ภาควิชาวิศวกรรมโยธา  
คณะวิศวกรรมศาสตร์ จุฬาลงกรณ์มหาวิทยาลัย  
ปีการศึกษา 2561  
ลิขสิทธิ์ของจุฬาลงกรณ์มหาวิทยาลัย

Thesis Title	MECHANICAL PERFORMANCES OF CONCRETE BEAMS WITH HYBRID USAGE OF STEEL AND FRP REINFORCEMENT
By	Mr. {Linh Van Hong Bui
Field of Study	Civil Engineering
Thesis Advisor	Professor Boonchai Stitmannathum, D.Eng.
Thesis Co Advisor	Professor Tamon Ueda, D.Eng.

---

Accepted by the Faculty of Engineering, Chulalongkorn University in Partial  
Fulfillment of the Requirement for the Doctor of Philosophy

..... Dean of the Faculty of Engineering  
(Associate Professor Supot Teachavorasinskun, D.Eng.)

DISSERTATION COMMITTEE

..... Chairman  
(Professor Teerapong Senjuntichai, Ph.D.)

..... Thesis Advisor  
(Professor Boonchai Stitmannathum, D.Eng.)

..... Thesis Co-Advisor  
(Professor Tamon Ueda, D.Eng.)

..... Examiner  
(Associate Professor Phoonsak Pheinsusom, Ph.D.)

..... Examiner  
(Assistant Professor Pitcha Jongvivatsakul, Ph.D.)

..... External Examiner  
(Professor Piti Sukontasukkul, Ph.D.)

ลิน แวน ฮง บุย : พฤติกรรมเชิงกลของคานคอนกรีตที่เสริมด้วยเหล็กร่วมกับพอลิเมอร์เสริมเส้นใย. (MECHANICAL PERFORMANCES OF CONCRETE BEAMS WITH HYBRID USAGE OF STEEL AND FRP REINFORCEMENT) อ.ที่ปรึกษาหลัก : ศ. ดร.บุญไชย สถิตมั่นในธรรม, อ.ที่ปรึกษาร่วม : ศ. ดร.ทามอน อุเอตา

ในปัจจุบันวัสดุพอลิเมอร์เสริมเส้นใย (FRP) ชนิดแห้งถูกนำมาใช้เสริมแรงในชิ้นส่วนโครงสร้างคอนกรีตเสริมเหล็กเนื่องจากมีกำลังรับแรงดึงสูงและสามารถเพิ่มความทนทานของโครงสร้างคอนกรีตในสภาพสิ่งแวดล้อมที่มีฤทธิ์การกัดกร่อนสูงได้ อย่างไรก็ตามเนื่องจากวัสดุ FRP มีค่าโมดูลัสยืดหยุ่นต่ำและมีคุณสมบัติระหว่างความดันและความเครียดเป็นเส้นตรงยืดหยุ่นจนกระทั่งเกิดการวิบัติ จึงทำให้คอนกรีตที่เสริมแรงด้วย FRP เพียงอย่างเดียวอาจขาดความเหนียวได้ ดังนั้นงานวิจัยนี้จึงนำเสนอการใช้ FRP ร่วมกับเหล็กเสริมในการรับแรงเฉือนและแรงดัดเพื่อเพิ่มความสามารถในการรับแรงของโครงสร้าง

ส่วนแรกของงานวิจัยเป็นการทดสอบการรับแรงเฉือนของคานคอนกรีตที่เสริมกำลังรับแรงเฉือนโดยใช้แท่ง FRP ด้วยเทคนิคการฝังผ่านหน้าตัด (ETS) เพื่อศึกษาประสิทธิภาพของระบบการเสริมกำลังภายใต้ผลกระทบต่างๆ และนำเสนอวิธีการทำนายกำลังรับแรงเฉือนสำหรับการเสริมกำลังด้วยวิธี ETS นอกจากนี้ยังทดสอบแรงดึงเพื่อศึกษาแรงยึดเหนี่ยวระหว่างแท่ง ETS และคอนกรีตภายใต้อิทธิพลต่างๆ อีกทั้งได้นำเสนอแบบจำลองไฟไนต์เอลิเมนต์ของระบบการเสริมกำลังดังกล่าวและเปรียบเทียบความถูกต้องของแบบจำลองกับผลการทดสอบคาน จากผลการทดสอบพบว่า เมื่อเปรียบเทียบกับงานวิจัยในอดีต ประสิทธิภาพในการรับแรงเฉือนของคานคอนกรีตเสริมเหล็กเพิ่มขึ้นอย่างมีนัยสำคัญเมื่อเสริมกำลังด้วยวิธี ETS แบบมีอุปกรณ์ยึด (anchorage) นอกจากนี้ผู้วิจัยได้พัฒนาสมการของความเครียดเฉลี่ยของแท่ง FRP จากทฤษฎีโครงข้อหมุนจำลอง (truss analogy theory) ซึ่งสามารถทำนายกำลังรับแรงเฉือนของแท่ง FRP ที่ใช้เทคนิคการฝังผ่านหน้าตัดชนิดมีอุปกรณ์ยึดได้อย่างมีประสิทธิภาพ

ส่วนที่สองของงานวิจัยนำเสนอการวิเคราะห์พฤติกรรมของคานคอนกรีตที่เสริมกำลังรับแรงดัดโดยการใส่ FRP ร่วมกับเหล็กเสริมโดยใช้แบบจำลองไฟไนต์เอลิเมนต์แบบสามมิติ ความเหนียวของคานคอนกรีตเสริมแรงด้วย FRP และเหล็กเสริมภายใต้ผลกระทบที่สำคัญได้ถูกวิเคราะห์โดยการศึกษาตัวแปรศึกษา จากผลการวิเคราะห์สามารถนำเสนอสัดส่วน FRP ต่อเหล็กเสริม ตำแหน่งของ FRP และชนิดของ FRP ที่ทำให้โครงสร้างมีความเหนียวที่เพียงพอสำหรับการใช้งานได้

สาขาวิชา วิศวกรรมโยธา  
ปีการศึกษา 2561

ลายมือชื่อนิสิต .....  
ลายมือชื่อ อ.ที่ปรึกษาหลัก .....  
ลายมือชื่อ อ.ที่ปรึกษาร่วม .....

# # 5871429421 : MAJOR CIVIL ENGINEERING

KEYWORD: FRP, Steel reinforcement, Ductility, Strengthening

Linh Van Hong Bui : MECHANICAL PERFORMANCES OF CONCRETE BEAMS WITH HYBRID USAGE OF STEEL AND FRP REINFORCEMENT. Advisor: Prof. Boonchai Stitmannathum, D.Eng. Co-advisor: Prof. Tamon Ueda, D.Eng.

Fiber-reinforced polymer (FRP) bars have been recently employed to reinforce concrete members due to their high tensile strength and especially in corrosive environments to improve the durability of concrete structures. However, FRP composites have a low modulus of elasticity and a linear elastic behavior up to rupture, thus reinforced concrete (RC) components with such materials would express a lack of ductility. In order to increase the mechanical performances of RC beams, the hybrid usage (also called combined usage) of FRP and steel reinforcements in shear and flexure is proposed.

At first, an experimental investigation of concrete beams strengthened in shear by FRP bars using embedded through-section (ETS) technique is carried out to study the efficiency of the strengthening system under various effects. The prediction of shear contribution of the retrofitting system is also proposed. Additionally, the pullout tests are conducted to investigate the bond response between ETS bars and concrete under various influences. Furthermore, the finite element (FE) simulation of the tested beams to validate the effectiveness of the FE tool is offered. Comparison between the results attained from this study and the literature displays the significant improvement in the shear efficiency of the ETS strengthening system with the anchorage installation. Furthermore, for the concrete beams strengthened in shear using ETS method, the truss analogy theory with the developed average strain formulation is an effective method to predict the shear resisting force of the anchored ETS FRP bars.

In the second part of research, this study presents a numerical and analytical study on the structural behaviors of concrete beams with the combined usage of FRP and steel tension reinforcement employing three-dimensional (3D) FE modelling. The ductility of the hybrid FRP-steel

Field of Study: Civil Engineering

Student's Signature .....

Academic Year: 2018

Advisor's Signature .....

Co-advisor's Signature .....

## ACKNOWLEDGEMENTS

Firstly, I would like to express my deepest gratitude to my supervisors Professors Boonchai Stitmannathum and Tamon Ueda for their invaluable advices. I could not finish my study without their strong supports and insightful suggestions.

Secondly, I would like to acknowledge Dr. Pitcha Jongvivalsakul for her helps during my research. I also would like to thank the technician staffs and colleagues in the Structural laboratory of the Department of Civil Engineering for their assistance during the experimental conduction.

Thirdly, I would like to express the gratitude for the financial support of the ASEAN University Network/Southeast Asia Engineering Education Development Network-AUN/SEED-Net. In addition, I would like to acknowledge the supply of adhesive material from Sika (Thailand) LTD and I would like to also acknowledge the support of glass fiber-reinforced polymer (GFRP) bars from Panjawattana Plastic Public Co., LTD.

Finally, I must give the deep gratitude to Thailand and Japan, where have contained my unforgettable memories. Of course, the love from my family in Vietnam occupies a part in my heart, motivating and encouraging me during my PhD life.

## TABLE OF CONTENTS

	Page
ABSTRACT (THAI).....	iii
ABSTRACT (ENGLISH).....	iv
ACKNOWLEDGEMENTS .....	v
TABLE OF CONTENTS .....	vi
LIST OF FIGURES .....	1
LIST OF TABLES.....	5
Chapter 1 INTRODUCTION.....	7
1.1 Background and motivation.....	7
1.2 Scope and objective of the dissertation.....	8
1.3 Dissertation structure .....	10
Chapter 2 LITERATURE REVIEW .....	11
2.1 Introduction .....	11
2.2 Assessments of the current strengthening methods.....	11
2.3 The previous research of ETS technique .....	14
2.4 The previous studies of beams with hybrid FRP and steel tension bars.....	18
2.5 Concluding remarks.....	20
Chapter 3 EXPERIMENTAL INVESTIGATION OF CONCRETE BEAMS STRENGTHENED WITH EMBEDDED THROUGH-SECTION (ETS) STEEL AND FRP BARS.....	22
3.1 Introduction .....	22
3.2 Experimental program .....	24
3.2.1 Description of tested specimens.....	24

3.2.2 Procedure of ETS method .....	26
3.2.3 Results and discussion .....	27
3.2.3.1 Load-deflection response .....	27
3.2.3.2 Cracking and failure mechanisms .....	30
3.2.3.3 Strain in shear reinforcement .....	34
3.3 Analysis of shear contribution carried by ETS strengthened bars .....	36
3.3.1 Introduction to existing shear resisting models.....	36
3.3.2 Comparison between internal reinforced beams and ETS beams .....	38
3.3.3 Effect of types of ETS strengthening system .....	41
3.3.4 Effect of existing steel stirrups on ETS FRP efficiency .....	45
3.3.5 Comparison to near surface mounted (NSM) shear strengthening method.....	48
3.3.6 Efficiency of ETS strengthening system in case of combined usage through shear capacity analysis.....	52
3.3.6.1 Experimental shear resistance compared to current shear resisting methods .....	52
3.3.6.2 Modified average strain for shear resistance model.....	55
3.4 Conclusions.....	59
Chapter 4 SIMULATION OF CONCRETE BEAMS STRENGTHENED BY EMBEDDED THROUGH-SECTION (ETS) STEEL AND GFRP BARS WITH BOND MODEL .....	61
4.1 Introduction .....	61
4.2 Experiment on bond mechanism of ETS bars to concrete.....	62
4.2.1 Description of tested specimens.....	62
4.2.2 Results and discussion .....	64
4.2.2.1 Effect of mechanical anchorage presence.....	65



4.2.2.2 Effect of embedment length.....	66
4.2.2.3 Effect of bar diameter.....	67
4.2.2.4 Effect of ETS types.....	68
4.2.2.5 Effect of anchorage length (number of anchoring nuts).....	68
4.2.3 Analysis of bond response of ETS bars to concrete.....	69
4.3 Finite element (FE) modelling of concrete beams strengthened with ETS steel and GFRP rods.....	76
4.3.1 Experimental data.....	76
4.3.2 Finite element program.....	78
4.3.2.1 Element types.....	80
4.3.2.2 Material models.....	80
4.3.3 Results and discussion.....	83
4.3.3.1 Load-deflection relationship and shear contribution of ETS strengthening system.....	83
4.3.3.2 Cracking and failure mechanism.....	87
4.3.3.3 Strain in shear reinforcement.....	89
4.4 Conclusions.....	92
Chapter 5 DUCTILITY OF CONCRETE BEAMS REINFORCED WITH BOTH FIBER- REINFORCED POLYMER AND STEEL TENSION BARS.....	94
5.1 Introduction.....	94
5.2 Experimental data to validate the finite element (FE) models.....	96
5.3 Validation of three-dimensional (3D) finite element (FE) models.....	99
5.3.1 Finite element program.....	99
5.3.1.1 Element types.....	100
5.3.1.2 Material models.....	100

5.3.2 Results and discussion .....	103
5.4 Parametric study by means of the finite element (FE) analysis .....	109
5.4.1 Design of parametric investigation .....	109
5.4.2 Effect of reinforcement ratios among concrete compressive strength and FRP types .....	111
5.4.3 Effect of reinforcement arrangement.....	113
5.4.4 Effect of FRP types.....	115
5.4.5 Ductility-related indices .....	117
5.5 Conclusions.....	125
Chapter 6 GENERAL CONCLUSIONS AND FUTURE DEVELOPMENTS .....	127
6.1 General conclusions.....	127
6.2 Future developments.....	132
REFERENCES .....	134
VITA.....	140

## LIST OF FIGURES

Figure 2.1 Strengthening technique of ETS method (Godat et al. 2013) .....	12
Figure 3.1 Configuration of the tested beams (dimensions in mm).....	27
Figure 3.2 Procedure of ETS shear strengthening technique.....	28
Figure 3.3 Preparation for recording the test data.....	28
Figure 3.4 Load-deflection response of the tested beams .....	29
Figure 3.5 Crack failure of the tested reference and ETS strengthened beams.....	32
Figure 3.6 (a) Crack patterns of a representative beam A3 and (b) general behavior of an ETS representative beam A3 .....	33
Figure 3.7 Strain in shear reinforcement.....	34
Figure 3.8 Comparison in shear contribution of internal stirrups and ETS reinforcement.....	39
Figure 3.9 Comparison in shear performance of the strengthened beams with different types of ETS bars .....	43
Figure 3.10 Effect of ETS Young's modulus on reinforcement strain with (a) vertical arrangement, (b) diagonal arrangement (no data for steel case) and (c) transverse steel.....	43
Figure 3.11 Shear failure tends to convert into flexural failure of ETS strengthened beams (B1 and B2) with mechanical anchorage attachment.....	44
Figure 3.12 Effect of existing steel stirrup ratios on (a) shear contribution of ETS strengthening system, (b) strain in stirrups and (c) strain in ETS reinforcement .....	46
Figure 3.13 Failure cracking pattern at side and at bottom of the beams strengthened using (a) NSM method and (b) ETS method .....	48

Figure 3.14 Comparison to the NSM shear strengthening method in shear contribution, note: reduction (%) = $[v_f(\text{low percentage of stirrups}) - v_f(\text{high percentage of stirrups})] \times 100 / v_f(\text{low percentage of stirrups})$ .....	50
Figure 3.15 Shear model of Ueda et al. (1996) .....	53
Figure 3.16 Comparison between analytical results using existing shear models and tested data.....	53
Figure 3.17 Modification of average strains in ETS strengthening system .....	56
Figure 3.18 Comparison between analytical results using modified average strain and tested data.....	56
Figure 4.1 Configuration of the tested specimens, the anchorage device (anchoring nuts) at end of GFRP bar and the pullout test setup.....	64
Figure 4.2 Comparison in the bond and strain responses between the cases with and without anchorage.....	66
Figure 4.3 Comparison in the bond response between the cases of embedment length changes .....	67
Figure 4.4 Comparison in the bond responses under the effects of ETS bar diameter and ETS types.....	68
Figure 4.5 Comparison in the bond responses between the cases of anchorage length changes, and pullout failure of specimen C8.....	69
Figure 4.6 The free body diagrams of the ETS bar interface .....	70
Figure 4.7 (a) Computed local bond stress-slip relationships at the different locations of the strain gauges (C4) and (b) strain distribution of ETS bar along bond interface (C4) .....	71
Figure 4.8 Experimental and regressed strain-slip curves at loaded end of the tested specimens .....	73
Figure 4.9 Comparison between theoretical and experimental maximum pullout forces.....	74

Figure 4.10 Experimental and analytical bond stress-slip curves at (a) loaded end of the tested specimens and (b) at interfacial locations of a representative specimen C4 .....	74
Figure 4.11 Configuration of the tested beams (dimensions in mm) .....	78
Figure 4.12 A half typical FE model for numerical program by using ANSYS 14.0.....	79
Figure 4.13 Models of concrete in compression and tension and bond model COMBIN39.....	81
Figure 4.14 Stress-strain relationships of steel and GFRP reinforcement.....	83
Figure 4.15 Comparison between tested and numerical results in load-deflection relationship .....	84
Figure 4.16 Comparison between tested and simulated data in terms of shear contribution of ETS strengthening system.....	86
Figure 4.17 Shear strain in XY plane compared to tested shear failure cracks of analyzed specimens.....	88
Figure 4.18 (a) Crack propagation in shear span of a representative beam R3: comparison between experimental and numerical results, (b) stress evolution at maximum load in reinforcement (ETS bars, stirrups, tension bars) of a representative beam B1 .....	90
Figure 4.19 Comparison between measured and simulated data in terms of strain in ETS reinforcement .....	91
Figure 4.20 Comparison between measured and simulated data in terms of strain in steel stirrups.....	92
Figure 5.1 Geometrical dimension of the tested beams (Aiello and Ombres 2002)....	97
Figure 5.2 Geometrical dimension of the tested beams (Qu et al. 2009) .....	98
Figure 5.3 Geometrical dimension of the group tested beams (Lau and Pam 2010) ..	99
Figure 5.4 A quarter typical FE model for numerical program by using ANSYS 15.0 ...	99

Figure 5.5 Models of concrete in compression and tension .....	100
Figure 5.6 Stress-strain relationships of steel and FRP reinforcement .....	101
Figure 5.7 Comparison of load-midspan deflection relationship between the tested and FE results: the first two specimens are steel and FRP RC beams, respectively, and the remaining specimens are hybrid beams .....	102
Figure 5.8 Stress in FRP bar, stress of steel reinforcement, and concrete strain at ultimate load of the representative hybrid beam B3.....	105
Figure 5.9 Crack propagation under the load stages of the representative hybrid FRP-steel RC beam B3 .....	106
Figure 5.10 General behavior of hybrid beams .....	106
Figure 5.11 Comparison between tested and simulated results in strain distribution .....	108
Figure 5.12 (a) Reinforcement arrangement cases, and (b) cases of reinforcement ratios among concrete compressive strength and FRP types (each group has a steel RC beam with the same flexural capacity design) .....	110
Figure 5.13 Effect of hybrid reinforcement ratio with different concrete compressive strengths and effect of reinforcement arrangement.....	112
Figure 5.14 Effect of reinforcement ratio together with FRP types.....	114
Figure 5.15 Relationship of reinforcement ratio and ductility index in the beams of parametric study.....	119
Figure 5.16 Relationship of reinforcement ratio and ductility factor in the beams of parametric study.....	121
Figure 5.17 Relationship of reinforcement ratio and absorption energy in the beams of parametric study .....	122

## LIST OF TABLES

Table 3.1 Reference, ETS shear strengthening configuration of the tested beams.....	25
Table 3.2 Properties of materials of the tested beams .....	25
Table 3.3 Experimental results of ultimate load ( $F_{max}$ ), ultimate displacement ( $u_{Lmax}$ ), and shear resistance ( $V_{max}$ and $V_f$ ) .....	29
Table 3.4 Main average diagonal shear crack angles of the tested beams.....	31
Table 3.5 Reinforcement configuration and ETS shear contribution ( $V_f$ ) of the tested beams in previous study .....	38
Table 3.6 Properties of materials of the beams in the previous study .....	38
Table 3.7 Reinforcement configuration and ETS/NSM shear contribution ( $V_f$ ) of the tested beams in previous studies .....	51
Table 3.8 Average strain from experimentation, before modification, computation, and after modification .....	54
Table 3.9 Shear contribution of ETS reinforcement from experimental and analytical results using modified average strain.....	57
Table 4.1 Properties of materials of the tested specimens .....	63
Table 4.2 Configuration, ultimate load, maximum slip and failure mode of the tested specimens .....	63
Table 4.3 Analysis of pullout test results.....	73
Table 4.4 Reference, hybrid and ETS shear strengthening configuration of the 11 tested beams.....	77
Table 4.5 Properties of materials of the 11 tested beams.....	79
Table 4.6 Numerical and experimental results in load capacity ( $P$ ), shear strength ( $V$ ) and shear contribution of ETS system ( $V_f$ ).....	87
Table 5.1 The properties of the tested beams .....	97

Table 5.2 The mechanical properties of materials.....	98
Table 5.3 Experimental and numerical results on load carrying capacity, absorption energy and failure mode.....	107
Table 5.4 Details of the parametric study on reinforcement ratios, concrete compressive strength and types of FRP, and simulated absorption energy and yielding load .....	122
Table 5.5 Effects of reinforcement arrangement and types of FRP reinforcement ...	124
Table 5.6 Absorption energy, ductility factor and ductility index of the experimental results.....	118





## Chapter 1 INTRODUCTION

### 1.1 Background and motivation

The countries, especially the developing countries, in the world are making efforts towards the sustainability in the multifarious fields, and one of areas is the sustainability in the construction and infrastructures. Therefore, the strengthening and rehabilitating existing reinforced concrete (RC) structures has been continuously increasing in the last decade because of the deterioration of concrete or the improvement of design guidelines which become stricter. One of the most attractive strengthening materials for the RC members is fiber-reinforced polymers (FRP) due to their high tensile strength, strength-to-weight ratio, corrosion resistance and durability.

Nowadays, the two common methods with FRP used for the strengthening of concrete structures are externally bonding (EB) and near-surface-mounting (NSM). There were various studies and application cases, which have been investigated on these retrofitting methods. These techniques were the effective solutions for enhancing the load-carrying capacity of concrete structures. However, as reported in the past research, the aforementioned strengthening methods still remain the main disadvantages as the tedious surface and groove preparation required as well as the occurrence of debonding of the FRP composites (delamination of the concrete cover). In the recent years, the advent of the embedded through-section (ETS) method overcomes the drawbacks of the EB and NSM methods. As a definition, in the ETS technique the FRP or steel rods are embedded through previously drilled holes into the concrete core. All of the previous research concluded that the ETS technique was proved to be particularly efficient as increased significantly of the shear resistance of the RC beams. Moreover, the advantages of the ETS technique are using a small amount of adhesive materials and not needing the high skill of the worker to construct. In addition, the ETS method is also a cost competitive and feasible solution in comparison with those by applying the EB and NSM techniques.

On another aspect, FRP bars have been recently used to reinforce concrete members in flexure due to their high tensile strength and especially in corrosive environments to improve the durability of concrete structures. However, FRPs have a low modulus of elasticity and a linear elastic behavior up to rupture, thus the RC components reinforced with FRP bars would exhibit a less ductility in comparison with the similar members reinforced by the steel reinforcement. Hence, the study on the performances of concrete beams with combined usage of steel and FRP reinforcement to assure the ductility, the rigidity, the strength and the durability is necessary towards the practical use.

This research aims to gain the deep understanding of the mechanical performances of concrete beams with hybrid usage in shear and flexure of FRP and steel reinforcement. The experimental and numerical methods are the research methodology of this study. The results of research are analyzed and compared to the data obtained by the previous studies. The verification of outputs is also carried out to present the efficiency of the ETS technique in the shear strengthening of the RC beams, and the hybrid combination of steel and FRP tension bars in the flexural members. The outcomes of this study are expected to provide the reliable database for the future research and the actual application.

## 1.2 Scope and objective of the dissertation

To enhance the longevity of the RC structures, the ETS technique has been applied in the past works with success in the shear strengthening field. Indeed, the ETS technique is an efficient method that overcomes all of drawbacks of the EB and NSM techniques. Most of previous research indicated the improvements in the shear performance of the ETS technique in the comparison with the EB and NSM methods. In addition, the high strength and the small weight are the special properties of FRP material, making them attractive as reinforcement for concrete structures. However, due to a linear elastic stress–strain relationship up to failure of FRP, FRP reinforced concrete components exhibit brittle failure.

The long term goal of the research is to develop a new shear strengthening method for the RC beams as well as to understand the structural behaviors of hybrid FRP-steel RC beams towards the practical use. The study on the mechanical performances of concrete beams with hybrid usage of steel and FRP reinforcement in shear and flexure by means of the experimental program and numerical analysis is the core purpose of the present research. The specific objectives of this study are as below:

(a) to experimentally and analytically study ETS rehabilitation method of full-scale RC T-section beams in shear using steel and FRP rods under various effects such as the presence of mechanical anchorage at tension ends of ETS bars, the inclination of the ETS bars, the amount of existing steel stirrups, the ratio of ETS shear bars and the ETS material types;

(b) to experimentally and analytically compare the structural performances of concrete beams reinforced with ordinary shear reinforcement to that of the concrete beams strengthened with ETS bars;

(c) to investigate the design procedures in the current guidelines to evaluate the shear efficacy of the ETS steel/FRP in terms of the shear resistance of retrofitted RC beams;

(d) to develop a rational design model to calculate the shear contribution of ETS strengthening system in the retrofitted beams based on the existing design methods;

(e) to experimentally analyze the bond response of concrete blocks embedded by ETS steel/FRP rods by varying the influencing parameters such as the presence of mechanical anchorage, embedment length, ETS bar diameters, ETS types and anchorage length (number of anchoring nuts);

(f) to simulate the tested beams using finite element (FE) tool to validate the numerical results and to provide the reliable FE models for the concrete beams strengthened in shear with ETS bars;

(g) to investigate the ductility of concrete beams with hybrid usage of steel and FRP tension reinforcement under various influences to offer the feasible parameters of the hybrid FRP-steel RC beams for the practical use.

### 1.3 Dissertation structure

The research work in this study is reported through six chapters. Chapter 1 offers an introduction and motivation, discusses the objectives and presents the structure of the research work. Chapter 2 briefly shows the literature review of the previous research related to the current work. Chapter 3 presents the experimental and analytical study of the concrete beams reinforced with the internal steel shear reinforcement and the concrete members strengthened in shear with ETS steel and glass fiber-reinforced polymer (GFRP) bars. Chapter 4 conducts the pullout test to analyze the bond response between the ETS bars and concrete. Chapter 4 also presents the finite element (FE) simulation of the concrete beams retrofitted by ETS bars, which are tested in Chapter 3. Chapter 5 investigates the ductility of concrete beams with hybrid usage of steel and FRP tension reinforcement by means of FE modelling. Finally, general conclusions and recommendations for future work are furnished in Chapter 6.

## Chapter 2 LITERATURE REVIEW

### 2.1 Introduction

This Chapter offers a general look in shear of the reinforced concrete (RC) structures using the new shear strengthening methods. Specifically, this Chapter presents the assessment on the mechanical performances of the current shear strengthening techniques towards the most effective method what is going to be investigated in this study. In addition, the important findings in the previous studies on the embedded through-section (ETS) technique for shear strengthening with fiber-reinforced polymer (FRP) and steel bars of the RC beams are also shown in this Chapter. On the other hand, to consider the structural responses of the concrete beams with hybrid usage of FRP and steel tension bars, the explorations obtained in the past studies are also summarized to reach the critical points of the research work.

### 2.2 Assessments of the current strengthening methods

To strengthen the existing concrete structures, the different techniques have been employed successfully in the actual projects involving the RC beams and girders. The two most common methods have been adopted to strengthen concrete members are externally bonding (EB) and near surface mounting (NSM). There were numerous research on the EB and NSM techniques for strengthening of concrete structures. Moreover, since these methods were developed in the last two decades, they were introduced in the specification of the analysis, design and construction.

For the EB strengthening technique, the FRP composites are attached to the tension/shear zone of the RC members to carry the tensile/shear stresses by means of the epoxy adhesive (Hawileh et al. 2014). According to the review by Panigrahi et al. (2014), this method was using for the strengthening and repair of structures due to actions of ageing, poor maintenance, corrosion of steel reinforcement, defects in

construction, exposure to harmful environments and damage in case of seismic events, and the deficiency of the initial design such as demand in the serviceability state, the durability and ductility of reinforced concrete structures. Most studies indicated that the use of the EB technique would enhance the load carrying, shearing and flexural capacities of RC members (Dai et al. 2005, Panigrahi et al. 2014, Hawileh et al. 2014, Ali et al. 2014, Hong et al. 2014). At the present, the study of the EB strengthening method for the RC members is extending to consider the various and combined effects of elevated temperature and environment conditions, the interfacial behavior and the new approach of numerical analysis (Dai 2005, Burke et al. 2013, Domenico et al. 2015, and Firmo et al. 2015). However, Dai et al. (2005) showed that a primary concern for this technique was local debonding of FRP and concrete interfaces, leading a sudden drop in loads and loss of ductility of the whole FRP-RC composite system.

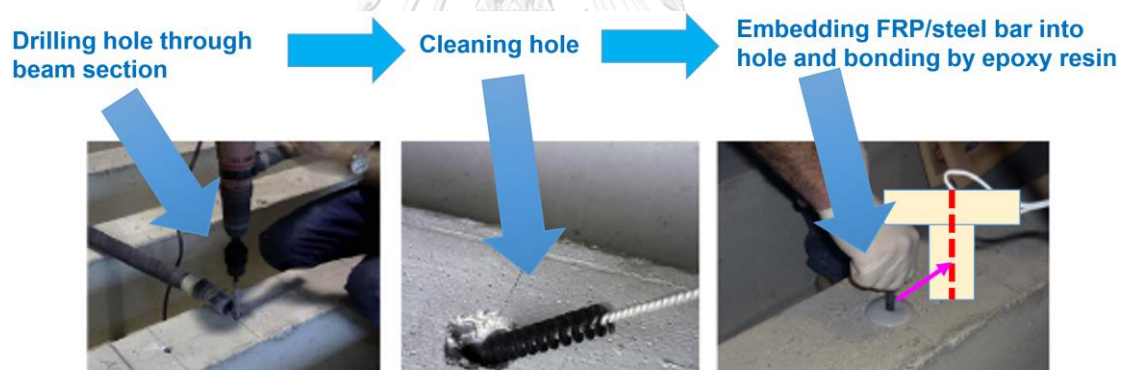


Figure 2.1 Strengthening technique of ETS method (Godat et al. 2013)

To apply the near surface mounting (NSM) method, Lorenzis et al. (2000) described as follows. Firstly, cutting a groove in the desired direction into the concrete surface and the groove is filled half-way with epoxy paste, the FRP rod is placed in the groove with light pressing. Then, more paste is filled into the groove to the surface. According to the results studied by Lorenzis et al. (2000), Rahal et al. (2011), Zhang et al. (2013), Akter et al. (2015), the structures strengthened by NSM bars would also increase significantly the load, shear and flexural capacities. In addition, the research of Rizkalla et al. (2004) stated that the NSM FRP strengthening

technique could be considered an efficient alternative to an externally bonded FRP strengthening system based on the improving of the experimental results on stiffness and flexural strength of members.

Generally, the various research have proven the effectiveness of the EB and NSM methods in the strengthening field. However, Chaallal et al. (2011) revealed that these two methods still remained the main disadvantages such as the tedious surface and groove preparation required as well as the occurrence of debonding of the FRP composites (i.e. delamination of the concrete cover). In addition, the employing of the EB and NSM techniques for the strengthening of RC members would enhance the load carrying capacity, but the ductility of RC members was decreased. Especially, for NSM technique that has placed the steel rods in groove at the surface of RC members, the structures would be attacked by the corrosive agents, therefore the durability of structures would gradually be reduced. Furthermore, the use of the EB and NSM methods needs a large amount of adhesive resin and high skill workers for construction.

Currently, embedded through-section (ETS) is an efficient method that overcomes all of drawbacks of the EB and NSM techniques. Godat et al. (2013) exhibited a simple definition of embedded through-section (ETS) technique that this method uses an adhesive to bond fiber-reinforced polymer (FRP) or steel bars embedded through pre-drilled holes into the concrete core. Figure 2.1 shows the steps for shear strengthening of a RC member by applying the ETS method. A rebar detector is used to verify the positions of reinforcement in the original structures, strengthening rods are therefore marked to orientate the drilling direction. The drilling positions can also be determined by the initial design. In the comparison with the other shear strengthening methods, the procedure indicates that the ETS shear strengthening technique are simply applied, wasted less time consuming, used less adhesive materials. In addition, the ETS method does not require the surface preparation of RC members and the high skill of workers to construct. Furthermore, as shown in the previous works, since the ETS bars are fully protected by concrete, the possible corrosion and fire exposure of the strengthening rods are prevented. Together with the aforementioned advantages, the bonding performance may be improved due to

the confinement of concrete to ETS bars. However, the research and application of ETS method are not much and less common.

### 2.3 The previous research of ETS technique

Till date, there were important investigations on the strengthening of RC members using ETS method. This Section presents the highlights of the experimental studies in the order of appearance of Valerio et al. (2009), Dalgre et al. (2011), Chaallal et al. (2011), Mofidi et al. (2012), Breveglieri et al. (2014), and Breveglieri et al. (2015).

As an initial study on the ETS strengthening method, Barros et al. (2008) carried out an experimental exploratory of the short beams to capture the main features of the carbon fiber-reinforced polymer (CFRP) bar contribution in shear resistance. In their study, the monitoring system was adopted to analyze the relationship between crack opening, crack sliding and strains in the CFRP strengthened bars with the applied load levels. Barros et al. (2008) revealed that a CFRP reinforcement ratio of 0.2% contributed for a 26% increment in terms of specimen shear resistance. On the other hand, to show the promising of the ETS strengthening method of RC structures, the authors found that the strain level in the CFRP reinforcement was enough significant at a crack width of 0.3 mm. Moreover, this study indicated that the contribution in shear of the CFRP bars was more effective when the specimens failed without bar-adhesive debonding.

In the study by Valerio et al. (2009), the comparison in shear performances of un-strengthened small scale and large scale beams to the equivalent beams strengthened in shear with the deep embedment (ETS) technique using experimental program was carried out. In addition, the pullout tests on carbon, glass, aramid and steel bars embedded into concrete with varying embedment lengths were also conducted. It is similar to the study by Barros et al. (2008) that the ETS strengthening method was feasible and effective for the RC beams in the shear resistance. Furthermore, the various findings are shown as follows. The system effectiveness relied on the bond between the ETS bar and concrete since the bond-slip response of the system was robust and ductile. The failure mode without debonding effect of



the beams strengthened by ETS bars exhibited the advantages in the shear contribution of the retrofitting system compared to that of employing the NSM method due to the ETS bars were embedded as the internal reinforcement. To take into account the shear strength prediction of the beams adopting ETS technique, this study concluded that the truss analogy, combined with current code predictions, was able accurately and safely to predict the capacity of the strengthened beams.

Dalfre et al. (2011) conducted an experimental program on the shear strengthening of two series of the reinforced concrete beams with a difference of cross section. In their study the ETS steel bars were designed as a stirrup of one arm following the American Concrete Institute (ACI) code. As observed in the test results, Dalfre et al. (2011) implied that by applying the ETS shear strengthening method, the retrofitted beam would have converted the brittle shear failure into the ductile flexural failure with the yielding of the longitudinal steel bars. In addition, the maximum strain in both stirrups and ETS bars was increased, and the gained values were around the yield strain and even some of them have even exceeded the yield strain (Dalfre et al. 2011). Furthermore, Dalfre et al. (2011) indicated that the effectiveness of the inclined ETS strengthening bars were more effective than that of the vertical ETS bars. Additionally, the decrease of the ETS bars spacing would increase the shear capacity of the ETS retrofitted RC beams.

In order to evaluate the effectiveness of the ETS shear strengthening system, Chaallal et al. (2011) studied on the performance of concrete beams strengthened by ETS bars in the comparison with that of concrete members retrofitted with EB and NSM bars. The experimental results in research of Chaallal et al. (2011) indicated that the shear capacity of the specimens without transverse steel strengthened by the ETS CFRP bars were increased significantly in comparison with the one attained by means of EB and NSM techniques. Chaallal et al. (2011) stated that the failure of the retrofitted members eventually occurred by concrete crushing or the highest strain of tension reinforcement, and the ETS CFRP bars reached the ultimate strain. Chaallal et al. (2011) also showed that the crack pattern on the surface of the concrete beams strengthened by ETS CFRP rods was distributed fairly within the concrete core. The same to the conclusion in the study by Barros et al. (2011), Chaallal et al.

(2011) implied that the load capacity of the strengthened beams would reach to their flexural capacity limit and the beams retrofitted with ETS bars were more ductile.

To enhance the understanding on the shear behavior of concrete beams strengthened by ETS bars through the study of Chaallal et al. (2011), Mofidi et al. (2012) carried out an analytical and experimental investigation on the shear strengthening of RC T-beams with ETS FRP rods. In their study, the authors considered the effects of the surface coating of FRP bars and steel stirrups on the shear contribution of ETS FRP systems. Additionally, the influences of ETS FRP bars spacing and ETS FRP rods diameter on the shear performance of the retrofitted RC beams were also analyzed. Also reported in the other studies, Mofidi et al. (2012) concluded that the ETS FRP strengthening method was an effective technique to increase the shear capacity of the retrofitted RC beams. With narrowly spaced internal steel reinforcement, the shear contribution of FRP would be decreased drastically in the strengthened RC members. Moreover, the efficacy of plain surface CFRP rods strengthened in beams was greater than the performance of sand-coated CFRP rods retrofitted in the similar members since the shear transfer mechanism between concrete-adhesive-ETS bars in the strengthened beams was well utilized. One of conclusions of this research, the applying of ETS FRP technique for strengthening RC beams brought to high efficiency due to increasing the shear capacity, reducing a large amount of steel stirrups, and enhancing the ductility of structures. On the other hand, the corrosion and fire attack of the strengthened RC beams would be limited by using ETS method, therefore the durability of the retrofitted structures was improved significantly.

Breveglieri et al. (2014) presented an experimental program with the real size scale of RC beams, designed to fail in shear, strengthened with ETS bars. Breveglieri et al. (2014) showed that using ETS technique for strengthening of a beam, a significant increase of the load carrying capacity would be obtained. It was obvious that the inclined ETS bars were much more effective than vertical ones in the shear resistance of the strengthening system. In the next study by Breveglieri et al. (2014), Breveglieri et al. (2015) indicated that using the steel stirrups would decrease the

strengthening effectiveness of ETS bars and the detachment of bars to concrete did not occur since the ETS bars were embedded in core of concrete section. Especially, the behavior of the RC beams strengthened by ETS bars could be converted from shear brittle failure modes to flexural ductile failure modes (Breveglieri et al. 2014 and Breveglieri et al. 2015). Besides, due to the higher confinement provided by the concrete surrounding the bars embedded into the core of the strengthened components, which leads advantages on the bond strength, Breveglieri et al. (2015) stated that the ETS technique could be highly effective for the shear strengthening. Therefore, by comparing to the NSM and EB methods, which the strengthening system is attached to the surface of members, the ETS technique can be a technical and economic alternative since it mobilizes the beam's concrete core that is generally less damaged zones of a beam (Breveglieri et al. 2015).

The bond behavior between the ETS strengthened rods and concrete is an important point that affects directly the mechanical performances of concrete beams strengthened with the ETS shear reinforcement. However, the bond mechanism of ETS installed bars to concrete has not been deeply investigated in the past works. Indeed, there were two ETS pullout test studied by Godat et al. (2012) and Caro et al. (2017), then Godat et al. (2013) and Barros et al. (2013) developed two-dimensional finite element models to confirm the experimental results. Godat et al. (2012) carried out an experimental test of 13 direct-shear test specimens by analyzing the influences of concrete strength, hole diameter, bar diameter, bar surface area, and bar bond length on the bond behavior of FRP-strengthened reinforced concrete beams. Their experimental results showed that debonding could be avoided by providing a sufficient bar length and high concrete strength. Moreover, Godat et al. (2012) recommended that, for the ETS strengthening technique, a hole of diameter should be  $1.5d_b$  to obtain a proper bond between the concrete and the bar.

However, the less bonding performance of the ETS retrofitting system to concrete is also appeared in the past works, especially the vertical case of strengthening. Moreover, the active effectiveness of the ETS bars with the cases of low bonding effect is drastically reduced by the presence of the existing transverse steel, it means

that the shear contribution of the ETS retrofitted rods is nearly insignificant after debonding of the strengthening tool to concrete due to the shear transfer mechanism between ETS bars-adhesive-concrete was not maintained. Besides, the available shear design methods for the beams strengthened by ETS FRP shear bars and reinforced with internal FRP reinforcement exhibited the drastic underestimations compared with the test results. Therefore, to trigger the ultimate effectiveness of ETS strengthening system either the bonding performance between ETS bars and concrete is enhanced or the bonding efficacy is compensated by the additional spare after debonding occurred. Additionally, the rational shear design model for predicting the shear contribution of the ETS retrofitting system in the RC strengthened beams has to be developed from the original methods to obtain the fair estimation compared with the experimental data.

#### **2.4 The previous studies of beams with hybrid FRP and steel tension bars**

Since fiber-reinforced polymer (FRP) reinforcement requires an expensive material, the partial replacement of steel reinforcement by FRP reinforcement is economically feasible. To prevent the corrosion of steel reinforcement in the reinforced concrete (RC) beams in aggressive environments, the most external reinforcement (closest to the concrete surface) could be replaced by FRP reinforcement. Therefore, concrete beams reinforced by both steel and FRP reinforcements have been considered an interesting topic for experimental and numerical research. The studies of Aiello and Ombres (2002), Qu et al. (2009), Lau and Pam (2010), Ge et al. (2015) and Yoo et al. (2016) have been conducted on deflection, curvature, ductility, crack width of concrete beams with hybrid usage of FRP and steel tension reinforcement. The study by Aiello and Ombres (2002) provides various findings as follows. The hybrid combinations of steel and FRP reinforcement were advantageous in the deformability consideration. The deformability of FRP reinforced concrete (RC) beams under service conditions was reduced by using the adequate amount of steel reinforcement. It was emphasized that placing FRP bars nearly the outer surface and steel bars at the inner level of the tensile zone would increase the stiffness of beams. Moreover, the crack

width and spacing decreased with the presence of steel reinforcement in comparison with the one attained by beams reinforced with only FRP bars. Using the moment-curvature law, the behavior of concrete beams reinforced by steel and FRP bars could accurately predict, and the ACI code furnished a good prediction of the deflections and crack width at the serviceability phase. A design method was proposed to determine the effective moment of inertia for steel RC beams and FRP RC beams based on the calibrated experimental results.

By conducting an experimental and theoretical program, Qu et al. (2009) showed that the usage of steel reinforcement in combination with glass fiber-reinforced polymer (GFRP) bars enhanced the flexural performance of GFRP RC beams. This research indicated that the axial stiffness ratio between GFRP and steel bars had little influence on flexural capacity, whereas the effective reinforcement ratio was a reasonable parameter for predicting the ultimate moment of hybrid reinforced concrete beams. In order to predict the failure mode of hybrid beams, the balanced effective reinforcement ratio could be used. Their study proposed the flexural capacity equation which was valid for hybrid GFRP-steel RC members by using normal effective reinforcement ratios. The ductility of beams was increased by adding the steel reinforcements. At the service load level, the model of Bischoff (2007) was adopted to calculate the deflection of concrete beams reinforced with GFRP and steel bars. In another experimental work, Lau and Pam (2010) concluded that increasing the degree of over-reinforcement and adding conventional steel bars could improve the flexural ductility of GFRP RC members. The requirement contents on the minimum GFRP flexural reinforcement given by ACI 440.1R-06 could be reduced by about 25% based on the results of this study.

Ge et al. (2015) experimented the flexural behaviors of hybrid concrete beams reinforced with BFRP (basalt fiber-reinforced plastic) bars and steel bars. This research used the proposed formula with the measured strengths of bars and concrete to compute the flexural capacity and made the comparison with the experimental results. It was shown that the experimental results had a good agreement with the simplified proposed formula, therefore the suggested equations could be used in future applications. Decreasing the area ratios of BFRP to steel reinforcement, the

deflection of hybrid RC beams decreased, whereas the stiffness reduction factor increased. The average crack spacing of the hybrid FRP-steel RC beams was in the middle of the average crack spacing of the steel RC beams and FRP RC beams. In contrast to the above-mentioned studies, Yoo et al. (2016) investigated the flexural behavior of ultra-high-performance fiber-reinforced concrete (UHPFRC) beams reinforced with GFRP and steel bars. Their research showed that the ductility of UHPFRC beams reinforced by GFRP and steel bars were similar or slightly less than those of single GFRP bar-UHPFRC beams due to the premature rupture of steel reinforcement.

Up to now, there were several researches on the numerical analysis of the hybrid FRP-steel RC beams as Kara et al. (2015, 2016), Hawileh (2015), Oller et al. (2015), Yoo and Banthia (2015), Bencardino et al. (2016), Zhang et al. (2016) and Qin et al. (2017). These studies used the numerical method for estimating the curvature, deflection and moment capacity of hybrid FRP-steel RC beams. The ductility definitions were also suggested in those papers. Most studies showed a good agreement in the comparison between the numerical and experimental results. However, the numerical studies based on finite element (FE) modelling were limited to 2D analysis. Besides, the FE analysis studies employed a little experimental data from the literature, thus the outcome of simulation did not gain the high reliability. Furthermore, the ductility evaluation by the existing studies was not good enough for introducing the hybrid FRP-steel beams to the practical use. Therefore, additional numerical and analytical investigations are necessary.

## **2.5 Concluding remarks**

The aforementioned reviews indicate that the ETS technique was an effectiveness strengthening solution for the RC beams due to the significant increase of the load carrying, the shear capacities and the ductility of RC members. On the other hand, the performance of the RC beams with the hybrid usage of FRP and steel tension reinforcement were also analyzed in the previous studies. This Section presents the summary of the main contents what have been studied.

*The ETS technique for the shear strengthening of RC beams is studied as follows:*

Experimental programs of the concrete beams strengthened with ETS bars were conducted in terms of the load-carrying capacity, strain in reinforcement, cracking mechanism to find the performances in shear of the ETS strengthening method. In addition, the comparisons in shear responses of the ETS strengthened RC beams with EB and NSM methods were also indicated.

The effects of ETS inclination, ETS types and existing steel stirrups on the shear strengthening efficacy for RC beams were evaluated. Most data indicated that the efficiency of adopting plain surface CFRP rods were greater than that of employing sand-coated CFRP rods. Besides, all of results showed that the shear resistance of the inclined ETS bars were much more effective than that of vertical ETS bars. Furthermore, the strengthening effectiveness of ETS bars in a retrofitted member would be decreased with the presence of the existing transverse steel.

*The studies on concrete beams reinforced with FRP and steel tension bars are investigated as follows:*

Experimental and numerical investigations of concrete beams reinforced with hybrid FRP-steel reinforcements considering effects of the amount of reinforcement, the hook angle in the stirrup installation and the types of FRP tension reinforcement were shown.

## Chapter 3 EXPERIMENTAL INVESTIGATION OF CONCRETE BEAMS STRENGTHENED WITH EMBEDDED THROUGH-SECTION (ETS) STEEL AND FRP BARS

### 3.1 Introduction

The shear strengthening of reinforced concrete (RC) beams using fiber-reinforced polymer (FRP) and steel bars have been used to improve the longevity of the structures with success in the practical projects. Among shear retrofitting methods, embedded through-section (ETS) technique is an efficient technique that overcomes all of the drawbacks of the previous techniques such as externally bonding (EB) and near surface mounting (NSM) methods. Simply, the ETS method employs an adhesive to bond FRP or steel bars embedded through pre-drilled holes into the concrete core. Under the special characteristics in the application of the ETS technique, the corrosion and fire attack to reinforcement would be limited. However, the studies on the shear strengthening of the RC beams using the ETS method are not much and are less common.

There were several experimental studies on the strengthening of RC members by using ETS method such as Dalfre et al. (2011), Chaallal et al. (2011), Mofidi et al. (2012), Breveglieri et al. (2014), and Breveglieri et al. (2015). As reported in Chapter of the literature review, the shear resistance of the strengthened RC beams would significantly increase by using the ETS method and the response of the ETS shear strengthened members would have converted brittle shear failure into a ductile flexural failure with the yielding of the longitudinal steel bars. In addition, these studies provided various findings as follows. By applying the ETS shear strengthening method, the maximum strain in both stirrups and ETS bars was increased, and the gained values were around obtained the yield strain or even exceeded the yield strain. With narrowly spaced existing steel reinforcement, the shear contribution of ETS strengthening system would be decreased drastically in the strengthened RC beams. Furthermore, consider concrete beams strengthened by ETS bars, the



strengthening performance using the inclined ETS bars were more effective than that employing the vertical ETS bars, and the decrease of the rods spacing would increase the shear capacity of the strengthened RC beams. On the other hand, according to Breveglieri et al. (2014), Godat et al. (2013) and Barros et al. (2013), the cause by the larger available resisting bond length assured in the former configuration was reasonable to explain for the great performance of the concrete beams strengthened using the ETS method. Indeed, the bond behavior between the ETS strengthened rods and concrete is an important point that affects directly the mechanical performances of concrete beams strengthened with the ETS shear reinforcement. However, the less bonding performance of the ETS retrofitting system to concrete, which reduced the shear resisting capacity of the strengthened bars, was also appeared in the past works, especially the vertical case of strengthening. Moreover, the active effectiveness of the ETS bars with the cases of low bonding effect is drastically reduced by the presence of the existing transverse steel, it means that the shear contribution of the ETS retrofitted rods is nearly insignificant after debonding of the strengthening tool to concrete due to the shear transfer mechanism between ETS bars-adhesive-concrete was not maintained. Besides, the available shear design methods for the beams strengthened by ETS FRP shear bars and reinforced with internal FRP reinforcement exhibited the drastic underestimations compared with the test results. Therefore, to trigger the ultimate effectiveness of ETS strengthening system either the bonding performance between ETS bars and concrete is enhanced or the bonding efficacy is compensated by the additional spare after debonding occurred. Additionally, the rational shear design model for predicting the shear contribution of the ETS retrofitting system in the RC strengthened beams should be developed from the original methods to obtain the fair estimation compared with the experimental data.

The objective of this study is to investigate the mechanical performances of concrete beams strengthened by ETS steel and FRP rods with the mechanical anchorage at the tension ends. The overall responses, including load-deflection behavior, crack patterns and strain of reinforcement, of the tested beams are investigated. The comparison between the shear contributions of ETS retrofitted bars

and internal reinforcement is carried out. Furthermore, the effects of the types of the ETS strengthening system and the existing steel stirrup amounts on the shear performance of the retrofitted beams are analyzed. Additionally, the comparison in the cracking mechanism and in the shear contribution of the strengthened bars between the ETS and NSM retrofitted beams is also conducted. On the other hand, the calculation of the shear resistance of the ETS reinforcement is carried out using the truss analogy models of ACI and JSCE, and the Ueda et al.'s (Ueda et al. 1996) model. Besides, to enhance the effectiveness of the existing shear design methods, the average strain formulation for the anchored ETS FRP rods is developed. The results obtained from this study are compared and validated with the data of the past studies to evaluate the shear strengthening efficiency of the ETS method.

## **3.2 Experimental program**

### **3.2.1 Description of tested specimens**

The design configuration of 11 specimens, including three reference beams (R1, R2 and R3), two concrete beams reinforced by internal diagonal-vertical shear reinforcement (A1 and A2), two concrete beams strengthened by ETS steel bars (A3 and A4) and four concrete beams retrofitted with ETS GFRP bars (B1, B2, B3 and B4), for experimental program is clearly shown in Fig. 3.1 and Table 3.1. To consider the shear resistance of concrete and existing stirrups, the three reference beams are respectively designed for the case of concrete only in the shear span L1 (beam R1), the case of two steel stirrups with diameter of 6 mm with 300 mm spacing in the shear span L1 (beam R2) and the case of two steel stirrups with diameter of 9 mm with 300 mm spacing in the shear span L1 (beam R3).

Table 3.1 Reference, ETS shear strengthening configuration of the tested beams

Beam ID	Number of ETS bars	Inclination of ETS bars ( $^{\circ}$ )	ETS bars spacing (mm)	Existing steel stirrups ratio (%)	ETS reinforcement ratio (%)
R1-0S-0ETS	0	NA	NA	0.00	NA
R2-2Sd6-0ETS	0	NA	NA	0.11	NA
R3-2Sd9-0ETS	0	NA	NA	0.24	NA
A1-2Sd6-5Sd6(90)	5	90	180	0.11	0.18
A2-2Sd6-5Sd6(45)	5	45	180	0.11	0.25
A3-2Sd6-5ETS Steel d12(90)	5	90	180	0.11	0.35
A4-2Sd6-5ETS Steel d12(45)	5	45	180	0.11	0.50
B1-2Sd6-5ETS FRP d10(90)	5	90	180	0.11	0.24
B2-2Sd6-5ETS FRP d10(45)	5	45	180	0.11	0.34
B3-2Sd9-5ETS FRP d10(90)	5	90	180	0.24	0.24
B4-2Sd9-5ETS FRP d10(45)	5	45	180	0.24	0.34

Table 3.2 Properties of materials of the tested beams

Beam ID	Concrete strength at tested day (MPa)	Young modulus of ETS bars (GPa)	Yielding/Rupt. strength of ETS steel/FRP bars (MPa)	Young modulus of adhesive (GPa)	Tensile strength of adhesive (MPa)
R1-0S-0ETS	35.4	NA	NA	NA	NA
R2-2Sd6-0ETS	35.4	NA	NA	NA	NA
R3-2Sd9-0ETS	38.2	NA	NA	NA	NA
A1-2Sd6-5Sd6(90)	35.4	200*	235*	NA	NA
A2-2Sd6-5Sd6(45)	35.4	200	235	NA	NA
A3-2Sd6-5ETS Steel d12(90)	35.4	200	390*	3.1**	21.0**
A4-2Sd6-5ETS Steel d12(45)	35.4	200	390	3.1	21.0
B1-2Sd6-5ETS FRP d10(90)	38.2	50**	1076**	3.1	21.0
B2-2Sd6-5ETS FRP d10(45)	38.2	50	1076	3.1	21.0
B3-2Sd9-5ETS FRP d10(90)	38.2	50	1076	3.1	21.0
B4-2Sd9-5ETS FRP d10(45)	38.2	50	1076	3.1	21.0

\*Values were used according to TIS 24-2548

\*\*Values were provided by manufacturer

Besides, the two concrete beams with hybrid usage of diagonal-vertical shear reinforcement (beams A1 and A2) are designed to compare with the concrete beams strengthened in shear by ETS bars only tested in the previous study. Additionally, the two concrete beams strengthened with vertical and diagonal ETS steel bars (beams A3 and A4) are also designed to compare with the concrete beams retrofitted in shear by ETS GFRP and CFRP bars. Moreover, the four ETS GFRP strengthened beams are designed to investigate the effects of the several parameters such as the mechanical anchorage at the tension ends of ETS bars, the presence of steel stirrups, the percentage of ETS bars and the mechanical properties of shear reinforcement on the shear strengthening efficacy. On the other hand, the positions of the attached strain gauges are also marked in Fig. 3.1. Table 3.1 shows the detail of configuration of the tested beams in this study, and Table 3.2 describes the properties of the materials of concrete, steel, FRP and adhesive employed in this experiment. The concrete compressive strengths were determined using the compressive test of concrete cylinders. While, the properties of steel and FRP reinforcement, and adhesive were provided by the manufactures.

### 3.2.2 Procedure of ETS method

Figure 3.2 shows the six steps for shear strengthening of RC members by applying the ETS method. In the comparison with the other shear strengthening methods, the procedure indicates that the ETS shear strengthening technique are simply applied, wasted less time consuming and used less adhesive materials. In addition, the ETS method does not require the surface preparation of RC members and the high skill of workers to construct. As shown in the previous works, since the ETS bars are fully protected by concrete therefore the possible corrosion of the strengthening rods is prevented. Together with the aforementioned advantages, the bonding performance may be improved due to the confinement of ETS bars in concrete. In addition, the test preparation of the experimental program is clearly described in Fig. 3.3.

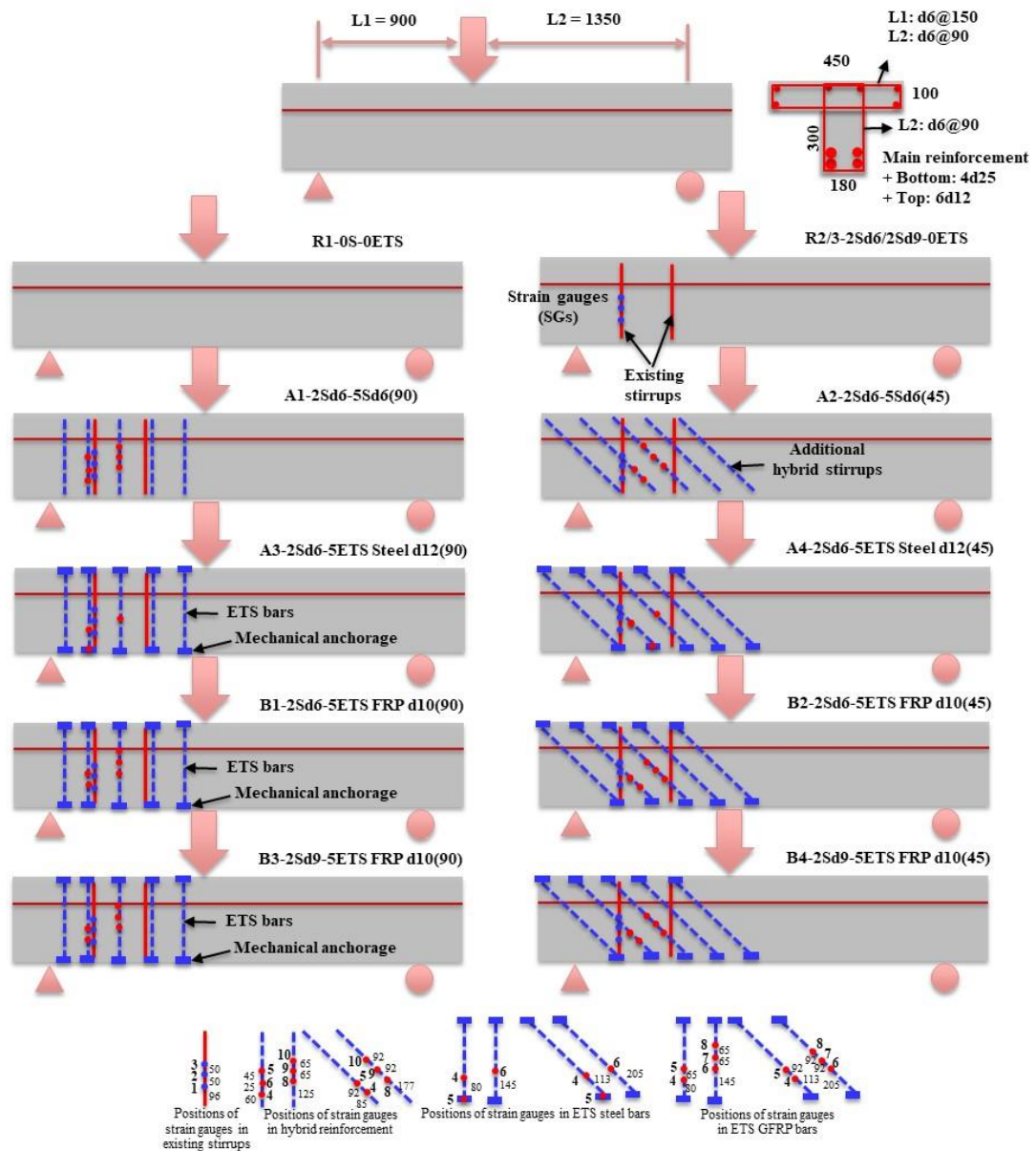


Figure 3.1 Configuration of the tested beams (dimensions in mm)

### 3.2.3 Results and discussion

#### 3.2.3.1 Load-deflection response

Figure 3.4 presents the load-deflection curves at loading points of the tested beams. The typical behavior during shear test was represented for all specimens and a similar performance was also observed before concrete starts to crack due to the same concrete shear strength of the tested members. Then, the crack propagated to

induce the loss of stiffness of beams which re-distributed the internal stresses and triggered the contribution of steel stirrups and ETS steel/GFRP bars to shear resistance.

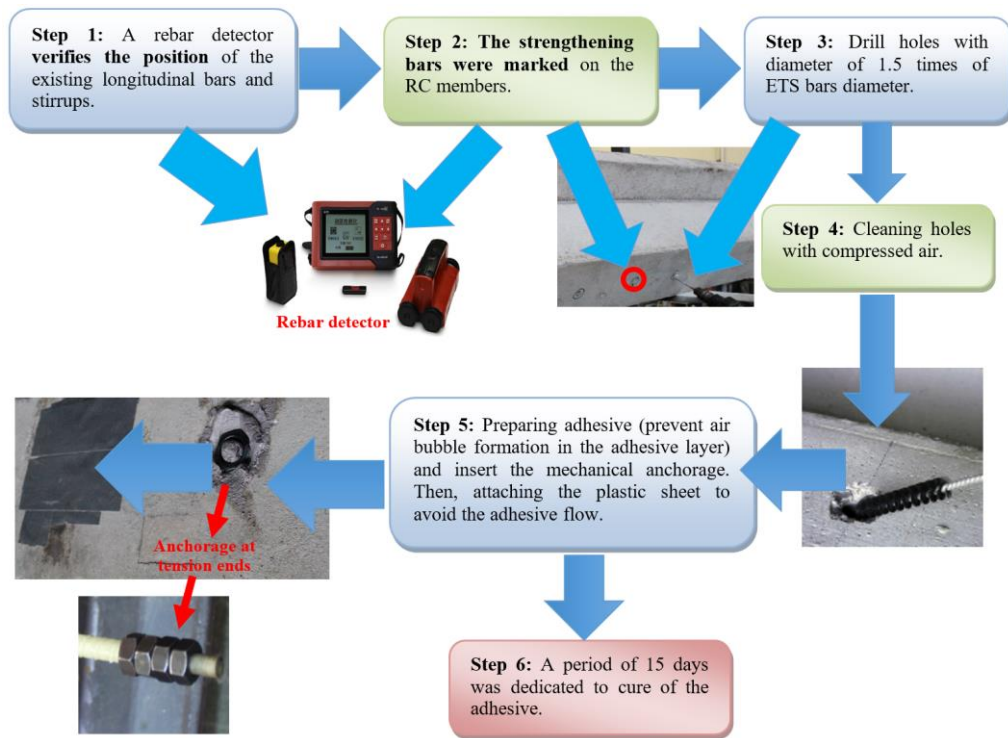


Figure 3.2 Procedure of ETS shear strengthening technique

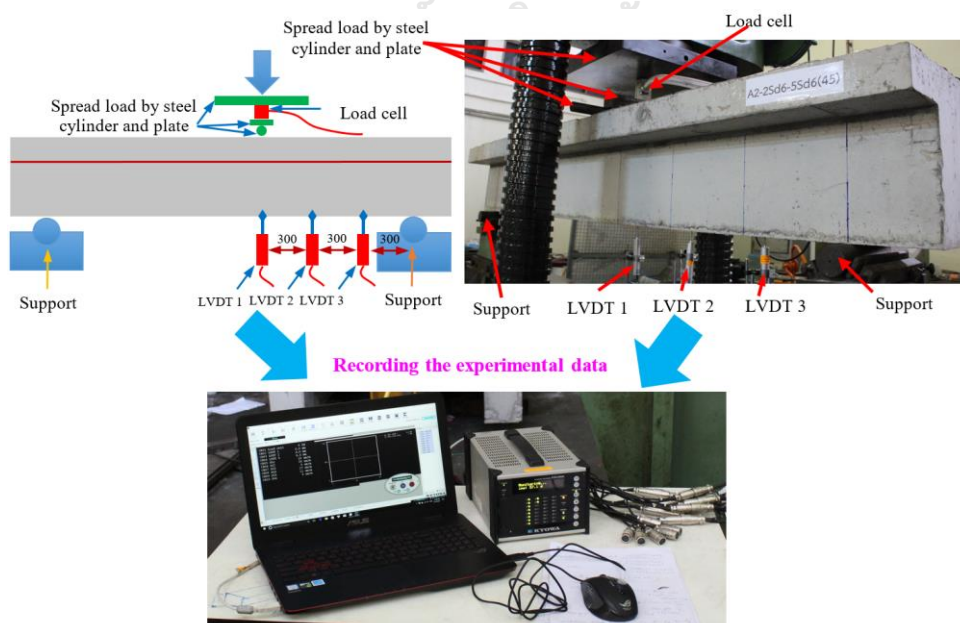


Figure 3.3 Preparation for recording the test data

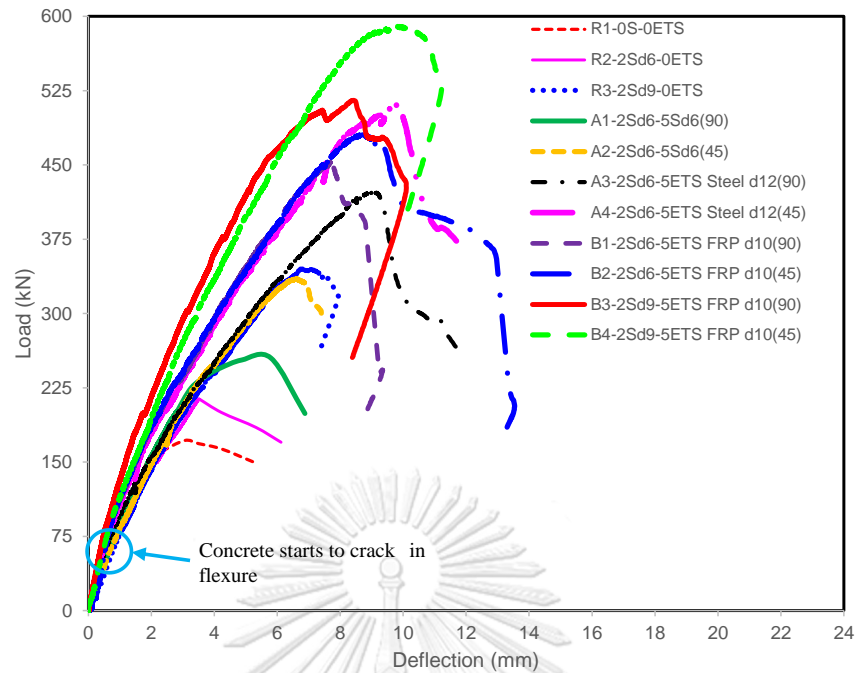


Figure 3.4 Load-deflection response of the tested beams

Table 3.3 Experimental results of ultimate load ( $F_{max}$ ), ultimate displacement ( $u_{Lmax}$ ), and shear resistance ( $V_{max}$  and  $V_f$ )

Beam ID	$F_{max}$ (kN)	$u_{Lmax}$ (mm)	$V_{max}$ (kN)	$V_f$ (kN)
R1	171.8	3.05	103.1	NA
R2	223.4	4.23	134.1	NA
R3	345.4	6.79	207.2	NA
A1	253.0	4.87	151.8	48.7
A2	335.1	6.60	201.0	97.9
A3	422.2	9.01	253.3	119.2
A4	510.5	9.69	306.3	172.3
B1	453.9	7.70	272.3	138.2
B2	481.5	8.67	288.9	154.8
B3	515.2	8.40	309.1	101.9
B4	589.9	9.82	353.9	146.7

It is obviously observed in Table 3.3 that the shear capacity of the members in series A1 and A2 results respectively in an enhancement by 48.7 kN and 97.9 kN compared to that of the reference beam R1. While, the beam series A3, A4, B1 and B2 show an increase in the shear capacity by 119.2 kN, 172.3 kN, 138.2 kN and 154.8 kN in the comparison with the failure shear load of the reference beam R2, respectively. Additionally, the beams B3 and B4 give an improvement in shear resistance of 101.9 kN and 146.7 kN compared to the shear load of the reference beam R3, respectively. These above observations indicate that the shear carrying capacity and rigidity of the beams increased as the shear reinforcement amount increased and as shear reinforcement inclined at  $45^\circ$ . In addition, the deflection at ultimate load of the beams retrofitted by ETS GFRP rods is slightly lower than that of the ETS steel retrofitted beams, and Table 3.3 shows the ETS steel strengthened beams resulted in the displacement at ultimate load with the values of 9.01 mm for the beam A3 and 9.69 mm for the beam A4, while the ultimate deflections of B1 and B2 were respectively 7.70 mm and 8.67 mm. It means that the ETS GFRP retrofitted members provide a feasible displacement ductility compared to the ETS steel strengthened beams.

### 3.2.3.2 Cracking and failure mechanisms

The failure cracking of the tested beams is shown in Fig. 3.5, therein the diagonal shear crack (as expressed in Fig. 3.5) is the critical failure crack in the beams at the ultimate load. All beams were failed in shear due to the significant and wider shear cracks in shear cracking zone of the members. Moreover, Fig. 3.5 indicates that the parallel diagonal cracks started to open up with a relative equal spacing from each other at an angle with respect to the beam axis varying between  $37^\circ$  and  $47^\circ$  that is displayed in Table 3.4. Since the concrete compressive strength adopted in the test specimens is similar, it is obvious from the experiment that the first diagonal crack in the shear cracking region occurred at a similar magnitude of the applied load for the all tested specimens, ranging in 130-170 kN approximately. By increasing the presence of shear reinforcement, more cracks were appeared in the ETS strengthened beams during the shear test since the shear transfer mechanism was



significantly triggered in the beams with the large amount of shear reinforcement. The beams retrofitted with ETS steel/GFRP bars (A3, A4, B1-B4) exhibit the more failure at flange of beams in the comparison with the ordinary RC beams (R1-R3, A1, A2) due to the ETS strengthening system was embedded thoroughly the section, making the shear transfer mechanism at the flange zone drastically activated. To find out the crack propagation in the tested specimens, Fig. 3.6(a) reveals that the major shear cracks initiated on the beam's web, midway between support and load point, then propagated towards both flange and support. After that, the crack reached the flange and triggered an immediate failure with a quasi-horizontal crack angle as shown in Fig. 3.5 and Fig. 3.6(a).

Table 3.4 Main average diagonal shear crack angles of the tested beams

Beam ID	Diagonal crack angle (degree)
R1	40.0
R2	39.0
R3	39.0
A1	37.0
A2	45.0
A3	44.0
A4	45.0
B1	41.0
B2	45.0
B3	43.0
B4	47.0

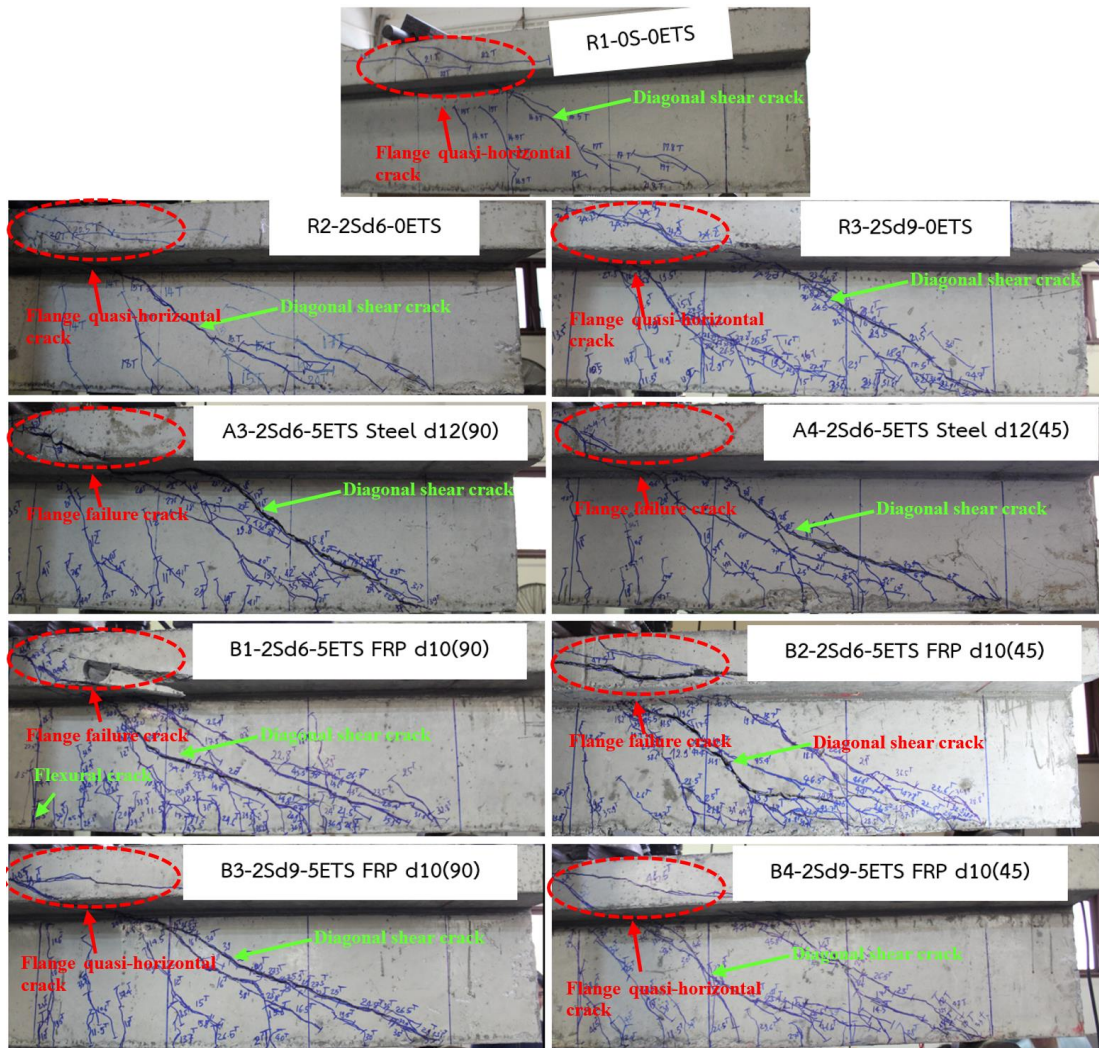


Figure 3.5 Crack failure of the tested reference and ETS strengthened beams

Figure 3.6(b) demonstrates the general behavior of a representative beam A3 during shear test. Initially, the flexural crack occurred in the flexural region under the applied load point of the tested beam at the force of 55 kN. The first shear crack on the member occurred at 130 kN approximately. Afterwards, the yielding of steel stirrup initially started at around 244 kN and this finding is also reported in the strain of shear reinforcement as Fig. 3.7. The main diagonal crack which intended to reach the loading and support points was extended at approximately 337 kN of applied load, and the ETS bars have activated in this stage. At the 400 kN of loading, the main diagonal crack was opening and propagated to the flange of the beam together with the yielding of existing stirrups, and the ETS reinforcement, moreover, have

significantly triggered. Continuously, the crack at flange was opened at around 414 kN, and the beam failed in shear at peak load of 422.2 kN. In addition, the rupture of the ETS bars, the debonding of the ETS bars to concrete and the leaving of the ETS bars to the mechanical anchorage were not observed in the tested specimens. By avoiding the failure mode of the debonding of strengthening system to concrete, the mentioned finding is a prominent point, bringing the improvement in the structural performance of concrete beams strengthened by ETS anchored bars. Indeed, the shear strengthening performance of the ETS retrofitted beams is closely discussed in Section 3.3.

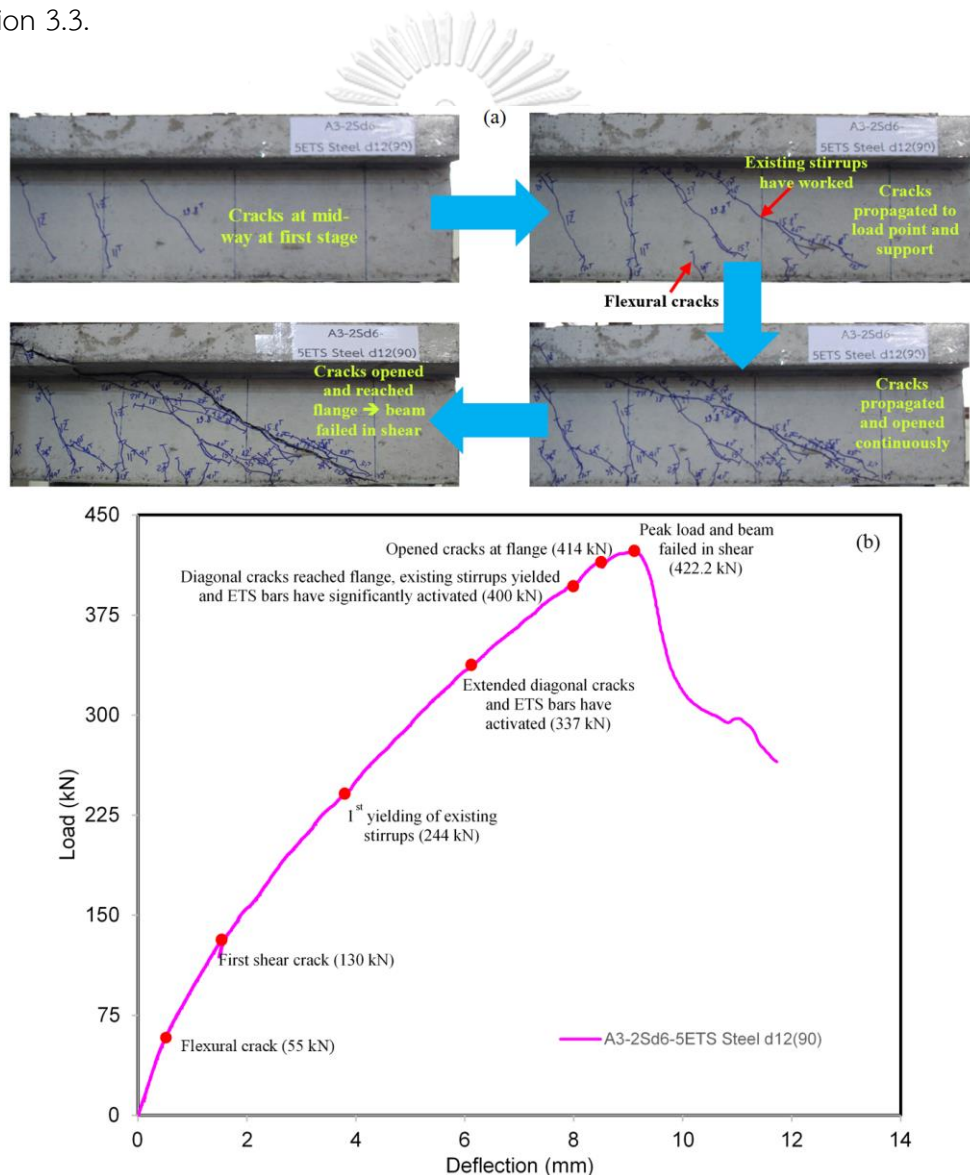


Figure 3.6 (a) Crack patterns of a representative beam A3 and (b) general behavior of an ETS representative beam A3

### 3.2.3.3 Strain in shear reinforcement

From Fig. 3.7, the recorded strain values depended on the distance between the strain gauges and shear failure cracks, and on available bond length of shear reinforcement, therefore, high strain values were obtained at the diagonal cracking zones. It is also indicated from Fig. 3.7 that the transverse reinforcement did not contribute drastically to shear capacity during the initial stage of loading, but it was started to contribute after formation of diagonal cracks. Generally, as shown in Fig. 3.7, the strain in diagonal shear reinforcement is lower than that in vertical shear reinforcement due to the inclined reinforcement arrangement provided the bigger percentage of reinforcement, which made the strain small. Since the amount of ETS cases (A3, A4) is higher than that of internal reinforcement (A1, A2), the strain in the ordinary embedded steel is greater than that in the ETS bars.

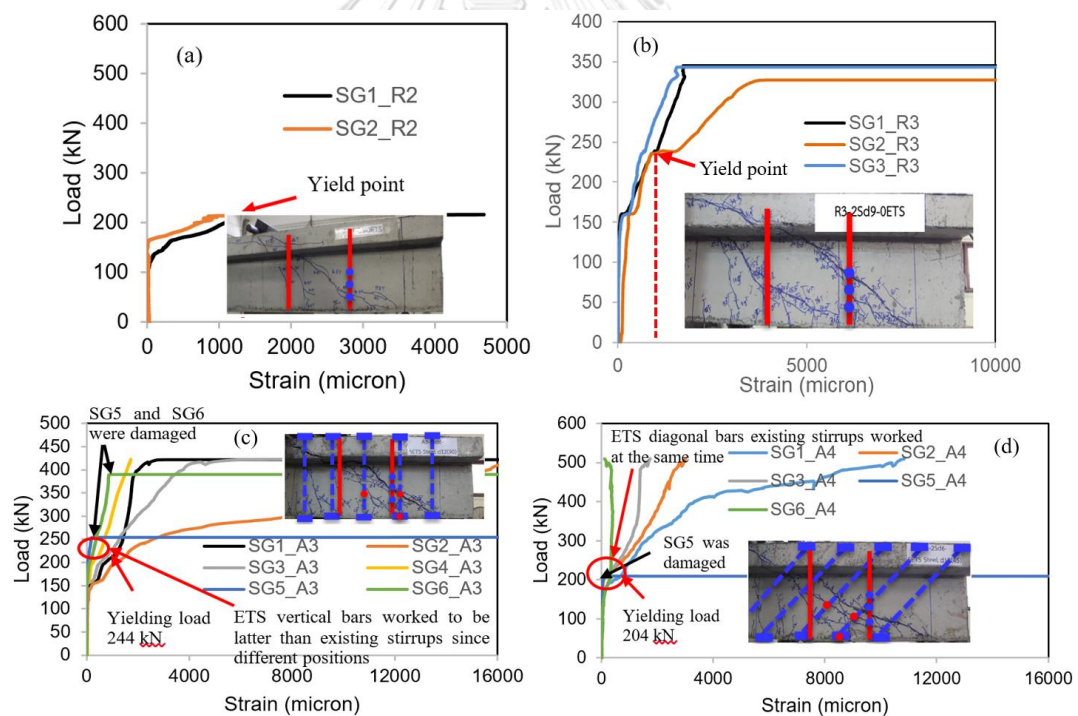


Figure 3.7 Strain in shear reinforcement

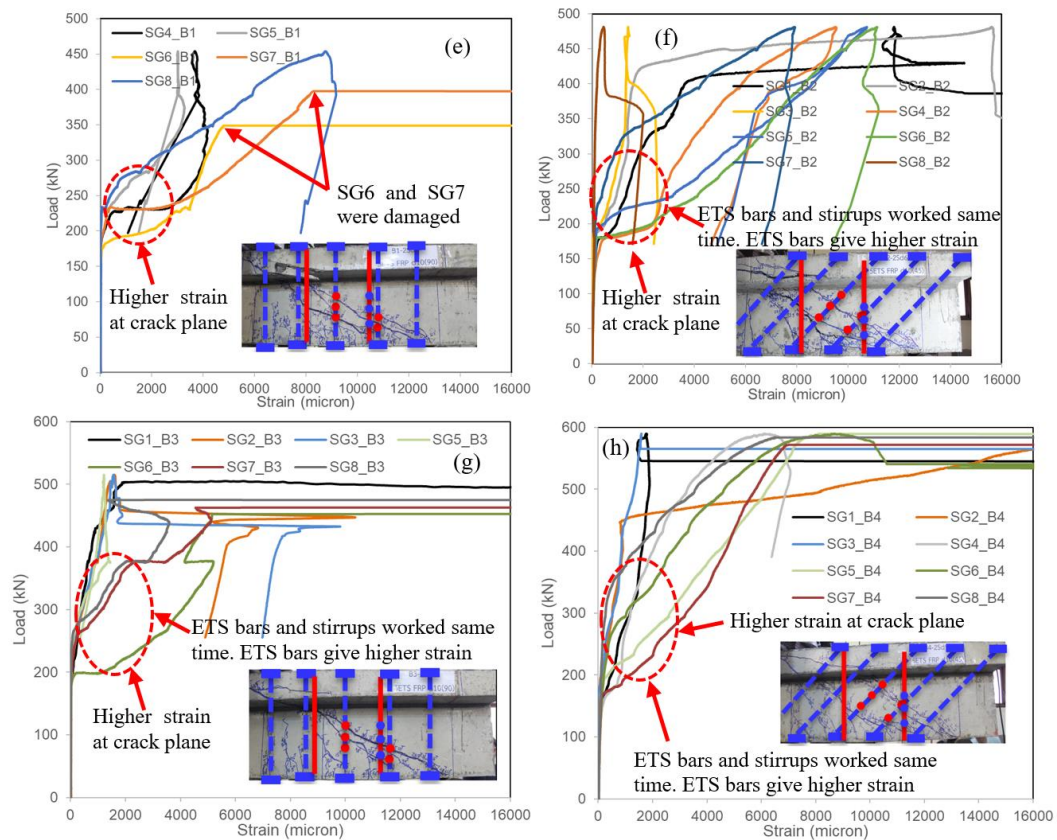


Figure 3.7 (continued)

Moreover, the strain in ETS GFRP rods is higher than that of the ETS steel reinforcement due to the low Young's modulus of GFRP material. In addition, for beam A3, Fig. 3.7(c) shows that the load level which triggered the shear contribution of vertical ETS reinforcement is higher than the load level that activated the existing transverse steel due to the big distance between the glued strain gauges in the ETS reinforcement and the failure crack, and due to the bonding performance that might exhibit an ineffective shear transfer mechanism of concrete-adhesive-ETS bars.

In the other words, the vertical ETS steel rods contributed to shear resistance later than the existing stirrups, and this statement was also reported in the previous studies by Mofidi et al. (2012) and Breveglieri et al. (2015). Whereas, the diagonal ETS steel reinforcement and ETS GFRP rods and existing steel stirrups in the beams A4 and B1-B4, respectively, were simultaneously triggered in shear resistance at the same load level since the bonding performance and the effective anchorage (using mechanical anchorage at the tension ends), which enhanced the shear transfer

mechanism of concrete-adhesive-ETS bars, were provided. This finding is different to the observation in the previous works by Mofidi et al. (2012) and Breveglieri et al. (2015), which activated the ETS strengthening system by the shear transfer bonding mechanism only. Besides, it is apparent from Figs. 3.7(e)-(h) that the strain of ETS GFRP bars increased with the constant slope and reached a maximum value at which the beam ultimately failed after the concrete struts were formed. Moreover, the strain in ETS GFRP rods is higher than that of the ETS steel reinforcement due to the low Young's modulus of GFRP material.

### 3.3 Analysis of shear contribution carried by ETS strengthened bars

To obtain the deep understanding on the mechanical performances of concrete beams strengthened in shear by ETS bars, the experimental results of the previous studies are adopted to make the comparison with the results of the current study. Indeed, Table 3.5 shows the detail of configuration of the tested beams in a previous study, Breveglieri et al. (2015), and Table 3.6 describes the properties of the materials employed in the experimental conduction by Breveglieri et al. (2015). The concrete dimension of the specimens tested in the past work is the same as the concrete dimension of the beams experimented in this study. In addition, the test results in terms of shear contribution of the strengthening system obtained by the present study and the previous work are compared with those computed by the truss analogy theory.

#### 3.3.1 Introduction to existing shear resisting models

In the previous studies, the authors indicated that the truss analogy theory, which is adopted in the ACI and JSCE codes, could predict well the contribution in shear of the ETS steel strengthening system in the RC beams. This Section presents the formulations to derive the shear contribution of the FRP strengthening system using in the ACI and JSCE standards as performed by Eqs. (3.1) and (3.2), respectively. Currently, as reported in the past works, the equation to predict the average stress in

FRP shear bars in the standards of ACI and JSCE is underestimated the actual values. Therefore, the purpose of this study is to improve the effective strength equation of FRP shear reinforcement in the current codes reaching the good estimation compared to the experimental data.

$$V_f = A_v f_f \frac{d(\cot \theta + \cot \alpha)}{s} \sin \alpha \quad (3.1)$$

$$V_s = A_v f_f \frac{7d(\cot \theta + \cot \alpha)}{8s} \sin \alpha \quad (3.2)$$

where,

$A_v$  (mm<sup>2</sup>) is the cross sectional area of the FRP shear reinforcement,

$f_f$  (MPa) is the effective strength of the FRP shear reinforcement, however in the case of ETS steel bars  $f_f$  (MPa) is yielding strength of steel reinforcement,

For ACI code:  $f_f = \min \left( 0.004E_f, f_{f,u}, f_{f,bend} = \left( \frac{0.05r_b}{d_b} + 0.30 \right) f_{f,u} \right)$

For JSCE code:  $f_f = E_{fw} \sqrt{\left( \frac{h}{0.3} \right)^{-0.1} f_c \frac{\rho_s E_s}{\rho_{fw} E_{fw}} \times 10^{-4}}$

$E_{fw}$  (GPa) and  $\rho_{fw}$  (%) are the Young's modulus and the ratio of the FRP shear reinforcement, respectively,

$f_{f,u}$  (MPa) is the ultimate strength of the FRP bar,

$f_{f,bend}$  (MPa) is the tensile strength of FRP bent bar,

$r_b$  (mm) is the bending radius of the FRP bar,

$d_b$  (mm) is the diameter of the FRP bar in the bent portion,

$f'_c$  (MPa) is the concrete compressive strength,

$E_s$  (GPa) and  $\rho_s$  (%) are the Young's modulus and the ratio of the tension reinforcement, respectively,

$d$  (mm) is the effective depth of the beam section, however,  $d$  is the height ( $h$ ) of the beam section for the case of ETS reinforcement,

$s$  (mm) is reinforcement spacing,

$\theta$  (°) and  $\alpha$  (°) are the crack angle and the inclination of shear reinforcement, respectively.

Table 3.5 Reinforcement configuration and ETS shear contribution ( $V_f$ ) of the tested beams in previous study

Study	Beam ID	Number of ETS bars	Inclination of ETS bars ( $^\circ$ )	ETS bars spacing (mm)	Existing steel stirrups ratio (%)	ETS reinforcement ratio (%)	$V_f$ (kN)
Breve- glieri	2S-C180-90 (C1)	5	90	180	0.11	0.16	77.1
	2S-C180-45 (C2)	5	45	180	0.11	0.22	175.6
et al. (2015)	0S-S300-90 (S1)	3	90	300	0.00	0.15	37.0
	0S-S300-45 (S2)	3	45	300	0.00	0.21	115.5

Table 3.6 Properties of materials of the beams in the previous study

Study	Beam ID	Concrete compressive strength at tested day (MPa)	Young modulus of ETS reinforcement (GPa)	Yielding/Rupture strength of ETS steel/FRP reinforcement (MPa)	Young modulus of adhesive (GPa)	Tensile strength of adhesive (MPa)
Breve- glieri et al. (2015)	2S-C180- 90 (C1)	29.7	160	1333	3.1	20.1
	2S-C180- 45 (C2)	29.7	160	1333	3.1	20.1
	0S-S300- 90 (S1)	29.7	200	549	3.1	20.1
	0S-S300- 45 (S2)	29.7	200	549	3.1	20.1

### 3.3.2 Comparison between internal reinforced beams and ETS beams

To evaluate the effectiveness of ETS shear strengthening method, Fig. 3.8 shows the comparison between the results attained from the current study and the data reported by Breveglieri et al. (2015) on the shear contribution of the hybrid internal reinforcement and the ETS bars. The selected beams which are A1 in this study compared to S1 in Breveglieri et al.'s study and A2 in this study compared to S2 in Breveglieri et al.'s were with the same shear strength and the same inclination of



transverse reinforcement through the initial design using truss analogy theory. It is indicated from Fig. 3.8 that the shear resistance of diagonal shear reinforcement is drastically higher than that of vertical shear reinforcement. This finding also agrees with the results computed by the truss analogy theory. Besides, it is also obvious from Fig. 3.8 that the shear resistance of ETS vertical bars is less than that of initially embedded shear reinforcement, 37 kN of shear resistance of ETS vertical system compared to 48.7 kN of shear contribution of vertical reinforcement. However, this fact is opposite to the results determined by using the truss analogy theory in Fig. 3.8, the ETS vertical bars exhibit the higher shear contribution compared to that of the vertical shear reinforcement.

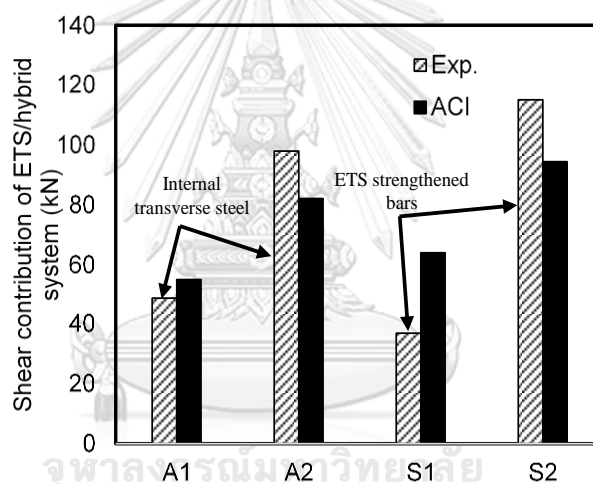


Figure 3.8 Comparison in shear contribution of internal stirrups and ETS reinforcement

To explain for the above observations, the close shape of hybrid vertical shear reinforcement provided an encouraging anchorage that significantly improved the contribution in shear of the transverse steel (this is suitable with the assumption in the truss analogy method) rather than the ETS system which the shear resistance was decided by bonding performance between ETS bars and concrete. However, the contribution of ETS diagonal reinforcement in shear (115.5 kN) is slightly greater than the contribution of hybrid diagonal reinforcement in shear (98.0 kN) due to the longer bond length of the ETS bars compared with the non-close shape of hybrid

shear diagonal reinforcement that offered a short bond length and a poor anchorage. The above fact triggers significantly the activation of the ETS bars reaching the yielding strength, therefore the mentioned finding agrees completely with the results computed by the ACI code. From the aforementioned discussions, it can be pointed out that the shear capacity of the beams reinforced in shear with hybrid diagonal-vertical reinforcement or strengthened in shear with the ETS bars is improved if the shear reinforcement is ultimately triggered by providing the long bond length or the encouraging anchorage. Furthermore, comparing to the members with hybrid shear reinforcement, the beam with the ETS diagonal strengthened system demonstrated the highest shear strengthening efficacy rather than the beam with the vertical ETS retrofitted bars.

On the other hand, the equation of ACI code is also employed to analyze the suitability of the truss analogy model for the shear resistance of hybrid system and ETS strengthening system. Fact, Fig. 3.8 indicates that truss analogy theory could predict well for the beams with hybrid usage of transverse reinforcement with the ratios of the experimental shear contribution ( $V_{f,Exp.}$ ) to the analytical shear contribution ( $V_{f,ACI}$ ) are 0.89 and 1.19 for the vertical (beam A1) and diagonal (beam A2) cases, respectively. Since the hybrid beams with internal shear reinforcement offered a good anchorage and bonding of the reinforcement to concrete, the hybrid transverse steel was triggered to reach the yielding strength, which is suitable to the assumption of the truss analogy theory. However, with the ratios of  $V_{f,Exp.}/V_{f,ACI}$  for the vertical (beam 0S-S300-90 (also called S1)) and diagonal (0S-S300-45 (also re-named S2)) strengthened ETS beams are 0.58 and 1.22, respectively, the truss analogy model was not good to predict the shear contribution of the ETS strengthening system. Especially, the beams with vertical ETS shear strengthening system, the shear resistance of the ETS bars in the tested data is significantly lower than that of the truss analogy computation. This is caused by the bonding performance between ETS bars-adhesive-concrete that made the stress in ETS steel bars could not reach the yielding strength before the member failed by debonding. In the contrast to the vertical ETS shear strengthening system, the beams strengthened by inclined ETS bars offered a conservative comparison between the tested data and analytical

results due to the bonding performance of ETS bars to concrete, which is decided by the longer bond length, was improved to increase the stress in ETS bars. In conclusion, the bonding characteristic of the ETS bars to concrete plays an important role not only in the experimental shear contribution of the ETS bars but also in the shear resistance prediction of the ETS strengthening system using the truss analogy method.

### 3.3.3 Effect of types of ETS strengthening system

To evaluate the effect of types of ETS bars on the shear contribution of strengthening system, Fig. 3.9 shows the comparison between the results attained from the current study and the data reported by Breveglieri et al. (2015) on the shear contribution of the ETS bars. The selected beams were initially designed with the same shear strength as the same inclination of transverse reinforcement. It is indicated from Fig. 3.9 that the shear resistance of diagonal ETS shear reinforcement was drastically higher than that of vertical ETS shear reinforcement. This finding completely agrees with the results computed using the ACI code. Also displayed in Fig. 3.9, the experimental shear resistance of the ETS CFRP vertical bars is less than that of the ETS GFRP vertical one, 77.1 kN of shear resistance of ETS CFRP system compared to 138.2 kN of shear contribution of ETS GFRP vertical reinforcement even though the rigidity ratio ( $E_{fw}\rho_{fw} + E_{sw}\rho_{sw}$ , GPa) of ETS CFRP is higher than that of ETS GFRP around 1.4 times. While, the values derived by the ACI result in the opposite way, the shear contribution of the vertical ETS CFRP is slightly higher than that of the vertical ETS GFRP since the effective strength of ETS CFRP bars computed by the truss analogy theory was higher than that of ETS GFRP calculated by the truss analogy method. To explain for the above-mentioned observations, the beam with ETS GFRP vertical system (with anchorage) provides an encouraging anchorage and a good confinement action to the ETS anchorage tension ends of concrete cover that significantly improved the contribution in shear of the strengthened bars rather than the ETS CFRP vertical system (without anchorage) in which the shear resistance was decided by bonding performance between ETS bars and concrete.

On the other hand, since the shear contribution of ETS strengthened rods is initially decided by the bonding resistance of ETS bars to concrete before the anchorage attended; therefore, when the bonding performance is improved through providing the longer bond length by the diagonal arrangement of ETS bars, the contribution of ETS CFRP diagonal reinforcement in shear (175.6 kN) is increased as the rigidity ratio increases, and it is greater than the shear resistance of ETS GFRP bars inclined at  $45^{\circ}$  (154.8 kN). This fact agrees well with the results observed by the truss analogy theory since the actual behavior is suitable for the assumption of the theoretical approach.

Moreover, to assess the effectiveness of the ETS steel and GFRP bars, although having the low stiffness and small amounts, the contributions in shear of the ETS GFRP strengthening systems is similar-levelly obtained to those of the ETS steel system (as presented in Fig. 3.9) even the ETS GFRP vertical system's shear contribution is higher compared to that of the ETS steel vertical bars due to the greater strength carried by GFRP bars. However, this finding is slightly different from the results exhibited by the ACI calculation, the computed shear contribution of the ETS steel cases is much higher than that of the ETS GFRP cases. These observations illustrate the efficacy of the anchorage, which helped to limit the detrimental influence after the bonding was activated, and imply that the truss analogy theory might be not good to predict the shear resistance of the ETS strengthening tool attached the mechanical anchorage. Indeed, generally, the ETS shear contribution values determined by the ACI are significantly underestimated in the comparison with those resulted through the test except the beams retrofitted by the ETS steel bars (A3, A4). The reason of the underestimation is mainly due to the equations of effective strain in the shear resisting models applying the truss analogy model underestimated the actual values (as shown in Table 3.8).

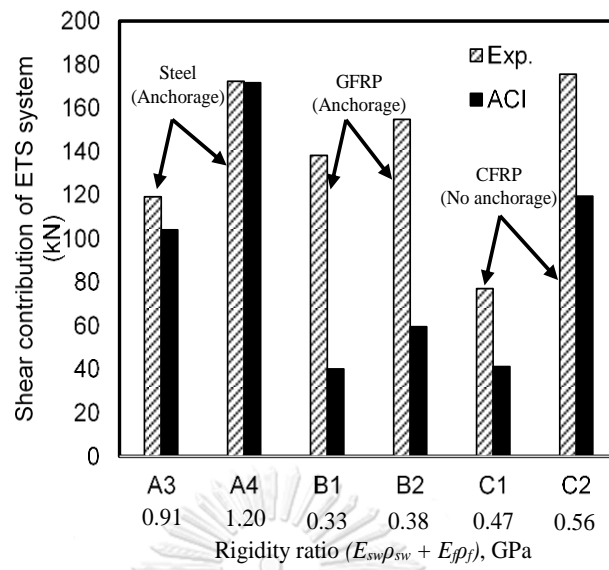


Figure 3.9 Comparison in shear performance of the strengthened beams with different types of ETS bars

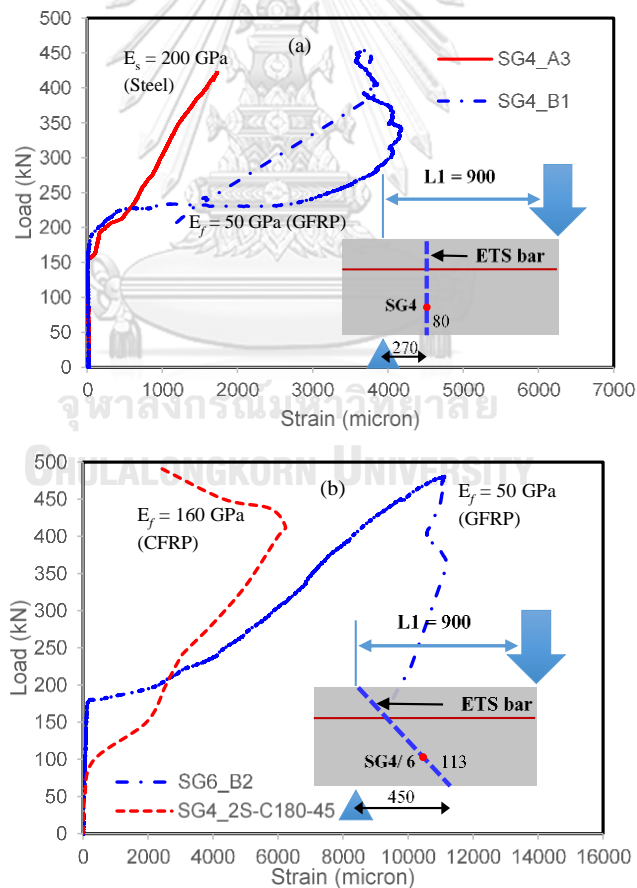


Figure 3.10 Effect of ETS Young's modulus on reinforcement strain with (a) vertical arrangement, (b) diagonal arrangement (no data for steel case) and (c) transverse steel

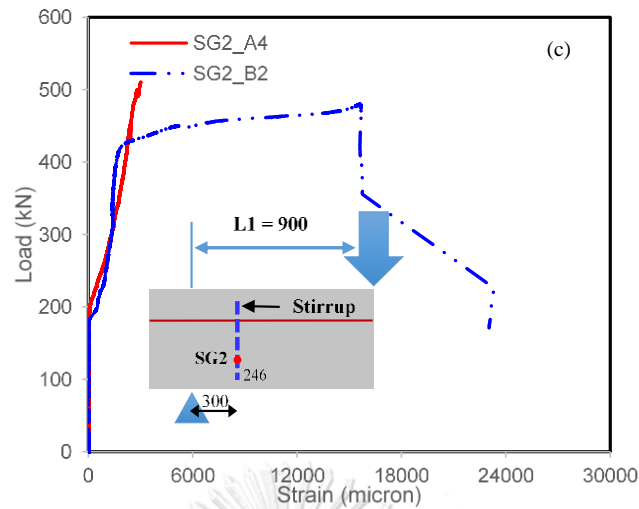


Figure 3.10 (continued)

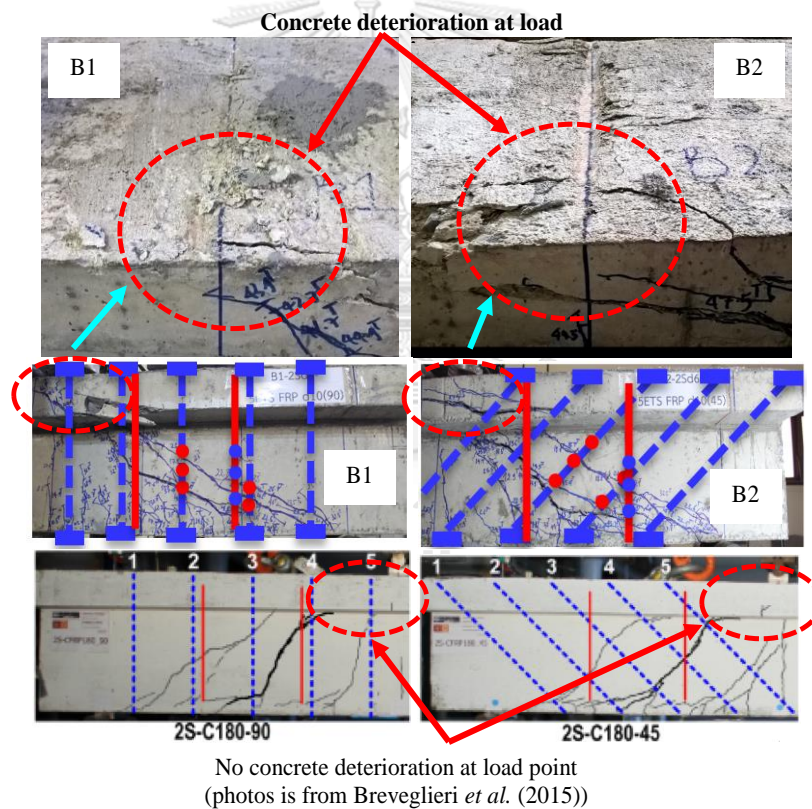


Figure 3.11 Shear failure tends to convert into flexural failure of ETS strengthened beams (B1 and B2) with mechanical anchorage attachment

Considering the crack failures in Fig. 3.11, the beams with the ETS GFRP system attached mechanical anchorage displayed more cracks in the comparison with the members strengthened with the ETS CFRP bars due to the anchorage triggered

significantly the shear transfer mechanism of ETS bars-adhesive-concrete. Also in Fig. 3.11, the shear failure modes of the beams B1 and B2, which is retrofitted with ETS GFRP bars installed mechanical anchorage, intended to convert into the flexural failures by crushing concrete at the load points. Therefore, the specimens B1 and B2 perform an improvement in the ductility aspect. In the contrast, the members strengthened by ETS CFRP bars failed in shear with the almost failure cracks at the web region of the beams (as shown in Fig. 3.11). In addition, Figs. 3.10(a), and (b) show the strains in ETS reinforcement, which are compared at the same positions of the recorded strain gauges, of the tested beams. Since the different concrete compressive strength of the investigated beams, the load triggered the activation of the ETS GFRP and steel bars is higher than the load triggered the resistance of the ETS CFRP rods. It is obvious from Figs. 3.10(a) and (b) that the strains in ETS GFRP strengthened bars are greater than those of the ETS CFRP and steel strengthened bars due to the low stiffness of GFRP reinforcement ( $E_{fw}\rho_{fw}$ ) and the use of mechanical anchorage, resulting in the significant strain development. This finding is also suitable for the truss analogy prediction computed by Eq. (3.4) as shown in Table 3.8 and Fig. 3.17, the strain in shear reinforcement was high as the stiffness of ETS bars was small. On the other hand, the strains in steel stirrups of the two beams A4 and B2 with different cases (steel and GFRP) of ETS reinforcement are shown in Fig. 3.10(c). Clearly, the strains in the same position of the stirrups of the specimens A4 and B2 are similar at all points before yielding, therefore the different ETS strengthening system types do not affect the strain response of the existing transverse steel.

#### 3.3.4 Effect of existing steel stirrups on ETS FRP efficiency

To assess the efficiency of shear ETS FRP strengthening system in the members with combined usage of shear reinforcement, two groups of beams with different existing steel stirrup amounts, B1-B2 (stirrups of 2Sd6) and B3-B4 (stirrups of 2Sd9), are considered. Figure 3.12(a) reveals that the presence of stirrups reduced the resistance of ETS strengthened bars in shear, indeed the shear contributions of the ETS retrofitting

systems decrease 36.3 kN (from 138.2 kN down to 101.9 kN for vertical cases) and 8.1 kN (from 154.8 kN down to 146.7 kN for diagonal cases) as increase the amount of existing transverse steel from 2Sd6 ( $\rho_{sw} = 0.10\%$ ) up to 2Sd9 ( $\rho_{sw} = 0.24\%$ ). Together with the mentioned findings, the results computed by the ACI also indicate that the shear resistance of ETS retrofitting system decreased as the content of existing transverse steel increased. The fact above can be caused by increasing steel stirrups amount, the shear resisting carried by the transverse steel high; therefore, under the same failure mode of concrete fracture in shear zone, the shear resistance of the strengthened bars in the beams reinforced by higher stirrups percentage is less than that of the retrofitted rods in the members reinforced by lower stirrups content. These aforementioned findings in the reduction of the shear resistance of the strengthening rods by increasing the ratio of available steel stirrups have also been shown in the previous studies by Mofidi et al. (2012) and Breveglieri et al. (2015). Apparently, the decrease in the shear contribution of the vertical ETS retrofitted rods is greater than that of the diagonal ETS strengthened bars because in the vertical cases of ETS retrofitted rods, the steel stirrup ratio is similar to the ETS ratio ( $\rho_{sw} = 0.24\%$ ) that makes the activation of the ETS strengthening system is not drastic. Thus, with low percentage transverse steel compared to the percentage of the ETS reinforcement, the detrimental effect induced by presence of existing stirrups does not occur in the specimens strengthened by ETS bars with mechanical anchorage insert.

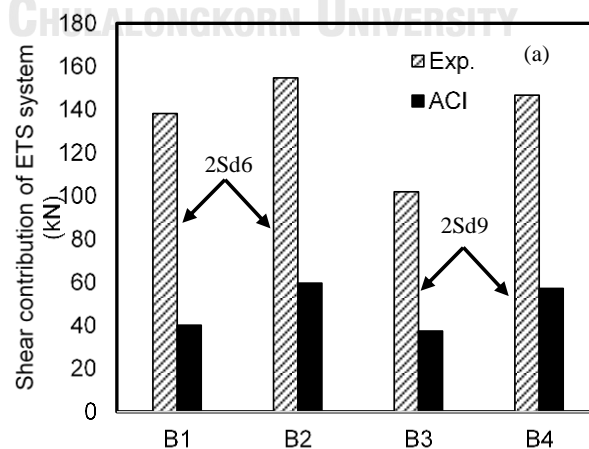


Figure 3.12 Effect of existing steel stirrup ratios on (a) shear contribution of ETS strengthening system, (b) strain in stirrups and (c) strain in ETS reinforcement



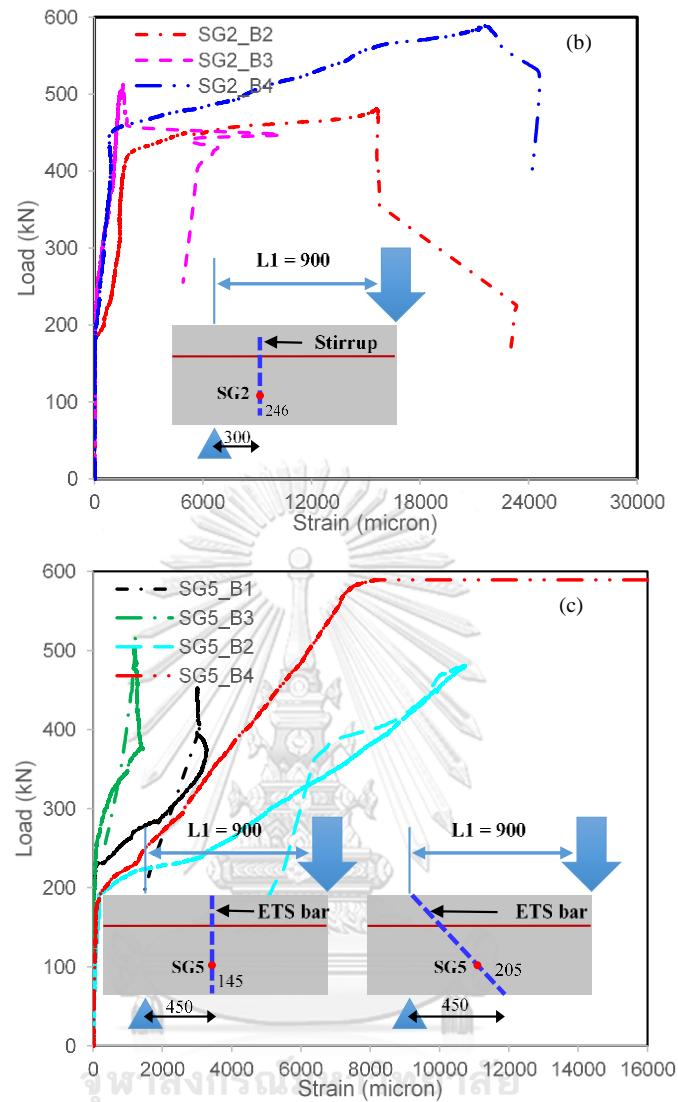


Figure 3.12 (continued)

Figure 3.12(b) shows the strains in the transverse reinforcement at the same location of the two beams B2 and B4. Clearly, the stirrups in the two investigated beams were yielded before the beams failed and the strains in the transverse steel of 9 mm diameter is lower than that in the stirrup of 6 mm diameter at all points. Thus, the shear resistance of the ETS bars is reasonably distributed with the steel stirrups of bigger bar size and this makes obviously the contribution of the ETS reinforcement in shear small. Furthermore, Fig. 3.12(c) demonstrates the strain response in the ETS retrofitted bars of the four beams B1, B2, B3 and B4 at the same location of the attached strain gauges. The beams with lower percentage of steel stirrups (B1 and B2) give higher strains of the

ETS reinforcement in the comparison with the specimens with higher transverse steel ratio (B3 and B4) at whole curves. This finding is completely confirmed with the prediction by the truss analogy theory (as shown in Table 3.8), the increase of the existing transverse steel (from 2Sd6 to 2Sd9) reduced the strain in ETS retrofitting system, leading the reduction of the shear contribution of ETS bars.

### 3.3.5 Comparison to near surface mounted (NSM) shear strengthening method

As clearly indicated in the previous literature, the cracking behavior of the strengthened beams and the bond performance of the strengthening system to concrete are most important factors in the shear strengthening effectiveness employing the retrofitting techniques. Therefore, this Section focuses on the comparison of cracking behavior of the strengthened specimens using two methods ETS and NSM, and also concentrates on the comparison in shear contribution of the ETS strengthening system to that of the NSM retrofitted bars.

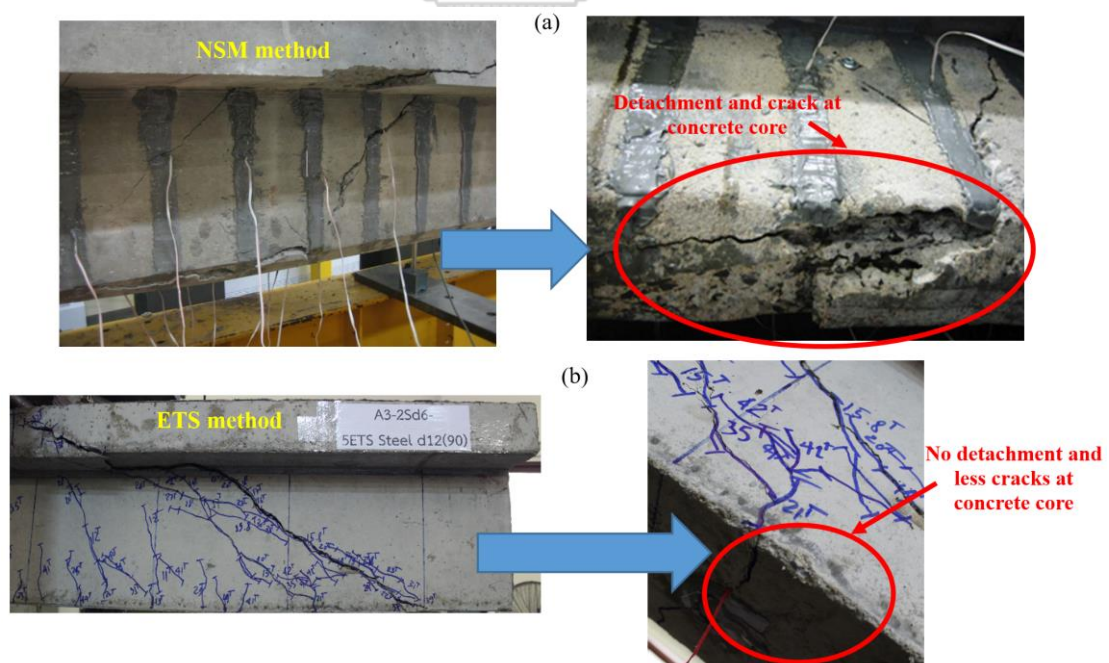


Figure 3.13 Failure cracking pattern at side and at bottom of the beams strengthened using (a) NSM method and (b) ETS method

To compare to the crack pattern of beam A3-2Sd6-5ETS d12(90) at ultimate load, the cracking failure of a beam strengthened by NSM bars in the study of Chaalla et al. (2011) are collected. Together with a statement in the research by Chaalla et al. (2011), the effect of transverse steel in the reduction of strengthening effectiveness is less pronounced in the ETS technique compared with the EB and NSM techniques, Fig. 3.13(b) indicates that by using ETS method for shear strengthening the cracking pattern was more spread on the surface of the beam. Whereas, Fig. 3.13(a) implies the cracking pattern of the beam retrofitted by NSM bars was propagated from the surface of the beam to the beams' confined core and the detachment of concrete cover was also occurred. It is obviously understood that the bond length and hence the bond force reduces when the cracks open and pass the strengthening system, therefore, the debonding in the NSM bars happened, whereas the debonding did not occur in the beams with the ETS technique, leading the less spread cracking pattern. This finding demonstrates that the shear cracking failure of the concrete beams strengthened using ETS method is seemingly safer than that of the specimens retrofitted with the NSM technique.

On the other hand, as shown in Table 3.7, the experimental data of the ETS/NSM shear strengthening method are collected from the studies by Breveglieri et al. (2015), and Dias and Barros (2008). The concrete geometry dimension of the investigated specimens applying the ETS and NSM methods are the same, therefore the shear contribution of the strengthening system could be directly compared. It is clearly described from Fig. 3.14(a) and Table 3.7 that the shear resistance of the diagonal strengthened bars is higher than that of the vertical retrofitted rods since the longer bond length of diagonal cases provided the greater shear resisting transfer. This fact also means that the shear contribution of the strengthening tool increased as the amount of retrofitted rods increased.

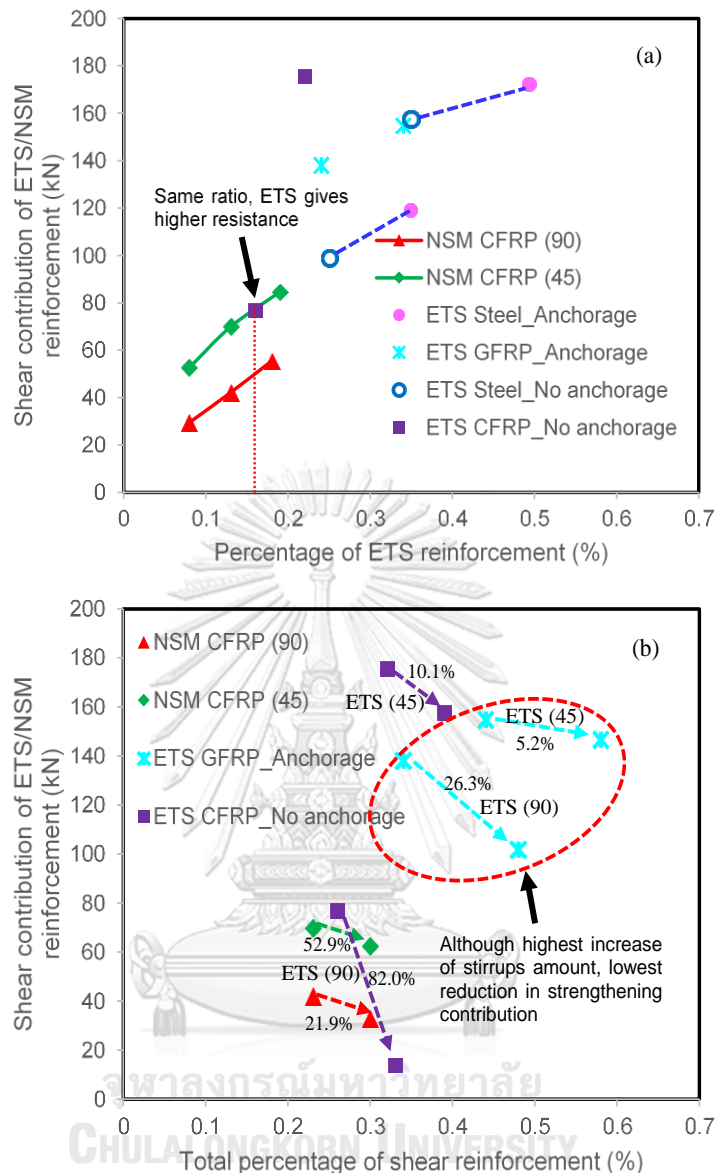


Figure 3.14 Comparison to the NSM shear strengthening method in shear contribution, note: reduction (%) =  $[V_f(\text{low percentage of stirrups}) - V_f(\text{high percentage of stirrups})] \times 100 / V_f(\text{low percentage of stirrups})$

As presented in Fig. 3.14(a) and Table 3.7, at the same CFRP ratio, the concrete beams strengthened using the ETS method provide the higher shear contribution of the retrofitting system compared to the members strengthened in shear by NSM technique. Additionally, consider trend lines of the plots in Fig. 3.14(a), the shear contribution of ETS strengthening tool always offers higher values than that of the retrofitted bars employing

the NSM technique. One of reasons of this is the good anchorage leading the encouraging confinement of the concrete core to ETS bars that make the shear transfer mechanism of concrete-adhesive-ETS bars significantly enhanced, triggering the contribution of ETS bars in shear drastically. Moreover, the short bond length of the NSM rods, which could not pass the beam flange, and the NSM bars placed at the outer concrete core may reduce the shear transfer mechanism of concrete-adhesive-NSM rods and induces the shear resistance of the NSM strengthening system small accordingly.

Table 3.7 Reinforcement configuration and ETS/NSM shear contribution ( $V_f$ ) of the tested beams in previous studies

Study	Beam ID	Inclination of ETS/NSM bars ( $^\circ$ )	Existing steel stirrups ratio (%)	ETS/NSM reinforcement ratio (%)	$V_f$ (kN)
Breveglieri	2S-C180-90 (C1)	90	0.11	0.16	77.1
et al. (2015)	2S-C180-45 (C2)	45	0.11	0.22	175.6
(ETS method)	4S-C180-90 (C3)	90	0.17	0.16	13.9
	4S-C180-45 (C4)	45	0.17	0.22	157.8
	2S-4LV (C5)	90	0.11	0.08	29.5
	2S-7LV (C6)	90	0.11	0.13	42.1
Dias and Barros	2S-10LV (C7)	90	0.11	0.18	55.4
(2008) (NSM method)	2S-4LI45 (C8)	45	0.11	0.08	52.7
	2S-7LI45 (C9)	45	0.11	0.13	69.8
	2S-10LI45 (C10)	45	0.11	0.19	84.6
	4S-7LV (C11)	90	0.17	0.13	32.9
	4S-7LI45 (C12)	45	0.17	0.13	62.5

Figure 3.14(b) and Table 3.7 present the shear contribution of the strengthened bars decreased as the increase of the existing stirrup percentage. In general, since the good confinement into concrete core and the long bond length of the ETS strengthened rods are offered, the reduction in the shear contribution of the ETS retrofitting tool by increasing the transverse steel content is less than that of the NSM strengthening system

by enhancing the steel stirrups amount. Also from Fig. 3.14(b) the members strengthened with the ETS GFRP bars and with the mechanical anchorage attachment offer the lowest reduction (as shown in Fig. 3.14(b), the shear contribution reduction of the ETS diagonal bars is 5.2%) in shear contribution by enhancing the transverse reinforcement amount. Therefore, for the concrete beams retrofitted by ETS bars, the mechanical anchorage is an effective device to reduce the detrimental effect on the shear resistance of the ETS strengthened bars in the retrofitted members with high percentage of internal steel stirrups, causing by the anchorage mechanism provides fully effective strength in ETS bars.

### 3.3.6 Efficiency of ETS strengthening system in case of combined usage through shear capacity analysis

#### 3.3.6.1 Experimental shear resistance compared to current shear resisting methods

Obviously, the previous sections indicated that the original truss analogy models could not be employed to predict the shear resistance of the ETS FRP strengthening system (both cases with and without anchorages) in the RC beams. Therefore, to provide the comprehensive comparison between the existing shear resisting models, Fig. 3.15 demonstrates the shear resisting method proposed by Ueda et al. (1996). The shear contribution of the FRP shear reinforcement is calculated as follows. Notably, the notations are consistent in the whole Chapter. The influence of hybrid ETS FRP and transverse steel on the shear resistance of ETS FRP bars is considered by the total stiffness of shear reinforcement,  $E_{fw}\rho_{fw} + E_{sw}\rho_{sw}$ . For the beams with the combined usage of ETS FRP bars and steel stirrups, the Young's modulus of the ETS FRP bars is not changed through the computation of its shear contribution. While, for the specimens with ETS steel bars and steel stirrups, the elastic modulus of the ETS steel bars is changed in the calculation of the shear contribution of ETS steel strengthened rods.

$$V_f = V_{web} + V_{str} = \rho_{fw} \overline{\sigma}_{web} bL_{web} + \overline{\tau}_{str} bL_{str} \quad (3.3)$$

where,

$$\bar{\tau}_{str} = (f'_c)^{1/3} \frac{1.28}{1 + \sqrt{a/d}}$$

$$\bar{\sigma}_{web} = E_{web} \bar{\varepsilon}_{web} \text{ and } \bar{\varepsilon}_{web} = 0.0053 \frac{\sqrt{f'_c}}{\sqrt{a/d} + 1} e^{\frac{-1000}{\rho_s E_s} - 0.05 \sqrt{\rho_{fv} E_{fv}}}$$

$a/d$  is the shear span ratio of the beam and the detail of the parameters is clearly shown in Fig. 3.15 (a).

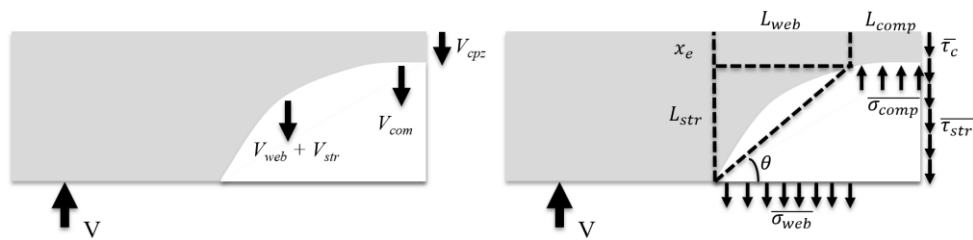


Figure 3.15 Shear model of Ueda et al. (1996)

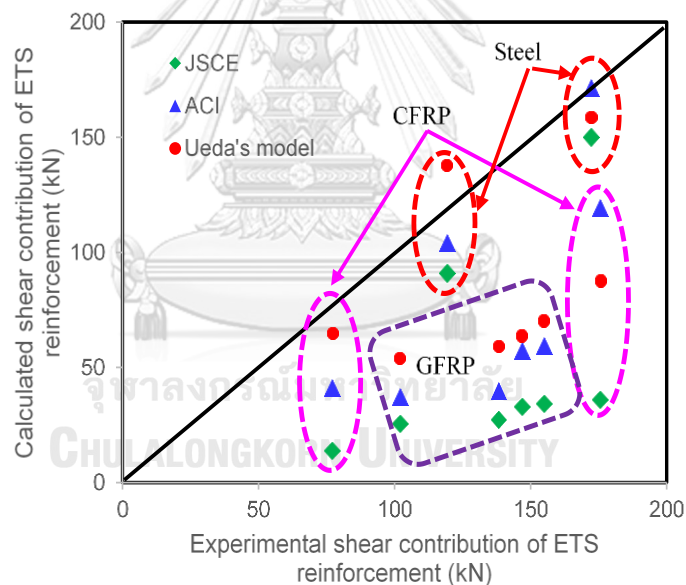


Figure 3.16 Comparison between analytical results using existing shear models and tested data

To verify the existing shear models, the experimental shear contributions of the strengthening systems in the ETS tested beams of this study A3, A4, B1, B2, B3, B4, and the tested specimens in the previous study by Breveglieri et al. (2015) 2S-C180-90, 2S-C180-45 are adopted to compare with the results obtained from the computation by applying the equations (3.1), (3.2) and (3.3). Furthermore, from the experimental data,

these investigated members were failed by either the ETS steel yielding or the shear cracking fracture of concrete at the flange at ultimate load, and no debonding failure was observed in those tested beams. It is obvious from Fig. 3.16 that the shear contribution of the ETS retrofitting system in the strengthened beams computed by the existing shear models underestimates with the shear resistance of the ETS bars in the investigated specimens collected from the experiment, especially the beams with ETS GFRP cases. In addition, the calculated results of the shear contribution of the ETS bars using Ueda et al.'s model offer a better prediction than those employing the equations of ACI and JSCE guidelines. The explanations of the underestimation in the shear resistance prediction employing the available models are as follows. Since the elastic modulus of the CFRP and steel bars are high, 160 GPa for CFRP and 200 GPa for steel, therefore the effective strengths determined by the models of ACI and JSCE provided the greater values than those by using the GFRP bars (low Young's modulus, 50 GPa) for strengthening the RC beams.

Table 3.8 Average strain from experimentation, before modification, computation, and after modification

Beam ID	$\varepsilon_{exp}$ (micron)	$\varepsilon_{beforemodi.}$ (ACI/JSCE/Ueda) (micron)	$\varepsilon_{fe}$ (Eq. (3.4)) (micron)	$\varepsilon_{aftermodi.}$ (Eq. (3.5)) (micron)	Yielding/ultimate strain (micron)
A3	1924	2000/2000/2492	2290	2000	2000
A4	1786	2000/2000/2005	2008	2000	2000
B1	12985	4000/3132/4566	13767	12689	21520
B2	10277	4000/2632/4268	10391	11780	21520
B3	10652	4000/3132/3281	10889	8763	21520
B4	9973	4000/2632/3121	10253	8274	21520
2S-C180-90 (C1)	7124	4000/1536/3423	7472	9195	12000
2S-C180-45 (C2)	5473	4000/1387/3078	5874	8143	12000



On the other hand, the members retrofitted by the ETS GFRP rods, which were inserted the mechanical anchorage at the tension ends, performed an improvement in the confinement action of the concrete cover to the tension ends of ETS with the anchorage attachment. Of course, this makes the activation of the ETS strengthening system was significantly triggered by the encouraging confinements of the concrete core to the ETS bars and the concrete cover to the anchorage ends of the ETS bars. Therefore, the actual effective strains (also called by actual average strains) in the ETS retrofitted bars are significantly higher than the theoretical average strains calculated by the existing shear models (see columns 2 and 3 of Table 3.8), and it is implied that the predicted values were drastically underestimated the tested results. Generally, for the shear resistance prediction of the ETS reinforcement in the RC strengthened beams, all models give the good estimations with the experimental data in the cases retrofitted by the ETS steel bars, especially Ueda et al.'s method. However, these models could not predict well for the shear contribution of the ETS FRP strengthened rods, especially the members retrofitted by the ETS GFRP bars with the anchorage insert. In conclusion, the Ueda's model could be employed to predict the shear resistance of the strengthening system in a concrete beam retrofitted with the ETS steel bars and failed with no debonding.

#### ***3.3.6.2 Modified average strain for shear resistance model***

As indicated in Section 3.3.6.1, the existing shear models displayed a disadvantage in the shear contribution prediction of the strengthening system in the concrete beams retrofitted by the ETS FRP bars, especially the low elastic moduli of FRP and the mechanical anchorage installation, due to the analytical average strains were not predicted well the real values. This Section makes effort to modify the predicted average strains in the ETS FRP strengthened bars reaching the actual effective strains from the tested results. Indeed, the effective strains in the ETS FRP retrofitting system are experimentally calculated by Eq. (3.4) and are shown in Table 3.8. It should be noted that the notations are consistent in the entire Chapter.

$$\varepsilon_{fe} = V_{f\_Exp.} / \left[ A_v E_{fw} \frac{z(\cot \theta + \cot \alpha)}{s} \sin \alpha \right] \quad (3.4)$$

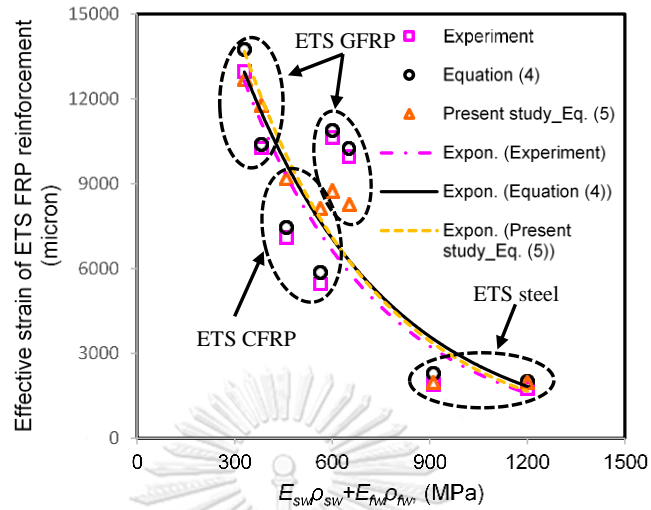


Figure 3.17 Modification of average strains in ETS strengthening system

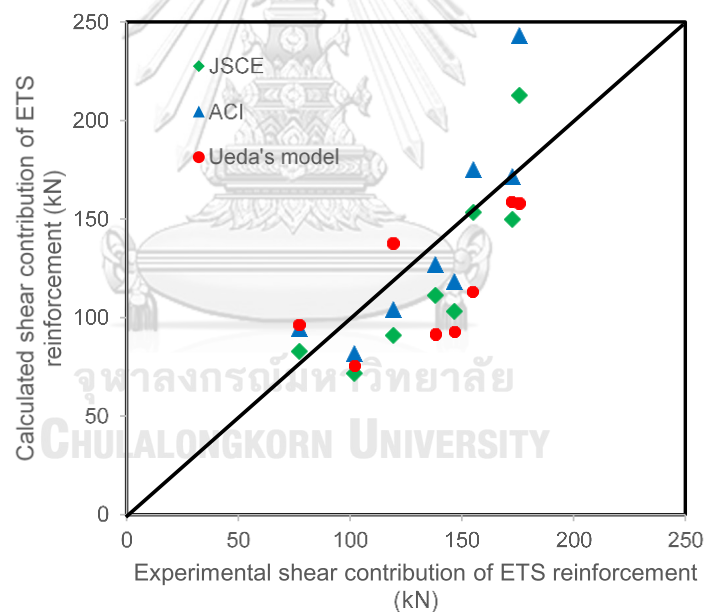


Figure 3.18 Comparison between analytical results using modified average strain and tested data

As seen from columns 2, 4 of Table 3.8 and Fig. 3.17, the average strains computed by Eq. (3.4) are nearly located the real effective strains defined by the recorded strain gauges. Therefore, Eq. (3.4) could be adopted to predict the effective strains of the ETS strengthened bars from the experimental shear contribution, and Eq. (3.4) is obviously

useful when the strain gauges were not glued in the shear reinforcement. To modify the average strains in the strengthened bars, the values computed from Eq. (3.4) and the formulation  $\frac{\sqrt{f'_c}}{\sqrt{a/d+1}} e^{\frac{-1000}{\rho_s E_s} - 0.05\sqrt{\rho_w E_w}}$  in Ueda's model are employed to build the regression relationship. Then, the effective strain is described as a function of  $\frac{\sqrt{f'_c}}{\sqrt{a/d+1}} e^{\frac{-1000}{\rho_s E_s} - 0.05\sqrt{\rho_w E_w}}$  by Eq. (3.5). Figure 3.17 and Table 3.8 (column 5) present the comparison between the average strains calculated by Eq. (3.5) and the effective strains collected from the test data. Fact, the comparison indicates that Eq. (3.5) could be used to define the average strains in the strengthening system of a beam retrofitted by the ETS FRP bars. Additionally, as observed from Fig. 3.17, the experimental data and the analytical results (Eqs. (3.4), (3.5)) reveal that the average strain in shear reinforcement decreased as the stiffness of shear reinforcement increased. Therefore, the shear contribution of the ETS reinforcement of the investigated beams in Section 3.3.6.1 is recalculated using the existing shear models with the update effective strain equation (Eq. (3.5)).

$$\varepsilon_{fe} = -0.00127 + 0.0162 \frac{\sqrt{f'_c}}{\sqrt{a/d+1}} e^{\frac{-1000}{\rho_s E_s} - 0.05\sqrt{\rho_w E_w}} \quad (3.5)$$

Table 3.9 Shear contribution of ETS reinforcement from experimental and analytical results using modified average strain

Beam ID	$V_{f\_Exp.}$ (kN)	$V_{f\_Exp.}/V_{f\_ACI}$	$V_{f\_Exp.}/V_{f\_JSCE}$	$V_{f\_Exp.}/V_{f\_Ueda's\ model}$
A3	119.2	1.15	1.31	0.86
A4	172.3	1.00	1.15	1.08
B1	138.2	1.08	1.24	1.51
B2	154.8	0.88	1.01	1.37
B3	101.9	1.24	1.42	1.34
B4	146.7	1.24	1.42	1.58
2S-C180-90 (C1)	77.1	0.81	0.93	0.80
2S-C180-45 (C2)	175.6	0.72	0.82	1.11
Mean (Cov)		1.02 (0.194)	1.16 (0.194)	1.21 (0.238)

Figure 3.18 and Table 3.9 show the comparison between the experimental data and the analytical results using the ACI, JSCE and Ueda et al.'s models with the update average strains determined by Eq. (3.5). The comparison performs a good agreement was obtained between experimental and analytical data. In addition, with the mean value of the ratio of the test values to the theoretical values is 1.02 and the coefficient of variation (COV) is 19.4% of the mean, the shear contribution of the ETS retrofitted bars calculated by the ACI model with the new effective strain formulation gives better results in the comparison with the shear resistance of the ETS strengthened rods computed by the JSCE and Ueda et al.'s models with the new average strain equation also. However, considering the shear contribution of the ETS strengthening system by applying the JSCE model with the developed effective strain model, the mean value of the ratio between experimental shear contribution to computed one is 1.16 and the COV is 19.4% of the mean, and most of specimens offer the lower calculated results than the data attained from the test; therefore, the developed JSCE model could be adopted for assuring a proper design safety format in the practical use.

Moreover, as presented in Table 3.9, the shear contributions of ETS FRP system computed by the developed model imply that the increase of the steel stirrups amount resulted in the reduction of the shear resistance of ETS FRP bars (B1-B2 compared to B3-B4). Additionally, the ETS CFRP vertical rods contributed to the shear capacity was less than the ETS GFRP vertical bars, while the ETS CFRP diagonal system exhibited the higher shear resistance compared to the ETS GFRP bars inclined at  $45^{\circ}$  (B1-B2 compared to C1-C2). These findings are completely fitted with the observations from the experiment since the modified effective strain equation (Eq. (3.5)) reflected accurately the real response of the ETS retrofitted bars. Indeed, as shown in Table 3.8, the increase of stiffness of shear reinforcement resulted in the decrease of the average strain of the ETS FRP retrofitted bars, and this behavior was also indicated in the study by Ueda et al. (1996). Although the total shear strength of the concrete beams with combined usage of steel and FRP bars increases as the reinforcement amount increases, it can be drawn that the shear capacity carried by ETS FRP reinforcement in the hybrid ETS FRP-steel beams is reduced as the contents

of the existing transverse steel large and the axial stiffness of shear reinforcement high.

### 3.4 Conclusions

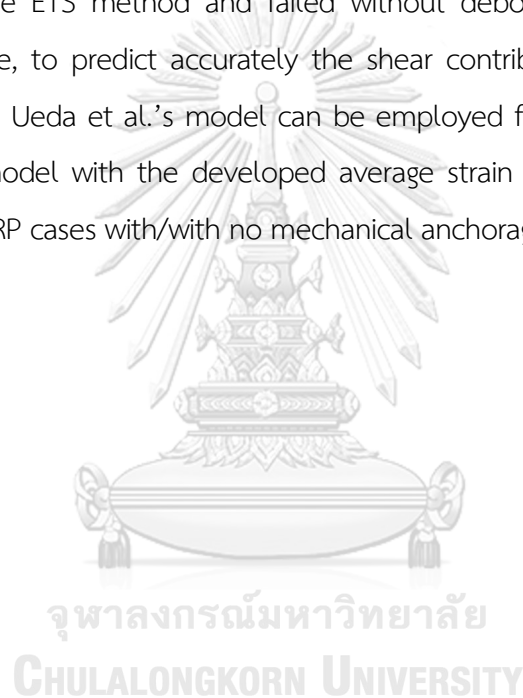
An experimental program to study on the mechanical behaviors of concrete beams strengthened by ETS steel/FRP bars was carried out. Additionally, the further comparisons between the tested results and the data in the previous studies are conducted to analyze the efficiency of the concrete beams retrofitted by ETS bars with the mechanical anchorage. On the other hand, the applicability of the existing shear models to predict the shear contribution of the ETS strengthening system is also validated and the average strain equation of the ETS FRP reinforcement in the available shear resisting methods is also developed. Based on the results of the analyses, conclusions can be drawn:

Due to the non-close shape configuration, the shear resistance of ETS vertical bars is less than that of hybrid vertical shear reinforcement. Whereas, the shear contribution of ETS diagonal system is slightly higher than the contribution of hybrid diagonal reinforcement in shear. The beams strengthened with ETS GFRP system (with anchorage) provide an encouraging anchorage and a good confinement action to the ETS bars of concrete core, therefore the shear contribution of the ETS GFRP is high. The presence of stirrups reduced the resistance of ETS strengthened bars in shear. With low percentage transverse steel compared to the percentage of the ETS reinforcement, the detrimental effect induced by presence of existing stirrups does not occur in the specimens strengthened by ETS bars with mechanical anchorage insert.

The shear failure modes of the beams, which is retrofitted with ETS GFRP bars installed mechanical anchorage, intended to convert into the flexural failures by crushing concrete at the load points, improving the ductility of the ETS strengthened members. The shear contribution of strengthening term adopting the ETS method always offers higher values than that of the NSM retrofitted bars, since the good anchorage and confinement of the concrete core to ETS bars, making the shear transfer

mechanism of concrete-adhesive-ETS bars was significantly enhanced and triggered the contribution of ETS bars in shear drastically.

The truss analogy theory can predict well the shear resistance of the initially steel shear reinforcement and ETS steel bars. However, this model cannot predict well the shear contribution of the low percentage of ETS reinforcement due to the beam failed by the debonding instead of the yielding of ETS reinforcement defined by the truss analogy approach. The current average stress equations of shear reinforcement is conservative especially for ETS FRP contribution. For the concrete beams retrofitted with the ETS method and failed without debonding of the strengthening system to concrete, to predict accurately the shear contribution of the strengthening system the original Ueda et al.'s model can be employed for the ETS steel cases, and the ACI or JSCE model with the developed average strain equation (Eq. (3.5)) can be used for the ETS FRP cases with/with no mechanical anchorage.



## Chapter 4 SIMULATION OF CONCRETE BEAMS STRENGTHENED BY EMBEDDED THROUGH-SECTION (ETS) STEEL AND GFRP BARS WITH BOND MODEL

### 4.1 Introduction

In the recent years the embedded through-section technique (ETS) can be considered a most efficient technique, among the shear retrofitting methods such as externally bonding (EB) and near surface mounting (NSM) methods, for strengthening in shear of the reinforced concrete (RC) members. Simply, the ETS method employs an adhesive to bond fiber-reinforced polymer (FRP) or steel bars embedded through pre-drilled holes into the concrete core. The corrosion and fire attack to reinforcement may be limited due to the fact that ETS bar is surrounded by concrete.

As reported in the experimental studies by Barros et al. (2011), Chaallal et al. (2011), Amir et al. (2012), Breveglieri et al. (2014), Breveglieri et al. (2015) and Linh et al. (2018a, b), the shear capacity of the strengthened RC beams would significantly increase by using the ETS method. Obtained findings in the past several works indicate that the response of the ETS shear strengthened members have converted brittle shear failure into ductile flexural failure with the yielding of the longitudinal steel bars. For the numerical investigation, only the study by Godat et al. (2013) presented the finite element (FE) simulation of the concrete beams strengthened by ETS bars tested in their past experimental works using DIANA. In their research, the overall behaviors of concrete beams retrofitted with carbon fiber-reinforced polymer (CFRP) bars such as load-deflection relationship and strain in ETS bars were considered. Their study indicated that although the perfect bond of the reinforcement and strengthening system to concrete was assumed, the agreement between the simulated results and the experimental data was acceptable.

On another aspect, the bond behavior of the strengthened rods to concrete is an important point that affects directly the performances of concrete beams

strengthened with ETS bars. The less bonding performance of the ETS retrofitting system to concrete, which reduced the effectiveness of ETS strengthening system, is also appeared in the past works, especially the vertical ETS case. As reported in Chapter 3, to trigger the ultimate effectiveness of ETS strengthening system either the bonding performance between ETS bars and concrete is enhanced or the bonding efficacy is compensated by the additional device, such as mechanical anchorage at the tension ends of ETS bars. However, only two experimental works of the ETS pullout tests (Godat et al. 2012 and Caro et al. 2017) were found. None has ever conducted experiments of ETS bars embedded into concrete blocks with mechanical anchorage at tension ends nor investigated strain profiles of the ETS bars to examine the bond response.

The principal objectives of this study are to investigate the bond mechanism of concrete specimens embedded by ETS steel and FRP rods with inserted anchoring nuts at the tension ends, and to simulate the ETS strengthened beams experimented in the previous works by the authors of this study through the FE modelling. The pullout tests to analyze the bond mechanism of the ETS bars to concrete under various effects of anchorage presence, embedment length, ETS bar diameter, ETS material types and anchorage length are conducted and examined. In addition, an analytical method for deriving the local bond stress-slip relationships of FRP bars-concrete interfaces is developed from the model proposed by Dai et al. (2005). The results obtained from the experimental program in terms of the pullout force-slip relationships, failure mode and strain profiles along embedment length are discussed. Besides, the FE models to simulate the beams strengthened with ETS bars tested in the previous study by the authors are built into ANSYS.

## **4.2 Experiment on bond mechanism of ETS bars to concrete**

### **4.2.1 Description of tested specimens**

The design configuration, material properties of nine specimens, the strain gauges attachment on the ETS steel/glass fiber-reinforced polymer (GFRP) bar and the



pullout test setup are shown in Fig. 4.1, Table 4.1 and Table 4.2. The specimens are divided into five groups to investigate the effects of anchorage (C1, C2), embedment length (C2, C3, C5, C6), bar diameter (C1, C4), ETS material types (C3, C7) and anchorage length (C3, C8, C9) on the bond response between ETS bars and concrete. The concrete blocks were drilled along the depth to insert the ETS bars by the epoxy layers, and the installation of mechanical anchorage at the tension ends of ETS bars was also implemented. As shown in Table 4.2, the maximum forces at tension fracture of ETS steel (12 mm diameter) and GFRP bars (8/10 mm diameter) are 60.7 kN and 54.1/84.5 kN, respectively.

Table 4.1 Properties of materials of the tested specimens

Specimens	$f_c$ (MPa)	$E_r$ (GPa)	$f_t$ (MPa)	$E_{adhesive}$ (GPa)	$f_{t\_adhesive}$ (MPa)
C1-C3, C5-C9	38.2	50	1076	3.1	21.0
C4	38.2	200	390	3.1	21.0

Table 4.2 Configuration, ultimate load, maximum slip and failure mode of the tested specimens

Spec.	$L_e$ (mm)	$d_b$ (mm)	ETS material	Anchorage	Number of anchoring nut	Ulti. force (kN)	$F_t$ (kN)	Max. slip (mm)	Failure mode
C1	150	10	GFRP	No	-	26.5	84.5	0.27	Pullout
C2	150	10	GFRP	Yes	4	30.3	84.5	0.42	Rupture
C3	120	10	GFRP	Yes	4	37.9	84.5	0.64	Rupture
C4	150	8	GFRP	No	-	32.1	54.1	1.16	Rupture
C5	200	10	GFRP	Yes	4	39.2	84.5	0.48	Rupture
C6	250	10	GFRP	Yes	4	37.4	84.5	0.98	Rupture
C7	120	12	Steel	Yes	4	60.7	45.2*	0.12	Rupture
C8	120	10	GFRP	Yes	2	34.0	84.5	0.55	Pullout
C9	120	10	GFRP	Yes	6	37.1	84.5	0.48	Rupture

Note:  $L_e$  (mm) is embedment length,  $d_b$  (mm) is ETS bar diameter and  $F_t$  (kN) is tensile force capacity of ETS bars. \*Yielding force of ETS steel.

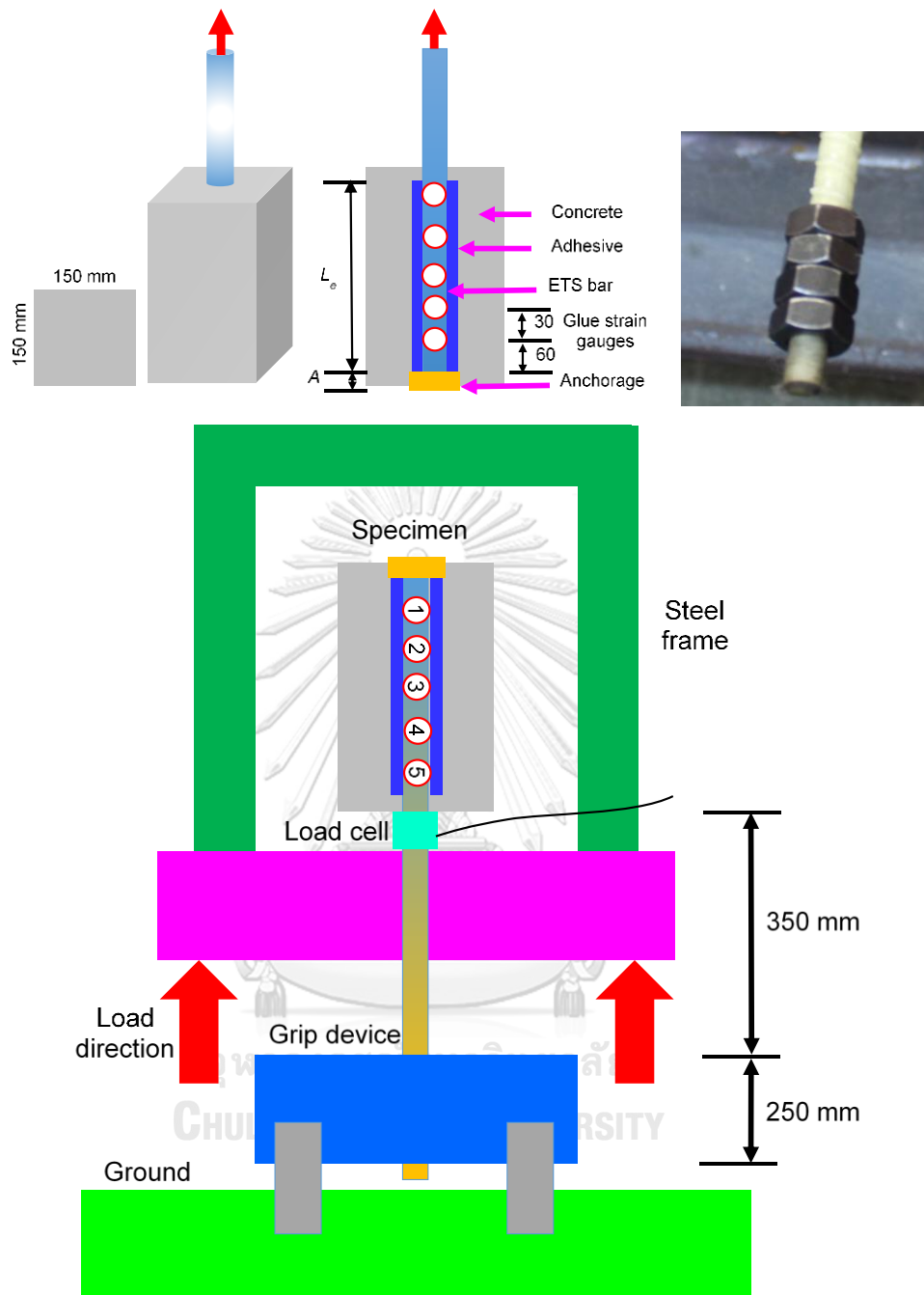


Figure 4.1 Configuration of the tested specimens, the anchorage device (anchoring nuts) at end of GFRP bar and the pullout test setup

#### 4.2.2 Results and discussion

This Section shows the discussion on the tested results by considering the effects of the factors on the bond response directly. The influences of the mechanical anchorage

presence, the embedment length, the ETS bar diameter, the ETS types and the anchorage length on the pullout force-slip and average bond stress-slip relationships and the strain profiles along the bond length are presented and discussed. The average bond stress ( $\tau$ ) and the local slip ( $s_i$ ) at strain gauge closet to load end are computed as equations.

$$\tau = \frac{P}{\pi d_b L_e} \quad (4.1)$$

$$s_i = \frac{\Delta x}{2} \left( \varepsilon_0 + 2 \sum_{j=1}^{i-1} \varepsilon_j + \varepsilon_i \right) \quad (4.2)$$

where  $P$  (kN) is the pullout force,  $L_e$  (mm) is embedment length,  $d_b$  (mm) is ETS bar diameter,  $\Delta x$  (mm) is the strain gauge interval of 30 mm,  $\varepsilon_i$  (micron) is the strain of ETS bar at the free end,  $\varepsilon_i$  (micron) is the strain at gauge of  $i$ th-order.

#### 4.2.2.1 Effect of mechanical anchorage presence

To analyze this effect, the test results of the specimen C1 without mechanical anchorage attachment and the specimen C2 with mechanical anchorage presence are assessed. It is obvious from Fig. 4.2(a) that the initial response before the mechanical anchorage being activated is completely similar between the two specimens. From Table 4.2, the specimen C2 with mechanical anchorage attachment results in the significantly higher maximum pullout force and maximum slip than those obtained by the test of the specimen C1 without anchorage by 14.3% (for pullout force) and 54.5% (for slip). The final failure modes of the blocks C1 and C2 are the pullout of ETS bar and the rupture of ETS bar, respectively. Clearly, at the load same as the peak load of the specimen C1, where the specimen C1 failed by pullout of bar, the anchorage in the specimen C2 started to be activated, utilizing the contribution of the ETS bars ultimately. Therefore, the pullout force transfer after that load was shifted from the adhesive to the anchorage, so that the failure mode of the block C2 is different from the specimen C1. Indeed, Fig. 4.2(b) indicates that the strain of gauge (SG1) closest to the anchorage in the specimen C2 started to increase at the peak load of the test specimen C1. While the strain at SG5, which was closest to the load end of the ETS bars, of the specimens C1 and C2 is similar at the triggered load. These indicate that the use of anchorage

enhanced drastically the tension capacity of rod at the bar end and made the ETS retrofitted bar worked ultimately to change the failure mode.

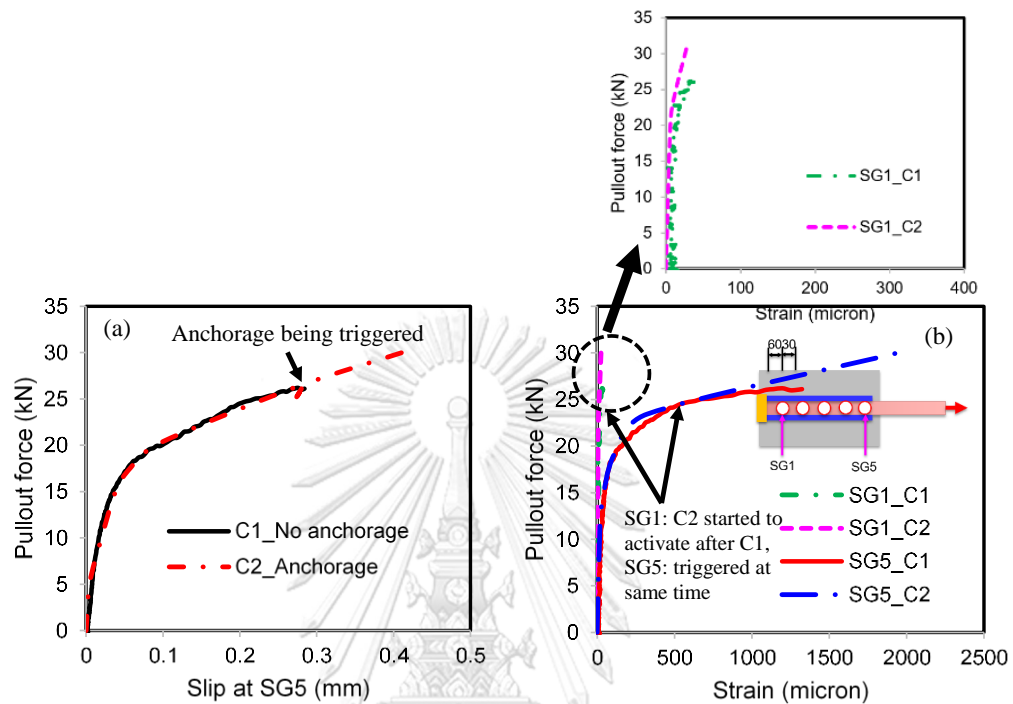


Figure 4.2 Comparison in the bond and strain responses between the cases with and without anchorage

#### 4.2.2.2 Effect of embedment length

Figure 4.3 shows the pullout force-slip of the investigated specimens C2, C3, C5 and C6. From Fig. 4.3, generally, the ultimate pullout forces of the specimens are similar since the failure mode is the GFRP bar rupture except the specimen C2 exhibited a lower pullout force due to the significant premature fracture. As shown in Table 4.2, the failure modes of the specimens C2, C3, C5 and C6 were the fracture of ETS GFRP bars due to the presence of anchorage at bar ends. As shown in Table 4.2, the ultimate pullout force is much smaller than the ultimate tensile force ( $F_t$ ) based on GFRP tensile strength since the premature tension rupture at the anchorage was occurred, and the premature rupture may depend on the detailing of anchorage.

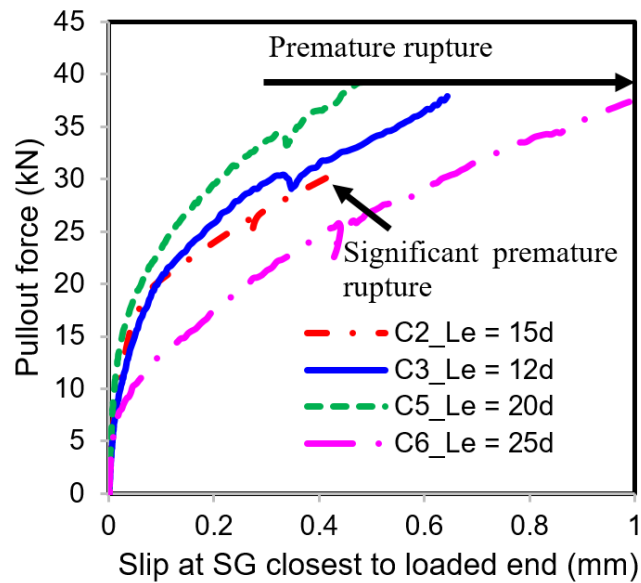


Figure 4.3 Comparison in the bond response between the cases of embedment length changes

#### 4.2.2.3 Effect of bar diameter

To consider the effect of bar diameter on the bond mechanism of ETS bars to concrete, the test results of the specimens C1 and C4, in which the rod diameters are 10 and 8 mm respectively, are compared. It is obvious from Table 4.2 and Fig. 4.4(a) that the specimen C1 with ETS GFRP bar diameter of 10 mm showed the lower ultimate pullout force and smaller maximum slip in the comparison with those of the specimen C4 with ETS GFRP bar diameter of 8 mm; 26.5 kN compared to 32.1 kN (for ultimate load) and 0.27 mm compared to 1.16 mm (for bond slip). The specimen C1 embedded by ETS GFRP bar with 10 mm of diameter induced the weak interface between the ETS bar-adhesive-concrete probably due to the poorer adhesive resin injection. While, with the smaller ETS bar size the adhesive resin was filled up more easily in C4. Hence, the ultimate pullout force of C1 was low and the maximum slip was small. In addition, the failure modes of the investigated specimens that are respectively pullout and ETS rupture failures for the blocks C1 and C4.

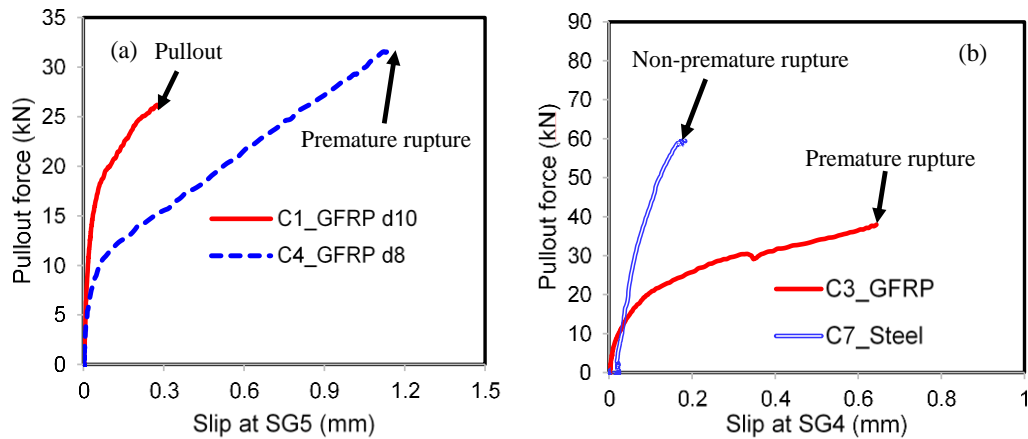


Figure 4.4 Comparison in the bond responses under the effects of ETS bar diameter and ETS types

#### 4.2.2.4 Effect of ETS types

The experimental data of the specimens C3 and C7 embedded by ETS GFRP bar and ETS steel bar, respectively, are employed to investigate the influence of the ETS types on the bond performance of the ETS bars to concrete. Table 4.2 and Figure 4.4(b) reveal that the concrete block embedded by ETS steel bar showed higher pullout force and smaller slip in the comparison with the specimen embedded with ETS GFRP rod. As observed from the tests, the failure modes of these investigated specimens are the ETS rupture failures for the both blocks C3 and C7. The high Young's modulus of steel of 200 GPa, the low yielding strain of steel of 2000 micron and the bigger size of ETS steel bar embedded in the specimen C7 can be a good reason to explain for the aforementioned findings. Besides, the mechanical properties of the ETS material exhibits that the rigidity of the concrete specimen with ETS steel bar was higher than that of the block embedded by ETS GFRP rod. Moreover, Table 4.2 also displays that ETS steel bar in C7 resulted in the rupture at pullout force higher than its tensile strength ( $F_t$ ) due to different rupture location in ETS steel bar, meaning that there is no premature failure for ETS steel case.

#### 4.2.2.5 Effect of anchorage length (number of anchoring nuts)

The specimens C3, C8 and C9 embedded by ETS GFRP rods with the nut amounts of anchorage were respectively  $A = 4$ ,  $A = 2$  and  $A = 6$  are tested and the experimental

results are discussed to investigate the effect of anchorage length on the bond response between ETS bars and concrete. It is clear from Fig. 4.5(a) and Table 4.2 that with the longer anchorage length (or more anchoring nuts) the specimens C3 and C9 resulted in the higher pullout force than that of the specimen C8 with the short anchorage length. The failure modes of the specimen C3 and C9 were the fracture of ETS bars, while the specimen C8 with short anchored ETS bar failed by the pullout of the ETS bar leaving the nuts in concrete (Fig. 4.5(b)). This fact indicates that the two nuts are not enough to assure the full tension capacity of ETS GFRP bar.

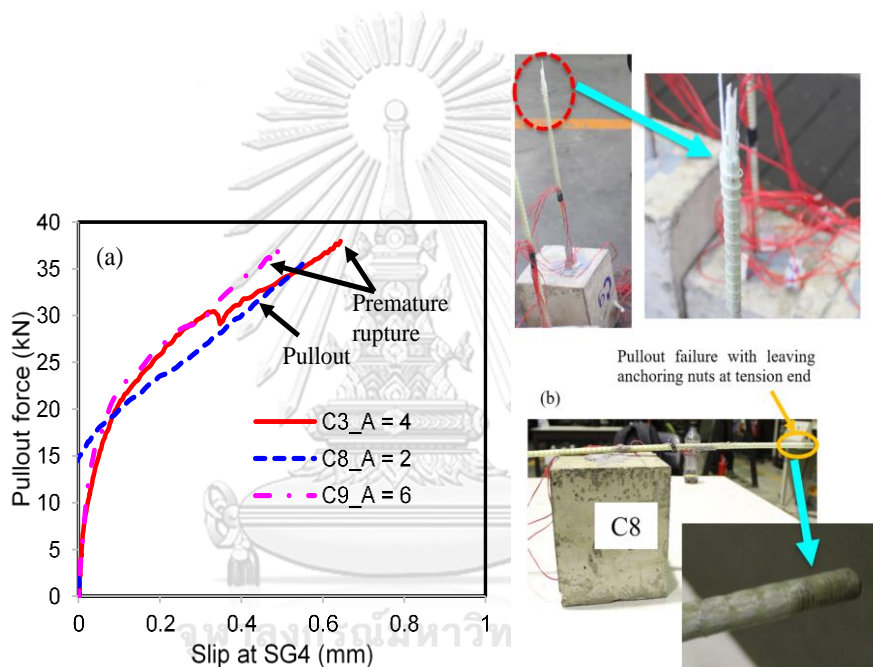


Figure 4.5 Comparison in the bond responses between the cases of anchorage length changes, and pullout failure of specimen C8

#### 4.2.3 Analysis of bond response of ETS bars to concrete

This Section presents a new development of the bond behavior in the ETS technique. Fig. 4.6 describes the equilibrium forces in arbitrary section and the free body diagrams of concrete-ETS bar interface. Obviously, from Fig. 4.6 the equilibrium equation can be obtained as follows.

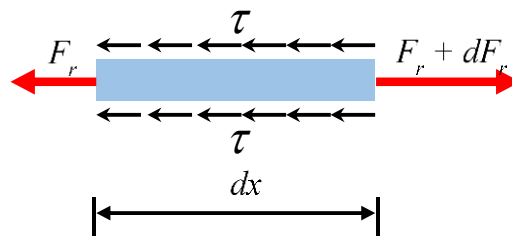


Figure 4.6 The free body diagrams of the ETS bar interface

$$dF_r(x) = A_r d\sigma_r(x) = p_r \tau(x) dx \quad (4.3)$$

where  $p_r$  is the perimeter of the bar, and  $\tau(x)$  is the bond stress and  $A_r$  is the cross-sectional area of ETS bar, respectively. Additionally,  $d\sigma_r(x)$  is the tensile stresses in ETS bar and  $dF_r(x)$  is the axial force in ETS bar at a segment  $dx$ . In addition, the uniaxial constitutive relationship for the linear elastic ETS bar elements is shown in Eq. (4.4).

$$F_r(x) = E_r A_r \varepsilon_r(x) \quad (4.4)$$

where  $F_r(x)$  is the axial force along the  $x$ -axis,  $E_r$  is the elastic modulus of bar and  $\varepsilon_r(x)$  is the axial strain at a distance  $x$ . Additionally, from the above equations, it can be written.

$$\frac{d^2 s(x)}{dx^2} = \frac{d\varepsilon_r(x)}{dx} = \frac{dF_r(x)}{E_r A_r dx} = \frac{p_r \tau(x)}{E_r A_r} \quad (4.5)$$

To analyze the local bond stress at the interfacial locations where attached the strain gauges, Eq. (4.5) can be performed as follows. The boundary condition of this analysis is the slip at the anchored end, which is zero.

$$\tau_i = \frac{E_r A_r}{p_r} \frac{\varepsilon_i - \varepsilon_{i-1}}{\Delta x} \quad (4.6)$$

where  $\tau_i$  (MPa) is average interfacial bond stress in the section  $i$ ,  $\varepsilon_i$  and  $\varepsilon_{i-1}$  (micron) are the strains at gauges of ( $i$ )th-order and ( $i-1$ )th-order, respectively.



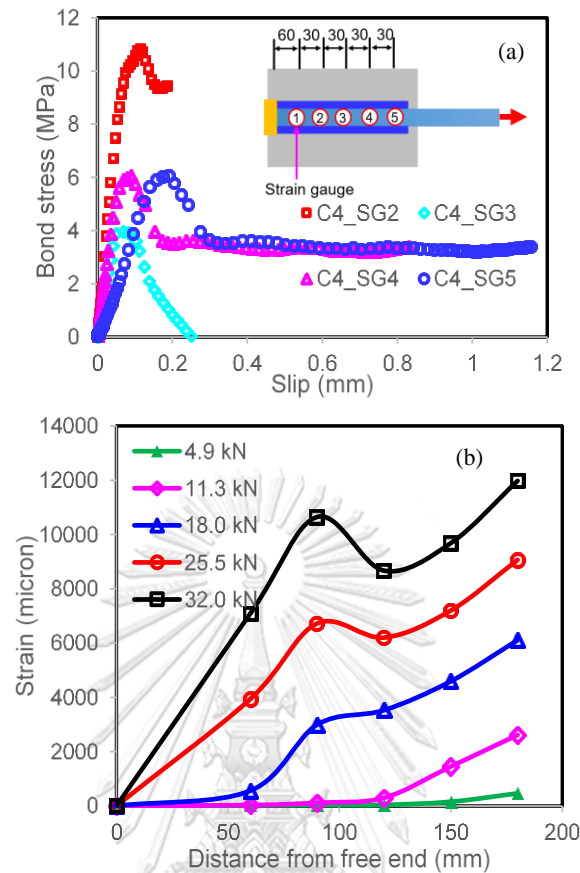


Figure 4.7 (a) Computed local bond stress-slip relationships at the different locations of the strain gauges (C4) and (b) strain distribution of ETS bar along bond interface (C4)

By using the mathematical formulation as Eq. (4.6) for local bond stress and Eq. (4.2) for local slip, the local  $\tau$ - $s$  relationships at the different interfacial locations in a pullout test of the representative specimen C4 are shown in Fig. 4.7(a). Similar to what have been observed by Dai et al. (2005), those  $\tau$ - $s$  relationships are fairly irregular at the different interfacial locations. The final scattering of the local  $\tau$ - $s$  relationships can be affected by the properties at the interfacial surface of concrete to ETS bars such as aggregate distribution, local bending of FRP rods due to improper epoxy filling. Therefore, it cannot be fair if one of curves is selected to represent for the  $\tau$ - $s$  relationship of the bond mechanism between ETS bars and concrete. Figure 4.7(b) is a representative strain distribution along the embedment length of the specimen C4. It is obvious from Fig. 4.7(b) that strain distribution along bonded

length was highly nonlinear profile, and the strain and the load transfer length increase as the applied load increases. To obtain the interfacial bond stress-slip relationships without the gauge attachment for recording the strain profiles along the ETS bars, the development of the method proposed by Dai et al. (2005) is carried out as follows.

In the Dai et al.'s method, the strain at each gauge attached in the ETS bars is expressed as an exponential function of the local slip calculated at this gauge (Eq. (4.7)). Equation (4.5) indicates that the  $\tau$ - $s$  relationships can be determined if the local strain and slip relationships were defined.

$$\varepsilon = f(s) = A(1 - e^{-Bs}) \quad (4.7)$$

where  $A$ ,  $B$  are experimental parameters as given in Table 4.3. Figure 4.8 shows the experimental and regressed curves of the strain and slip relationships at the loaded end of the tested specimens. It is obvious from Fig. 4.8 that the exponential expression as Eq. (4.7) could fit the experimental results very well, indeed the correlation factor values  $R^2$  of the relationship between the strains in ETS-FRP bars and the slips at the loaded end range 0.975 to 0.999 for all the specimens (as shown in Table 4.3). By substituting Eq. (4.7) into Eq. (4.5), the bond stress and slip relationship can be described as follows.

$$\tau = \frac{E_r A_r}{P_r} A^2 B e^{-Bs} (1 - e^{-Bs}) \quad (4.8)$$

The interfacial fracture energy  $G_f$  and the theoretical maximum pullout force  $P_{max}$  can be defined as follows.

$$G_f = \int_0^{\infty} \tau ds = \frac{A^2 E_r A_r}{2 P_r} \quad (4.9)$$

$$P_{max} = E_r A_r \varepsilon_{max} = E_r A_r A = E_r A_r \sqrt{2G_f \frac{P_r}{E_r A_r}} \quad (4.10)$$

where  $\varepsilon_{max}$  (micron) is the maximum strain of ETS bars corresponding to the maximum pullout force.

The maximum slip ( $s_{max}$ ) corresponding to the maximum bond stress ( $\tau_{max}$ ) can be derived as below.

$$\frac{d\tau}{ds} = 0 \therefore s_m = \frac{\ln 2}{B} \text{ and } \tau_m = 0.5BG_f \quad (4.11)$$

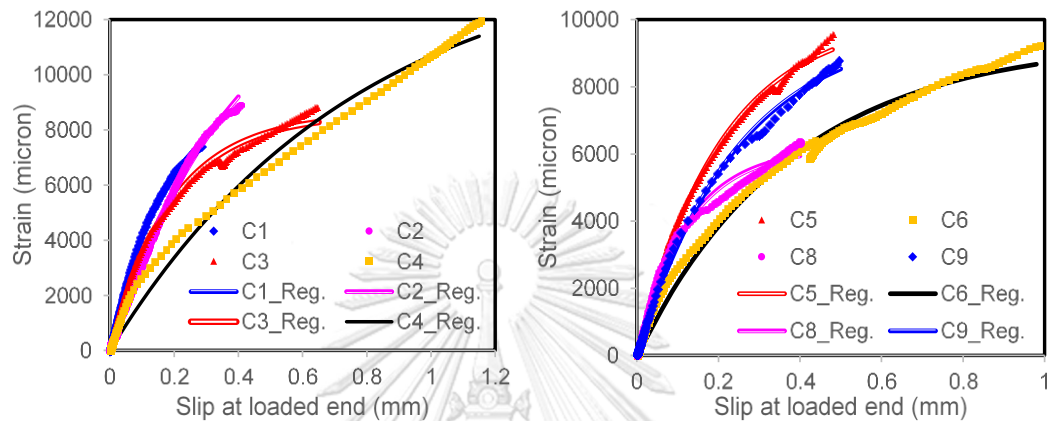


Figure 4.8 Experimental and regressed strain-slip curves at loaded end of the tested specimens

Table 4.3 Analysis of pullout test results

Spec.	$E_r A_r / p_r$ (kN/mm)	$A$ ( $\epsilon$ )	$B$ (1/mm)	$G_f$ (N/mm)	$R^2$	$\tau_{max}$ (MPa)	$s_{max}$ (mm)	$P_{max}$ kN (Expt.)	$P_{max}$ kN (Anali.)	$P_{anali}/P_{expt.}$
C1	125	0.01224	3.30	9.361	0.998	14.16	0.214	26.5	28.7	1.08
C2	125	0.01468	2.59	13.459	0.998	13.76	0.339	30.3	34.0	1.15
C3	125	0.00760	4.12	3.612	0.998	10.52	0.119	37.9	34.7	0.92
C4	100	0.00778	3.96	3.029	0.995	6.00	0.175	32.1	30.1	0.94
C5	125	0.01123	3.69	7.881	0.999	14.53	0.188	39.2	37.6	0.96
C6	125	0.00432	8.66	1.166	0.996	4.05	0.080	37.4	36.2	0.97
C8	125	0.00617	7.88	2.377	0.996	9.36	0.088	34.0	26.7	0.76
C9	125	0.01053	3.52	6.932	0.975	12.20	0.197	37.1	34.4	0.93
									Mean	0.96
									Cov. (%)	12.1

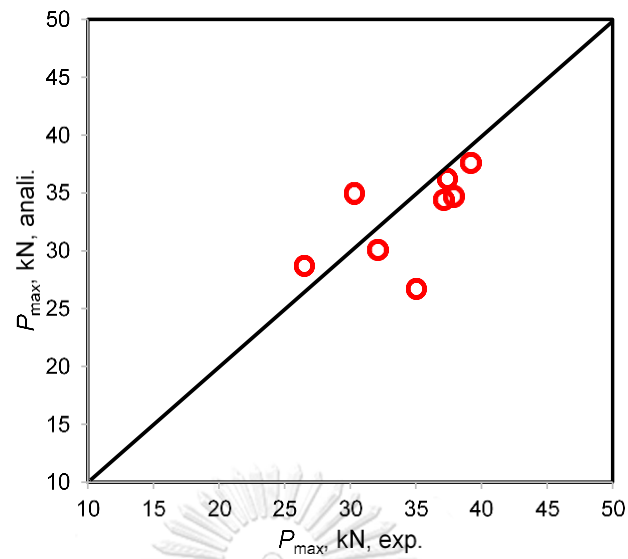


Figure 4.9 Comparison between theoretical and experimental maximum pullout forces

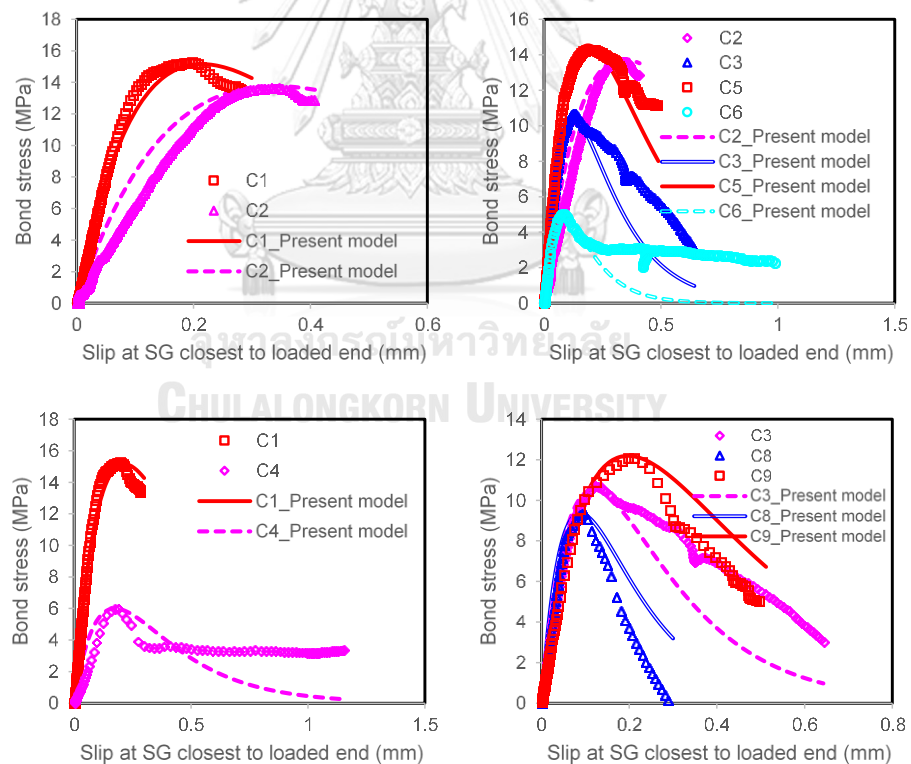


Figure 4.10 Experimental and analytical bond stress-slip curves at (a) loaded end of the tested specimens and (b) at interfacial locations of a representative specimen C4

The comparison between the analytical maximum pullout forces computed by Eq. (4.10) and the experimental maximum pullout loads is indicated in Fig. 4.9. As presented in Table 4.3, with the mean value of the ratio of the theoretical values to the tested values is 0.96 and the coefficient of variation is 12.1% of the mean, the good agreement can be obtained. By applying the above-mentioned process, Eqs. (4.7) and (4.8), the experimental and analytical curves of the bond stress and slip relationship at the gauges closest to loaded end of the tested specimens are displayed in Fig. 4.10. It can be seen from Fig. 4.10 that the results computed by the developed ETS bond model fitted well with the tested data, especially in the ascending branch of the curves. It means that the developed bond model can be assumed to represent for the bond stress-slip relationship between ETS bars and concrete although there were the variations on the bond stress-slip curves at the different interfacial locations, causing by the scatter of strain in the experiment.

Fig. 4.10 also presents the  $\tau$ - $s$  relationships under various effects of anchorage availability, embedment length, bar diameter and anchorage length. Due to the influence of anchorage at bar end, the strain in ETS bar of the anchored specimen (C2) was smaller than that in ETS bar of the non-anchored block (C1), making the maximum bond stress of the specimen C2 lower than that of the specimen C1. For the effect of ETS bar diameter, as reported by Shrestha et al. (2017) and Dai et al. (2005), the bond stress increases as the stiffness ( $E_r A_r / p_r$ ) of the bonded system enhanced. In addition, the longer the anchorage length (or more anchoring nuts) resulted in the higher bond stress due to the anchorage affects the bond response reducing the strain at the stage before the anchorage become effectively. On the other hand, the interfacial ductility index ( $B$ ) and interfacial fracture energy ( $G_f$ ) are also affected by the various influences. The specimen without anchorage increased the ductility but decreased the fracture energy in the comparison with the specimen with anchorage attachment. Additionally, the higher stiffness results in lower ductility and larger energy, and the increase of anchoring nuts provides the better interfacial energy and the lower ductility index. Furthermore, the interfacial ductility index ( $B$ ) and interfacial fracture energy ( $G_f$ ), which could be derived by Eqs. (4.9), (4.10) and (4.11) if the maximum strain in the ETS bars have been known, are the important

factors to apply the ETS bond model developed in this Chapter to the concrete members strengthened by the ETS FRP bars. Therefore, how the interfacial ductility index ( $B$ ) the interfacial fracture energy ( $G_f$ ) to be employed in the concrete beams retrofitted with ETS GFRP rods will be discussed in the next Section.

### 4.3 Finite element (FE) modelling of concrete beams strengthened with ETS steel and GFRP rods

#### 4.3.1 Experimental data

The experimental data of the study in this study are adopted to carry out the simulation using finite element (FE) method of the concrete beams strengthened by ETS bars and reinforced with hybrid shear reinforcement. The design configuration of 11 specimens, including three reference beams (R1, R2 and R3), two hybrid diagonal-vertical beams (A1 and A2), two concrete beams strengthened by ETS steel bars (A3 and A4), and four concrete beams retrofitted with ETS GFRP bars (B1, B2, B3 and B4), for experimental program is clearly shown in Fig. 4.11 and Table 4.4. The three reference beams are respectively designed for the case of concrete only in the shear span L1 (beam R1), the case of two steel stirrups with diameter of 6 mm with 300 mm spacing in the shear span L1 (beam R2) and the case of two steel stirrups with diameter of 9 mm with 300 mm spacing in the shear span L1 (beam R3). On the other hand, the positions of the attached strain gauges are also marked in Fig. 4.11 and Table 4.5 describes the properties of the materials employed in the experiment.

Based on the experimental program in Chapter 3, the comparison between the test results and FE simulation results in terms of the load-deflection curves, cracking mechanism, failure mode, strain response in reinforcement and shear contribution of ETS strengthened bars is conducted. In addition, the application of bond model developed in this Chapter is also applied in the FE simulation to reflect well the real behaviors of the members.

Table 4.4 Reference, hybrid and ETS shear strengthening configuration of the 11 tested beams

Beam ID	Number of ETS/hybrid bars	Inclination of hybrid/ETS bars ( $^{\circ}$ )	Hybrid bars/ETS bars spacing (mm)	Existing steel stirrups ratio (%)	Hybrid/ETS reinforcement ratio (%)
R1-0S-0ETS	0	NA	NA	0.00	NA
R2-2Sd6-0ETS	0	NA	NA	0.11	NA
R3-2Sd9-0ETS	0	NA	NA	0.24	NA
A1-2Sd6-5Sd6(90)	5	90	180	0.11	0.18
A2-2Sd6-5Sd6(45)	5	45	180	0.11	0.25
A3-2Sd6-5ETS Steel d12(90)	5	90	180	0.11	0.35
A4-2Sd6-5ETS Steel d12(45)	5	45	180	0.11	0.50
B1-2Sd6-5ETS FRP d10(90)	5	90	180	0.11	0.24
B2-2Sd6-5ETS FRP d10(45)	5	45	180	0.11	0.34
B3-2Sd9-5ETS FRP d10(90)	5	90	180	0.24	0.24
B4-2Sd9-5ETS FRP d10(45)	5	45	180	0.24	0.34

By using ANSYS commercial software, the 11 tested beams has been performed to investigate the structural behaviors. Table 4.4 also shows that the investigations were considered under various effects, such as the amount of shear reinforcement, type of ETS bar, inclination of shear reinforcement and anchorage attachment at the tension ends of ETS bars. In addition, the hybrid use of FRP and steel shear reinforcement is also assessed by means of the shear capacity of the beams. The influence of existing steel stirrups on the shear resisting force of ETS FRP strengthening system is discussed to figure out the reasonable content of ETS bars for the shear retrofitting of the beams.

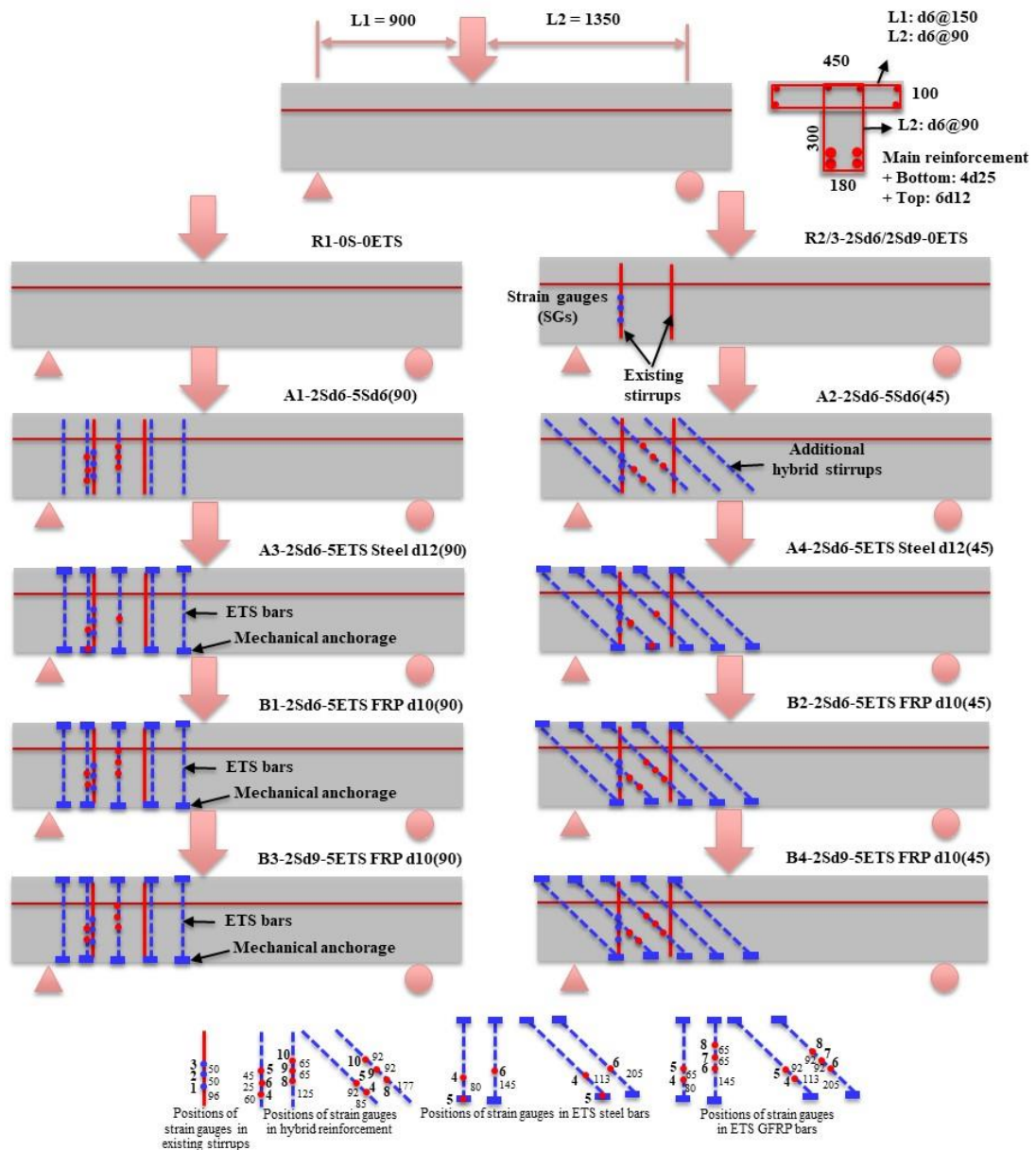


Figure 4.11 Configuration of the tested beams (dimensions in mm)

#### 4.3.2 Finite element program

In this study, numerical analyses are conducted by a commercially available software, ANSYS 15.0. A half FE model is applied to investigate the performance of the tested beams based on the symmetric condition as shown in Fig. 4.12. For this investigation, the mesh discretization is the  $25 \times 25 \text{ mm}^2$ . In addition, the descriptions



of element types and material models for the FE program are also presented in the previous work (Linh et al. 2017) of the authors of the present study.

Table 4.5 Properties of materials of the 11 tested beams

Beam ID	Concrete compressive strength at tested day (MPa)	Young modulus of hybrid/ETS reinforcement (GPa)	Yielding/Rupture strength of hybrid/ETS reinforcement (MPa)
R1-0S-0ETS	35.4	NA	NA
R2-2Sd6-0ETS	35.4	NA	NA
R3-2Sd9-0ETS	38.2	NA	NA
A1-2Sd6-5Sd6(90)	35.4	200*	235*
A2-2Sd6-5Sd6(45)	35.4	200	235
A3-2Sd6-5ETS Steel d12(90)	35.4	200	390*
A4-2Sd6-5ETS Steel d12(45)	35.4	200	390
B1-2Sd6-5ETS FRP d10(90)	38.2	50**	1076**
B2-2Sd6-5ETS FRP d10(45)	38.2	50	1076
B3-2Sd9-5ETS FRP d10(90)	38.2	50	1076
B4-2Sd9-5ETS FRP d10(45)	38.2	50	1076

\*Values were used according to TIS 24-2548

\*\*Values were provided by manufacturer

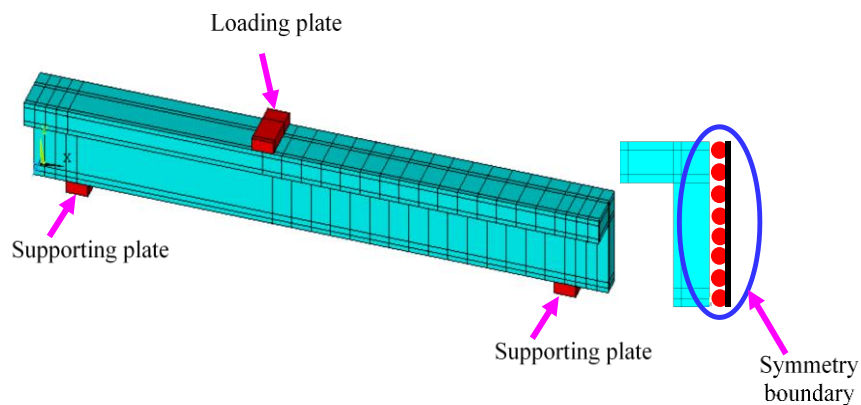


Figure 4.12 A half typical FE model for numerical program by using ANSYS 14.0

#### 4.3.2.1 Element types

SOLID65, LINK180, SOLID45 and COMBIN39 are used as the elements in ANSYS 14.0 for the nonlinear 3D modelling of concrete materials, reinforcement, rigid steel support and interfacial property, respectively. The SOLID65 element is capable of cracking in tension and crushing in compression. The element is defined by eight nodes and at each node has three degrees of freedom (Linh et al. 2017). While, the LINK180 is a uniaxial tension-compression element with three degrees of freedom at each node, the translations in the nodal x, y, and z directions (Linh et al. 2017). Besides, the SOLID45, which has the same properties as that of the SOLID65 except for the capability of cracking in tension and crushing in compression (Hawileh 2015, Linh et al. 2017), is applied for the supporting and loading plates. The non-linear spring element COMBIN39 in ANSYS is introduced to simulate the interfacial bond behavior of ETS bars and steel reinforcement to concrete in the FE models. The COMBIN39 requires the bond force-slip relationship at the interface of the reinforcement (including ETS bars and internal reinforcement) to input into program.

#### 4.3.2.2 Material models

Various constitutive models have been employed in FE simulations of the RC beams to describe the behavior of concrete under a wide range of complex stress and strain histories. These models included nonlinear elastic models, plasticity based models whether perfect plasticity models or elastic-plastic models (Godat et al. 2012). In this study, the model of Hognestad et al. (1955) is adopted to simulate the nonlinear response of concrete in compression. Equation (4.12) and Figure 4.13(a) show the more details of Hognestad et al. (1955) parabola.

$$f_c = f'_c \left[ 2 \left( \frac{\varepsilon}{\varepsilon_0} \right) - \left( \frac{\varepsilon}{\varepsilon_0} \right)^2 \right] \quad (4.12)$$

where

$f_c$  is the compressive stress of concrete (MPa) corresponding to the specified strain,  $\varepsilon$ ,

$f'_c$  is the concrete compressive strength (MPa),

$$\epsilon_0 = \frac{2f'_c}{E_c}, \text{ and } E_c \text{ is the elastic modulus of concrete (MPa).}$$

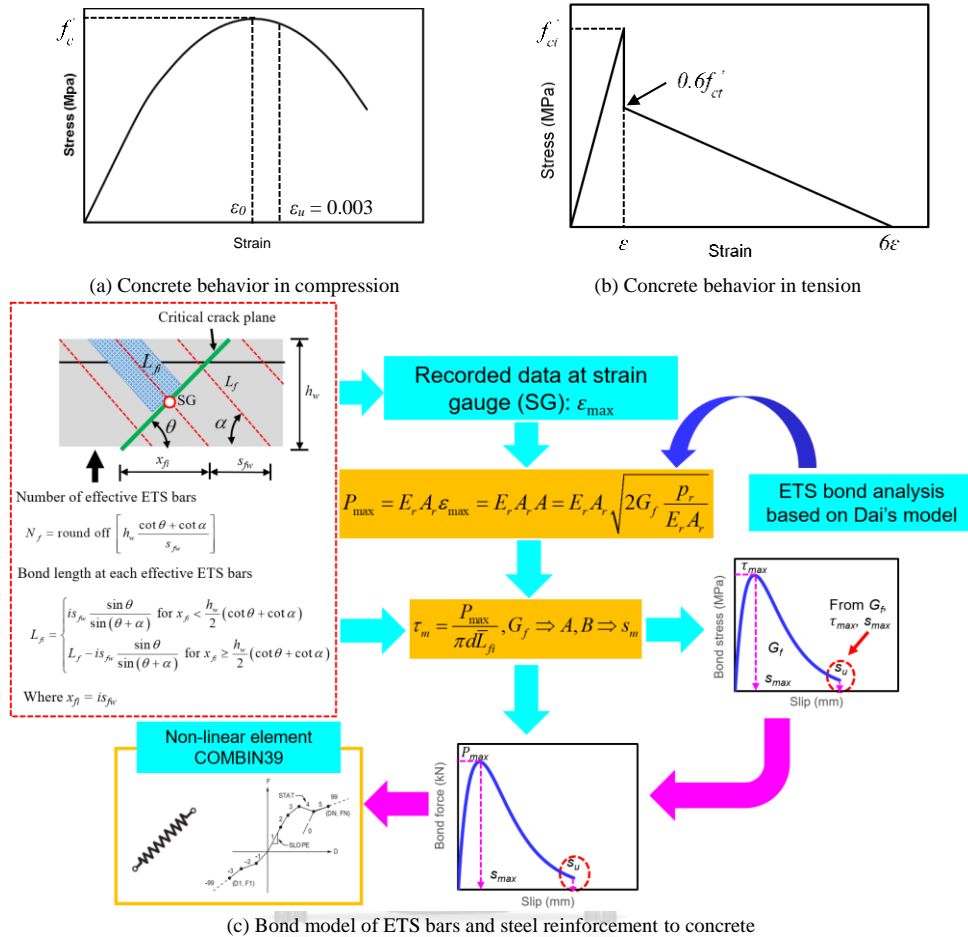


Figure 4.13 Models of concrete in compression and tension and bond model COMBIN39

Linh et al. (2017) showed the concrete behavior in tension according to the model of William and Warnke, which was recommended by ANSYS software. Fig. 4.13(b) shows the stress-strain relationship of concrete in tension. At first, the linear elasticity to the concrete tensile strength is used for concrete behavior in tension. Then, a steep drop in the concrete tensile stress by 40% is the stress relaxation in tension. And the rest of model is represented as the curve which descends linearly to zero tensile stress at a strain value six times larger than strain value at the concrete's tensile strength (Hawileh 2015). To simulate the bond behavior of reinforcement to

concrete in the FE models, a part of Fig. 4.13(c) reveals that each ETS bar, which the critical crack plane passed, contributed to shear resistance of the strengthening system through the bonding mechanism between the ETS bars-adhesive-concrete. In addition, the bond behavior is considered as a pullout response of each ETS bar to the covered concrete block. Number of the ETS bars, which contributed to the shear resistance, is defined by the amount of the ETS bars were crossed by the main crack plane and it is displayed in Eq. (4.13). Moreover, the effective bond length in the assumed concrete block covered the corresponding ETS bar is described as Eq. (4.14).

$$N_f = \text{round off} \left[ \frac{h_w}{s_{fw}} (\cot \theta + \cot \alpha) \right] \quad (4.13)$$

$$L_{fi} = \begin{cases} is_{fw} \frac{\sin \theta}{\sin(\theta + \alpha)} & \text{for } x_{fi} < \frac{h_w}{2} (\cot \theta + \cot \alpha) \\ L_f - is_{fw} \frac{\sin \theta}{\sin(\theta + \alpha)} & \text{for } x_{fi} \geq \frac{h_w}{2} (\cot \theta + \cot \alpha) \end{cases} \quad (4.14)$$

where  $x_{fi} = is_{fw}$ , and  $\theta$ ,  $\alpha$  are the crack, reinforcement angles respectively.

For the ETS bars and steel reinforcement where the strain gauge was glued, based on the ETS bond model developed in Section 4.3 and the equations above, the bond force-slip ( $P$ - $s$ ) relationship, corresponding to COMBIN39 element, derived by the interfacial fracture energy ( $G_f$ ) from the experiment is assigned into the FE models as Fig. 4.13(c). For the steel reinforcement where the strain gauge was not attached, the maximum bond stress and maximum slip are assumed based on fib Model Code 2010 (MC2010), as  $\tau_m = 2.5\sqrt{f'_c}$  (MPa) and  $s_m = 1$  (mm). Then, the bond force-slip ( $P$ - $s$ ) relationship, corresponding to COMBIN39 element, is similarly determined to the ETS bars and steel reinforcement for which the strain gauges were attached.

On the other hand, the steel reinforcement is described as the elastic fully plastic model based on the von Mises yield criterion, while the FRP bars are simulated as elastic-brittle materials till rupture. Figure 4.14 shows the stress-strain relationships of steel and FRP reinforcement which are applied in the FE simulations.

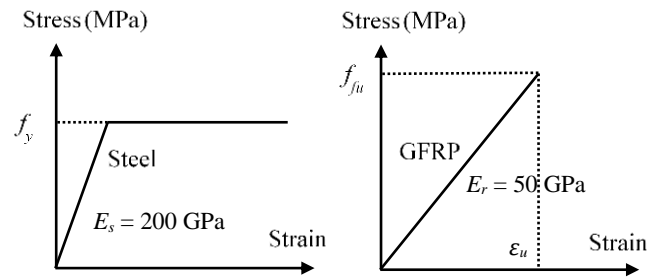


Figure 4.14 Stress-strain relationships of steel and GFRP reinforcement

### 4.3.3 Results and discussion

To verify the reliability of the FE method, the tested beams reinforced by hybrid shear steel stirrups and strengthened in shear with ETS steel and GFRP bars in Section 4.2 are simulated and the simulation results are investigated. The failure definition of beam specimens in the FE analysis is, after internal steel stirrups reaching yielding strength, either the stress in hybrid/ETS reinforcement reaching their yield/rupture strength or the concrete strain in compressive or diagonal region exceeding 0.003. The structural performances of the investigated beams by simulating in ANSYS 15.0 in terms of the load-deflection response, the cracking failure and the strain in shear reinforcement are compared with the results obtained from the corresponding experimental data.

#### 4.3.3.1 Load-deflection relationship and shear contribution of ETS strengthening system

Figure 4.15 shows the load-deflection curves of experimental and simulated results for the 11 beam specimens with the three reference beams (R1, R2, R3), the two specimens with internal shear reinforcement (A1, A2) and the six beams strengthened by ETS GFRP/steel bars (A3, A4, B1, B2, B3, B4). It is explicit that the FE results perform the good appraisal in the comparison with the tested data, and a maximum deviation less than 10% in the load-carrying capacity is found from Fig. 4.15 and Table 4.4. In general, the stiffness of the analyzed specimens is closed to that of the tested beams due to the bond-slip model was applied in the FE

simulation. This fact indicates that the bond-slip model based on Dai et al.'s method could be adopted to simulate the concrete beams strengthened by ETS steel/GFRP bars and the concrete beams reinforced with hybrid inclination of shear reinforcement. As shown in Fig. 4.15, the displacement corresponding to the peak load of the simulated beams is slightly smaller than that of the tested specimens. This discrepancy may be due to the displacement of the analyzed beams at high load level is partially decided by the bond behavior of steel tension reinforcement to concrete, which the maximum bond stress and slip were collected in MC2010. Moreover, Fig. 4.16 presents the comparison between tested and simulated data in terms of shear contribution of ETS strengthening system. It is obvious from Fig. 4.16 that the shear resistance of ETS bars computed by FE simulation is well agreed with that of ETS strengthened bars derived from experiment. Also from Fig. 4.16, it is similar to the test results that the shear contribution of strengthening system enhanced as the ETS bars inclined at  $45^\circ$ . Considering beams B1-B2 (stirrups 2Sd6) and B3-B4 (stirrups 2Sd9), the contribution in shear of ETS retrofitted rods reduced by increasing the stirrups amount and this finding is also observed in the experiment.

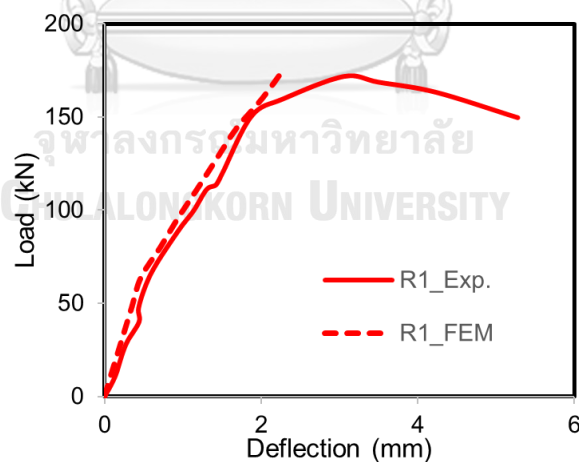


Figure 4.15 Comparison between tested and numerical results in load-deflection relationship

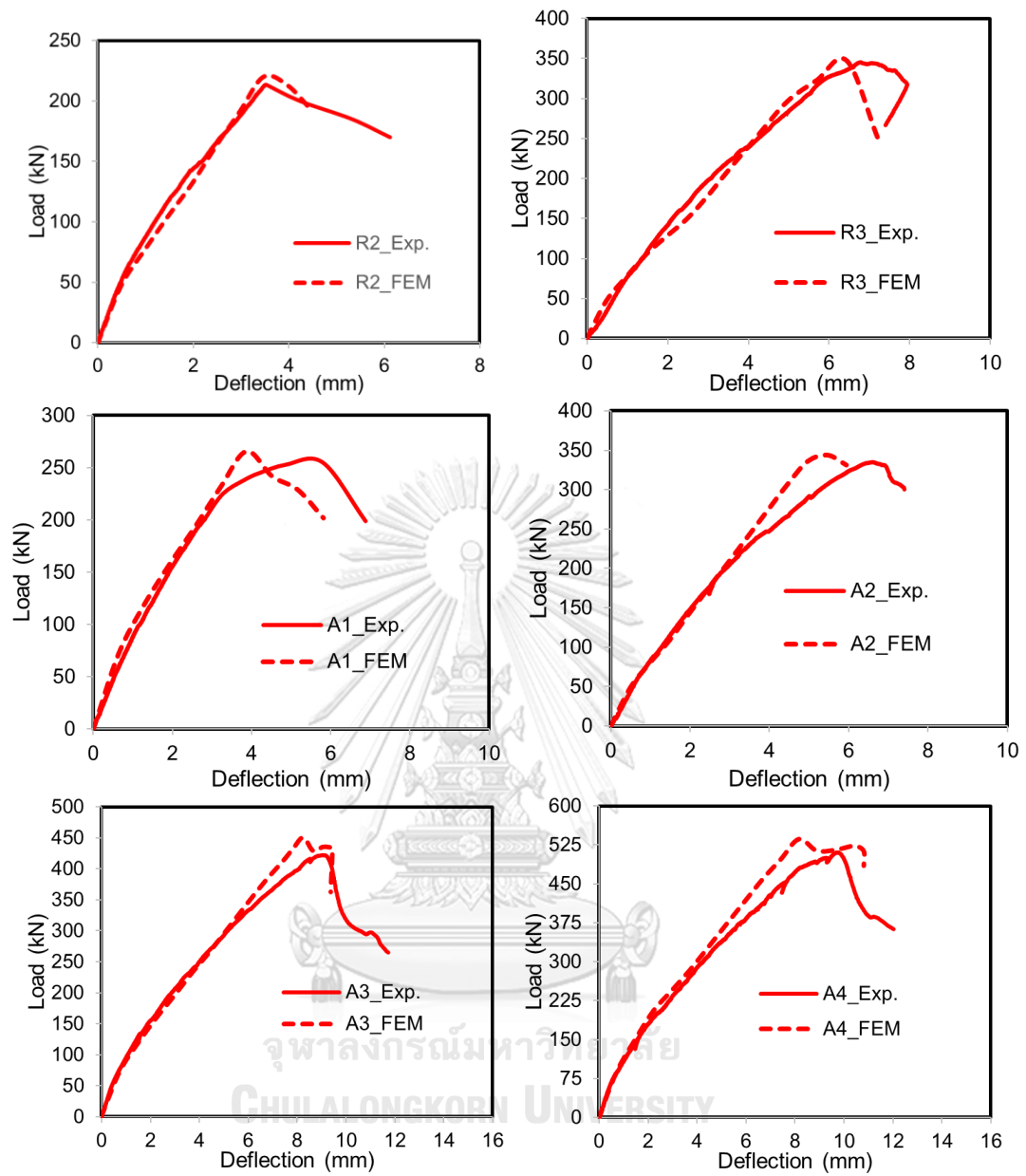


Figure 4.15 (continued)

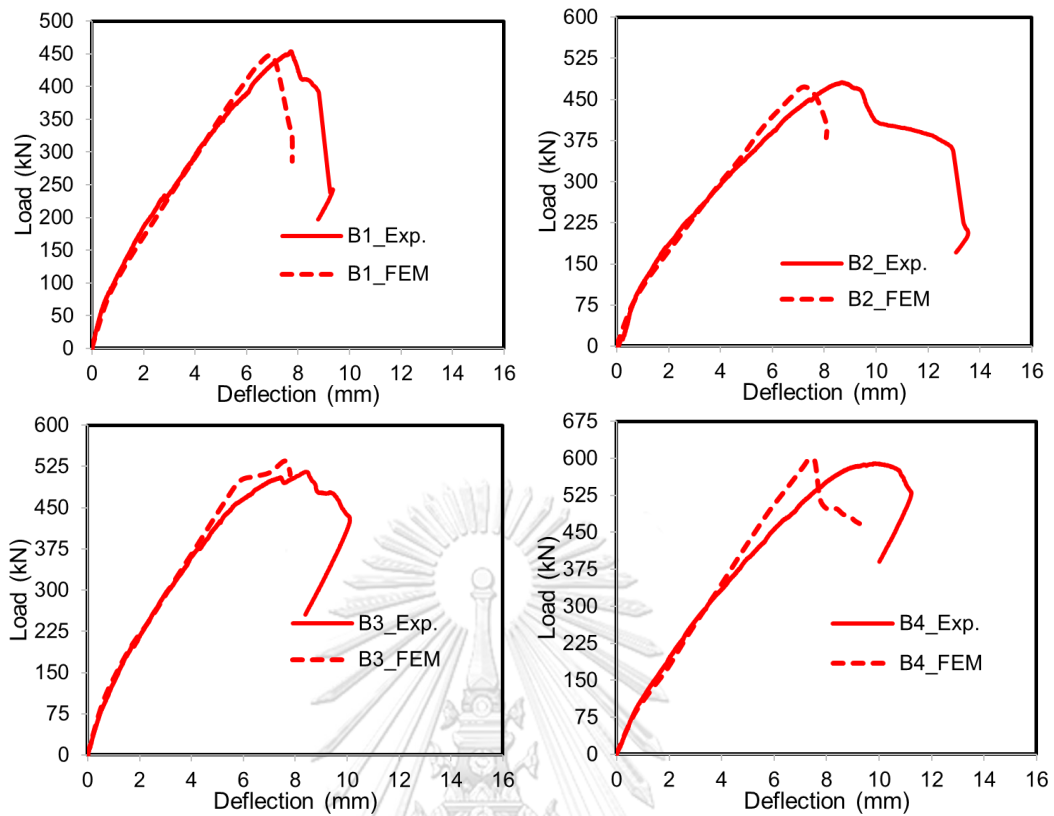


Fig. 4.15 (continued)

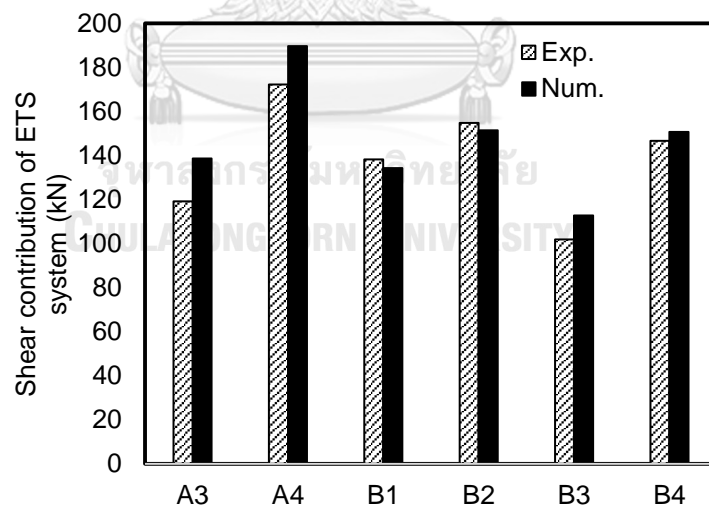


Figure 4.16 Comparison between tested and simulated data in terms of shear contribution of ETS strengthening system



Table 4.6 Numerical and experimental results in load capacity ( $P$ ), shear strength ( $V$ ) and shear contribution of ETS system ( $V_f$ )

Beam ID	$P_{exp.}$ (kN)	$P_{num.}$ (kN)	Difference in load (%)	$V_{exp.}$ (kN)	$V_{num.}$ (kN)	$V_{f,Exp.}$ (kN)	$V_{f,Num.}$ (kN)
R1-0S-0ETS	171.8	176.0	2.44	103.1	104.6	NA	NA
R2-2Sd6-0ETS	223.4	220.0	1.52	134.0	132.0	NA	NA
R3-2Sd9-0ETS	344.4	347.1	0.49	207.2	208.3	NA	NA
A1-2Sd6-5Sd6(90)	253.0	266.0	4.14	151.8	159.6	NA	NA
A2-2Sd6-5Sd6(45)	334.1	343.8	2.60	201.1	206.3	NA	NA
A3-2Sd6-5ETS Steel d12(90)	422.2	451.1	6.85	253.3	270.7	119.3	138.7
A4-2Sd6-5ETS Steel d12(45)	510.5	536.1	4.01	306.3	321.7	172.3	189.7
B1-2Sd6-5ETS FRP d10(90)	453.9	443.7	2.25	272.3	266.2	138.3	134.2
B2-2Sd6-5ETS FRP d10(45)	481.5	472.5	1.87	288.9	283.5	154.9	151.5
B3-2Sd9-5ETS FRP d10(90)	514.2	534.1	3.86	309.1	321.1	101.9	112.8
B4-2Sd9-5ETS FRP d10(45)	589.9	598.3	1.42	353.9	359.0	146.7	150.7

#### 4.3.3.2 Cracking and failure mechanism

Figure 4.17 shows shear strain in XY plane of the simulated beams comparing to the actual shear cracking failure of the tested beams. It is obvious from Fig. 4.17 that the actual shear failure cracks are almost located in the zone with highest shear strain of the simulated specimens. Thus, it can be said that the FE method could predict well the shear failure region of a beams reinforced/strengthened in shear by steel and FRP bars. Similar to the experimental observation, all simulated beams are failed in shear due to the significant and wider shear cracks in shear cracking zone of the members; additionally the rupture of the ETS bars and the debonding of the ETS bars to concrete were not occurred as in the tested beams. Indeed, as observed in

Fig. 4.18(b), at the failure load the stress in ETS FRP bars and steel tension reinforcement did not reach rupture strength and yielding strength, while the existing steel stirrups yielded and the concrete in shear zone was heavily fractured (as shown in Fig. 4.17 that shear strain in XY plane exceeded ultimate value). Moreover, Fig. 4.18(a) compares the crack pattern propagation at load steps of a representative specimen R3, which was tested and was simulated using FE tool. Clearly, Fig. 4.18(a) reveals the good agreement in the crack propagation between the tested work and the simulated work. The major shear cracks initiated on the beam's web, midway between support and load point, then propagated toward both flange and support. After that, the crack reached the flange and triggered an immediate failure with a quasi-horizontal crack angle.

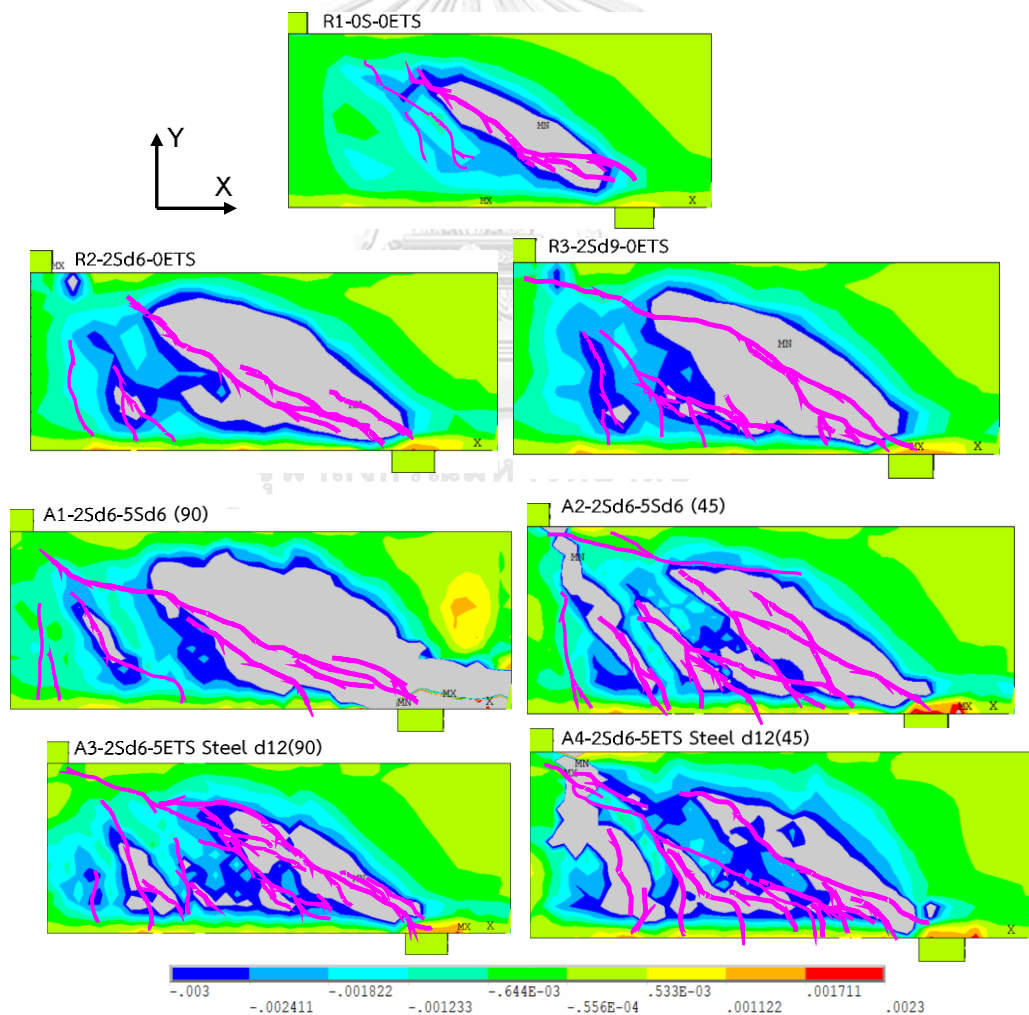


Figure 4.17 Shear strain in XY plane compared to tested shear failure cracks of analyzed specimens

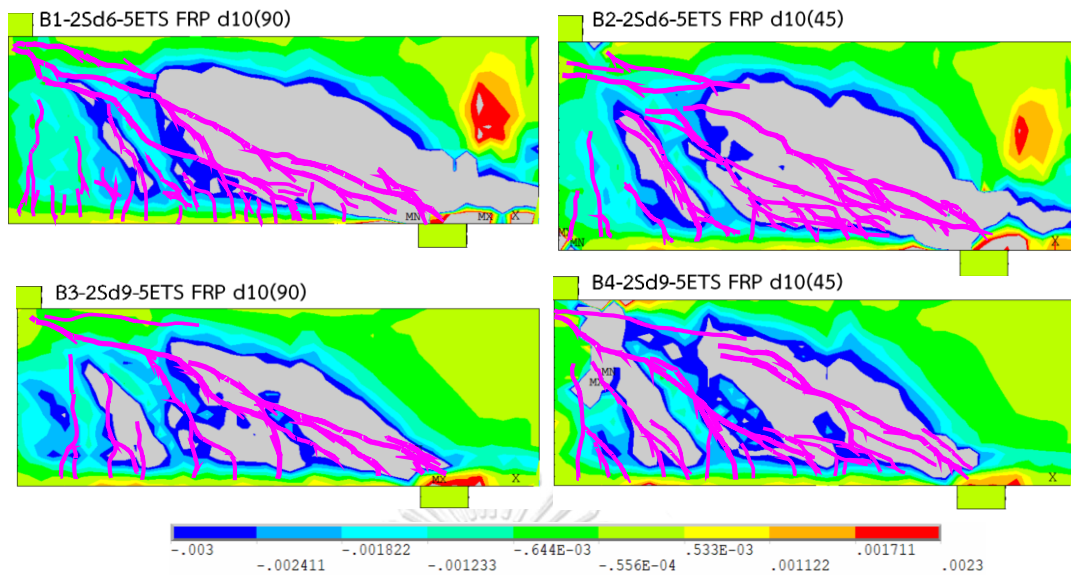


Fig. 4.17 (continued)

#### 4.3.3.3 Strain in shear reinforcement

Figure 4.19 shows the comparison between the measured data and numerical results in terms of the load-strain relationship of ETS bars of the investigated beams A3, B1, B2 and B3. The load-strain relationships in ETS bars derived from the simulation are well fitted with those in ETS bars recorded at the corresponding position of the test. Besides, also from Fig. 4.19 the load activating the ETS strengthening system in the FE simulation is generally lower than the force activating the ETS strengthening system in the experiment. Together with the experimental results, from Fig. 4.19 the numerical data indicates that for the same load, the strains in ETS GFRP strengthened bars (in B1) were greater than those of the ETS steel strengthened bars (in A3) due to the low Young's modulus of GFRP reinforcement. Additionally, for the beams with combined use of steel and ETS GFRP bars, the lower percentage of steel stirrups (B1) gives the higher strains of the ETS reinforcement under the same load in the comparison with the specimens with higher transverse steel ratio (B3) for the entire load range. This finding implies the shear resisting force of the ETS strengthened bars in the beams with the high amount of existing steel stirrups was smaller than the shear contribution of the ETS retrofitting system in the specimens with the less ratio of transverse reinforcement.

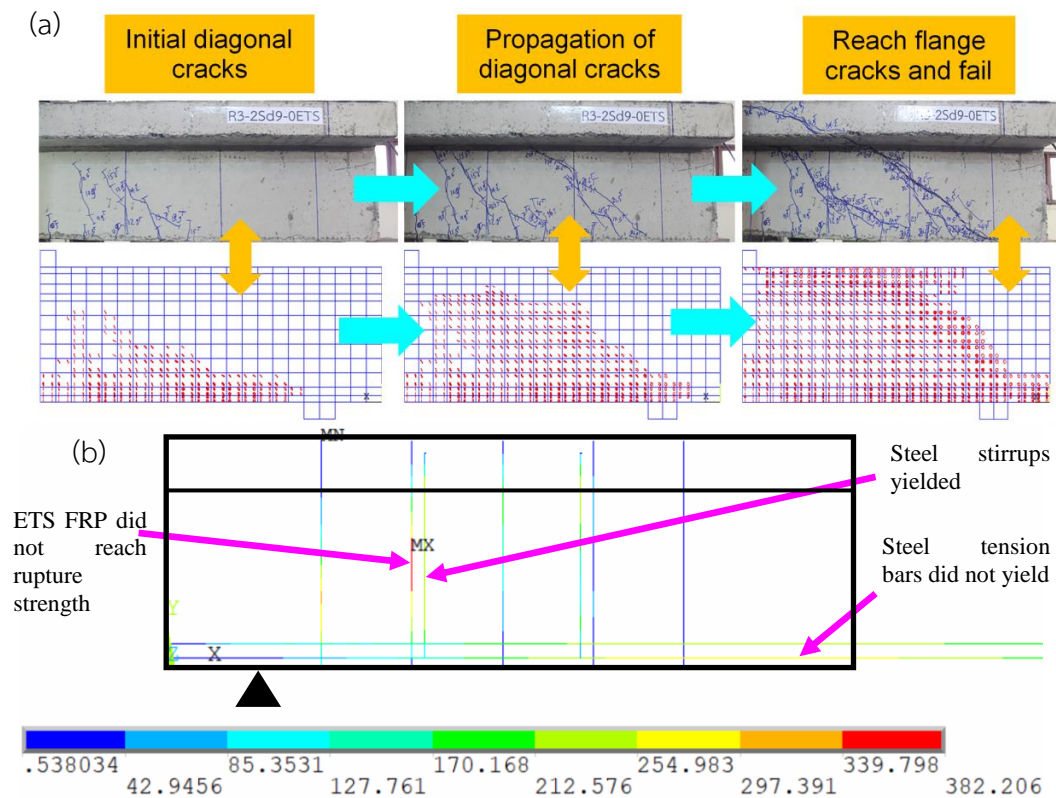


Figure 4.18 (a) Crack propagation in shear span of a representative beam R3: comparison between experimental and numerical results, (b) stress evolution at maximum load in reinforcement (ETS bars, stirrups, tension bars) of a representative beam B1

On the other hand, the strains in steel stirrups of the two beams A4 and B2 with different cases of ETS reinforcement (steel and GFRP) by means of the experiment and simulation are shown in Fig. 4.20(a). It is obvious that the FE results are fitted well with the measured data. Additionally, the same as the experimental observation, the strains determined by the FE simulation at the same position of the stirrups of the members A4 and B2 are similar at all points before yielding; therefore, the different ETS strengthening system types seemly do not affect the strain response of the existing transverse steel. Moreover, Fig. 4.20(b) indicates the good agreement in the comparison between tested data and simulated results in terms of the strains in the transverse reinforcement at the same location of the two beams B2, B3 and B4.

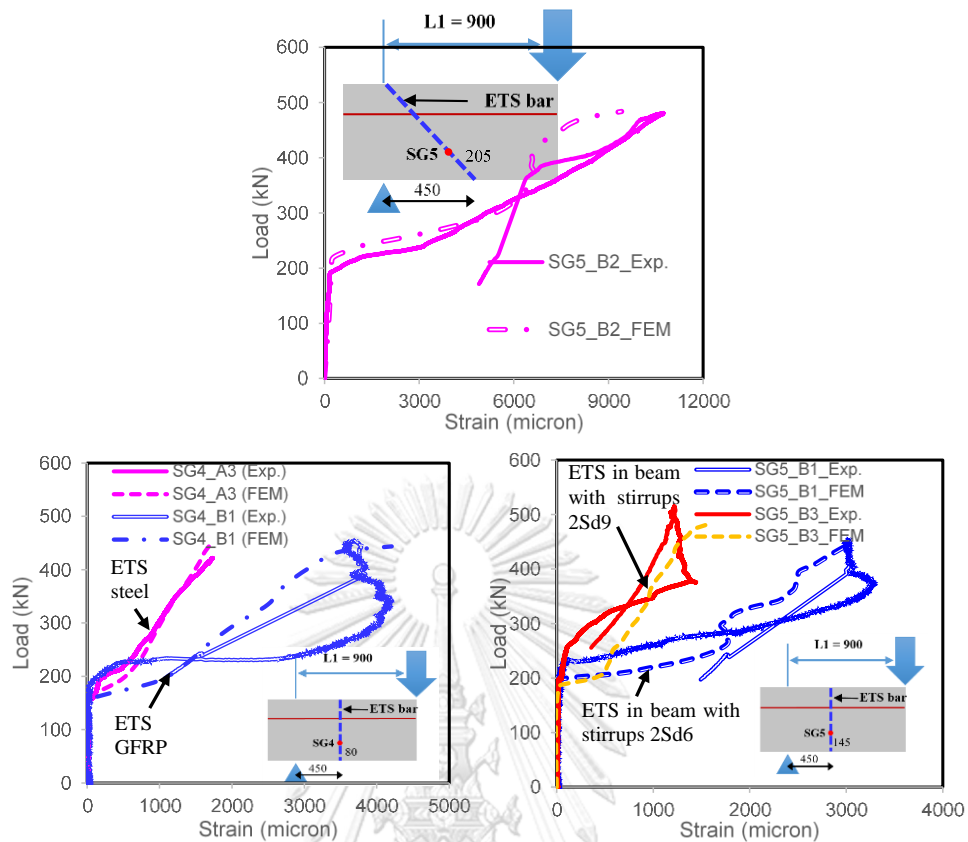


Figure 4.19 Comparison between measured and simulated data in terms of strain in ETS reinforcement

Considering the strain response of stirrups of the beams B2 and B4, the same as the results recorded from the experiment, the stirrups in these two analyzed specimens yielded before the beams failed and the strains in the transverse steel of 9 mm diameter are lower than that in the stirrup of 6 mm diameter for all the load range. Therefore, the shear resistance of the ETS bars is reasonably distributed with the steel stirrups of bigger bar size and this makes obviously the contribution of the ETS reinforcement in shear small. In addition, consider two beams B3 and B4 with the same existing steel stirrups and different inclinations of ETS bars, together with experimental results the strains defined by FE modelling at the same position (SG3) of the transverse steel of these specimens are similar for all the load range before yielding.

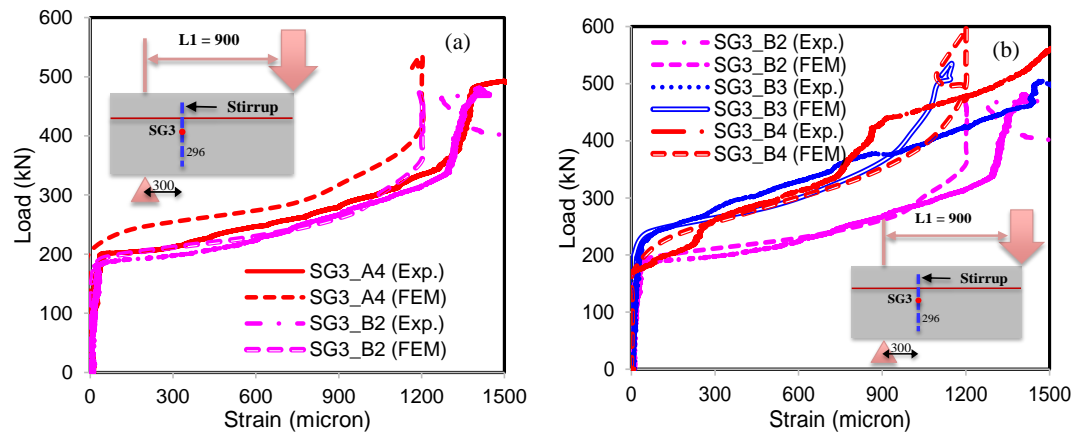


Figure 4.20 Comparison between measured and simulated data in terms of strain in steel stirrups

#### 4.4 Conclusions

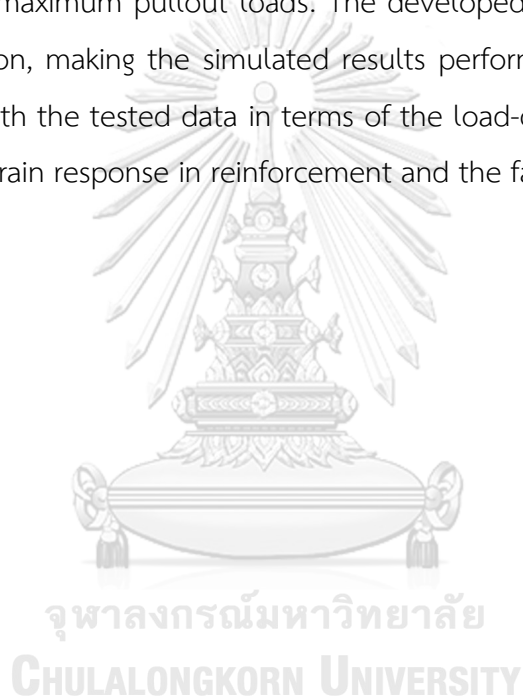
An experimental program to study the bond behavior between ETS steel/GFRP bars and concrete under various effects was carried out. Additionally, the bond model based on Dai et al.'s method was developed for analytically calculating and simulating the bond response between ETS GFRP bars and concrete. On the other hand, a FE program was developed to simulate the mechanical response of concrete beams reinforced/strengthened by internal reinforcement and ETS steel/GFRP bars. Based on the analyses, conclusions can be drawn as follows:

Before the mechanical anchorage being activated, the initial response of the specimen embedded by ETS bars with anchorage attachment is completely similar to the corresponding specimen embedded by ETS bars without anchorage. The specimen with mechanical anchorage presence results in the significantly higher maximum pullout force than that obtained by the test of the specimen without anchorage. In this study, the ultimate pullout force is much smaller than the ultimate tensile force ( $F_t$ ) based on GFRP tensile strength since the premature tension rupture at the anchorage was occurred.

In addition, the specimen with ETS GFRP bar diameter of 10 mm offered the lower ultimate pullout force and smaller maximum slip in the comparison with those of the specimen with ETS GFRP bar diameter of 8 mm. For the effect of ETS type, the tested

results reveal that the concrete block embedded by ETS steel bar offered higher pullout force compared to the specimen embedded with ETS GFRP rod. The longer anchorage length (or more anchoring nuts) resulted in the higher pullout force than that of the specimen with the short anchorage length. The specimen C8 with short anchored ETS bar failed by the pullout of the ETS bar leaving the nuts in concrete, implying the two nuts are not enough to assure the full tension capacity of ETS GFRP bar.

By developing the bond model based on Dai et al.'s method, the good agreement is obtained in the comparison between the analytical maximum pullout forces and the experimental maximum pullout loads. The developed bond model was applied in the FE simulation, making the simulated results performed the good appraisal in the comparison with the tested data in terms of the load-carrying capacity, the crack mechanism, the strain response in reinforcement and the failure mode.



## Chapter 5 DUCTILITY OF CONCRETE BEAMS REINFORCED WITH BOTH FIBER-REINFORCED POLYMER AND STEEL TENSION BARS

### 5.1 Introduction

Since fiber-reinforced polymer (FRP) reinforcement requires an expensive material, the partial replacement of steel reinforcement by FRP reinforcement is economically feasible. To prevent the corrosion of steel reinforcement in the reinforced concrete (RC) beams in aggressive environments, the most external reinforcement (closest to the concrete surface) could be replaced by FRP reinforcement. Therefore, concrete beams reinforced by both steel and FRP reinforcements have been considered an interesting topic for experimental and numerical research.

The experimental studies of Aiello and Ombres (2002), Qu et al. (2009), Lau and Pam (2010), Ge et al. (2015) and Yoo et al. (2016) were conducted to investigate deflection, curvature, ductility, crack width of concrete beams with hybrid usage of FRP and steel tension reinforcement. Their studies indicated that the hybrid usage of steel and FRP reinforcement was more advantageous in the consideration of deformability than the use of steel reinforcement. Generally, adding conventional steel bars could improve the flexural ductility of hybrid FRP-steel RC members. In another aspect, the crack width and spacing values were decreased with the presence of steel reinforcement in comparison with the crack width and spacing attained by beams reinforced with only FRP bars. The average crack spacing of the hybrid FRP-steel RC beams was in the middle of the average crack spacing of the steel RC beams and FRP RC beams.

Aiello and Ombres (2002) showed that using the moment-curvature law could accurately predict the behavior of concrete beams reinforced by steel and FRP bars, and the American Concrete Institute (ACI) code furnished a good prediction of the deflections and crack width in the serviceability phase. Aiello and Ombres (2002) also offered a design model to determine the effective moment of inertia for steel RC beams and FRP RC beams based on the calibration of the experimental results.



However, Qu et al. (2009) adopted the model of Bischoff (2007), which was initially studied by Branson (1977), to calculate the deflection of concrete beams reinforced with glass fiber-reinforced polymer (GFRP) and steel bars at the service load level.

By conducting an experimental and theoretical program, Qu et al. (2009) and Lau and Pam (2010) discovered that the use of steel reinforcement in combination with GFRP bars enhanced the flexural performance of GFRP RC beams. The studies by Qu et al. (2009) and Ge et al. (2015) proposed equations to compute the flexural moment capacity and strength of FRP bars for hybrid FRP-steel RC beams. The axial stiffness ratio between GFRP and steel bars had little influence on flexural capacity, whereas the effective reinforcement ratio was a reasonable parameter for evaluating the ultimate moment of hybrid FRP-steel RC beams. For the failure mode prediction of hybrid FRP-steel RC beams, the balanced effective reinforcement ratio could be employed. Based on the results of Lau and Pam (2010), the requirements for the minimum GFRP flexural reinforcement given by the ACI code could be reduced by approximately 25%.

Together with the experimental program, the numerical and analytical investigations such as Faza and GangaRao (1993), Tan (1997), Zhang et al. (2012), Kara et al. (2015, 2016), Hawileh (2015), Oller et al. (2015), Yoo and Banthia (2015), Bencardino et al. (2016), Zhang et al. (2016) and Qin et al. (2017) were conducted to propose the design method for concrete beams reinforced/strengthened by both FRP and steel tension reinforcement, and determining the curvature, deflection, ductility and moment capacity of hybrid FRP-steel RC beams. Most of those studies showed good agreement of the numerical and analytical results in the comparison with the experimental results. However, several important parameters were not studied in the past experiments and the previous FE simulations. The ductility evaluation of the hybrid FRP-steel RC beams is limited because of the lack of the research data and has not achieved the high reliability. This study, therefore, presents a numerical investigation on the structural behavior of concrete beams reinforced with FRP-steel bars under various conditions. The main contents of this study are as follows: (1) FE simulation of beams with hybrid usage of FRP and steel reinforcement, with experimental data available to show the reliability of FE

simulation results, (2) the parametric study by the FE simulation on ductility of beams reinforced with both FRP and steel tension reinforcement, and (3) the ductility analysis with ductility index to show feasible hybrid use of FRP-steel tension reinforcement.

## 5.2 Experimental data to validate the finite element (FE) models

The data in the experimental program of Aiello and Ombres (2002), Qu et al. (2009), Lau and Pam (2010) were adopted to verify the FE models. Aiello and Ombres (2002) presented an experimental investigation of five concrete beams ( $150 \times 200 \times 3000 \text{ mm}^3$ ) reinforced by both aramid fiber-reinforced polymer (AFRP) and steel reinforcement. One beam was reinforced by only AFRP bars, another one was reinforced with only steel reinforcement, and three others were reinforced with a hybrid AFRP-steel reinforcement. Four-point flexural loading tests were conducted on the beams. All the beams used the two steel bars of 8 mm diameter as the compression reinforcement, and transverse reinforcement with 8 mm diameter and 100 mm spacing were employed as shear reinforcement. More details of the beams investigated in this study are shown in Fig. 5.1 and Table 5.1.

Qu et al. (2009) studied the flexural behavior of concrete beams reinforced with both GFRP and steel bars. This research employed eight concrete beams ( $180 \times 250 \times 1800 \text{ mm}^3$ ), including two control beams reinforced with only steel or only GFRP bars, and six hybrid FRP-steel RC beams. All beams used two steel bars of 10 mm diameter as the compression reinforcement as well as steel stirrups with 10 mm diameter and 100 mm spacing. A four-point flexural loading test was conducted. In the following year, Lau and Pam (2010) studied the twelve specimens, simply supported and subjected to a point load at midspan, including plain concrete beams, steel-reinforced concrete beams, pure GFRP RC beams, and hybrid GFRP-steel RC beams. The two steel bars of 6 mm diameter were employed as the compression reinforcement, steel stirrups with 8 mm diameter and 50 mm spacing at the two ends of beams and 100 mm spacing at the rest of beams were applied as

shear reinforcement. Figures 5.2 and 5.3 and Table 5.1 show the more details of the beam specimens, which are investigated in the present study.

Table 5.1 The properties of the tested beams

Study	Beam ID	$A_s$ (mm <sup>2</sup> )*	$A_f$ (mm <sup>2</sup> )*	$\rho_r = A_f/A_s$
Aiello and Ombres (2002)	A1	100.6 (2d8)	88.4 (2d7.5)	0.8789
	A2	100.6 (2d8)	157.1 (2d10)	1.5625
	A3	226.2 (2d12)	235.6 (3d10)	1.0417
Qu et al. (2009)	B1	452.2 (4d12)	-	-
	B2	-	505.5 (4d12.7)	-
	B3	225.1 (2d12)	253.2 (2d12.7)	1.1201
	B4	201.1 (1d16)	395.9 (2d15.9)	1.9751
	B5	402.2 (2d16)	141.7 (2d9.5)	0.3525
	B6	402.2 (2d16)	253.2 (2d12.7)	0.6301
	B7	113.1 (1d12)	141.7 (2d9.5)	1.2535
	B8	12056.6 (6d16)	395.9 (2d15.9)	0.3292
Lau and Pam (2010)	G0.6-T1.0-A90**	981.8 (2T25)	567.1 (2G19)	0.5776
	G1.0-T0.7-A90**	628.4 (2T20)	981.8 (2G25)	1.5625
	G0.3-MD1.0-A90**	981.8 (2MD25)	283.5 (1G19)	0.2888

\* $A_s$  and  $A_f$ : The area of the steel and AFRP tension reinforcement, respectively

\*\*MD, T, G, and A90: The mild steel, high yield steel, GFRP reinforcement, and 90° hook angle in stirrups respectively

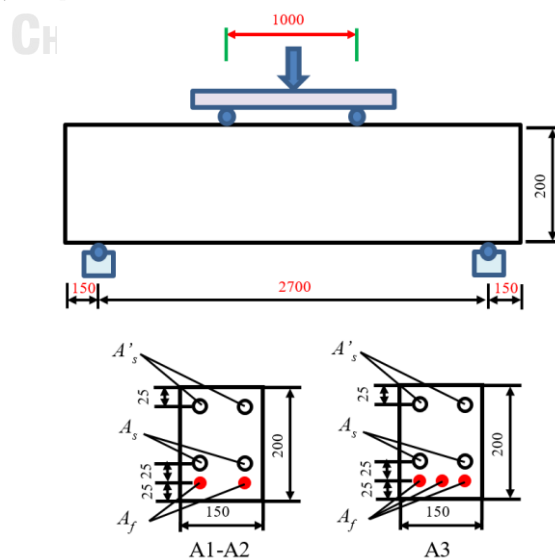


Figure 5.1 Geometrical dimension of the tested beams (Aiello and Ombres 2002)

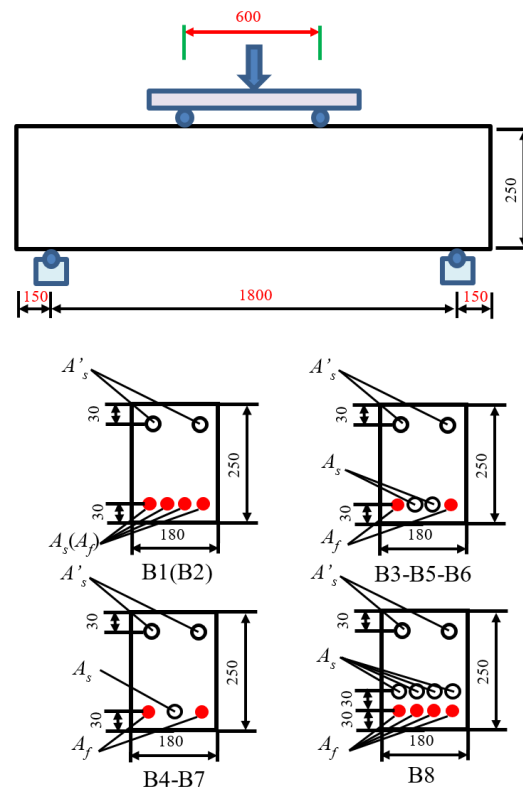


Figure 5.2 Geometrical dimension of the tested beams (Ou et al. 2009)

Table 5.2 The mechanical properties of materials

Study	Beam ID	$f'_c$ (MPa)	$f_y$ (MPa)	$f_{fu}$ (MPa)	$E_f$ (MPa)	$\rho_s$ (%)	$\rho_f$ (%)
Aiello and Ombres (2002)	A1	38	558	1674	49000	0.335	0.294
	A2	38	558	1366	50100	0.335	0.523
	A3	38	558	1366	50100	0.754	0.785
Ou et al. (2009)	B1	30.95	363	NA	NA	1.142	NA
	B2		NA	782	45000	NA	1.280
	B3	33.10	363	782	45000	0.571	0.640
	B4		336	755	41000	0.508	1.003
	B5	34.40	336	778	37700	1.015	0.358
	B6		336	782	45000	1.015	0.640
	B7	40.65	363	778	37700	0.286	0.358
	B8		336	755	41000	3.269	1.076
Lau and Pam (2010)	G0.6-T1.0-A90	44.6	550	588	39500	0.923	0.533
	G1.0-T0.7-A90	39.8	597	582	38000	0.591	0.923
	G0.3-MD1.0-A90	41.3	336	588	39500	0.923	0.266

Each study is indicated: beam ID, concrete compressive strength ( $f_c'$ ), steel yielding strength ( $f_y$ ), ultimate strength and elastic modulus of FRP reinforcement ( $f_{fu}$ ,  $E_f$ ), reinforcement content of steel and FRP bars are  $\rho_s$  and  $\rho_f$ , respectively.

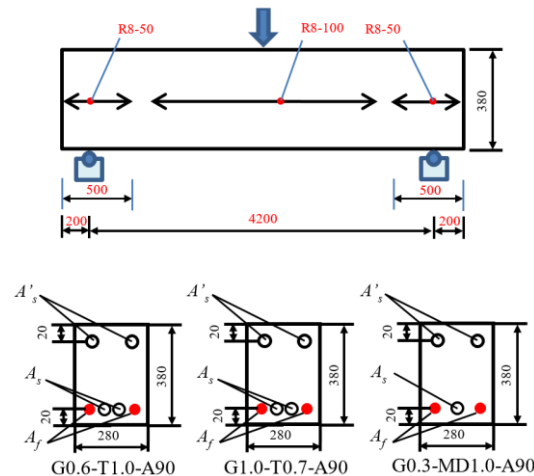


Figure 5.3 Geometrical dimension of the group tested beams (Lau and Pam 2010)

### 5.3 Validation of three-dimensional (3D) finite element (FE) models

#### 5.3.1 Finite element program

In this study, numerical analyses were conducted by a commercially available software, ANSYS 15.0. A quarter FE model was applied to investigate the performance of the tested beams based on the symmetrical condition as shown in Fig. 5.4. For this investigation, the mesh discretization is  $10 \times 10 \text{ mm}^2$ . In addition, the descriptions of the element types and material models for the FE program follow from the previous work (Linh et al. 2017) of the authors of the present study.

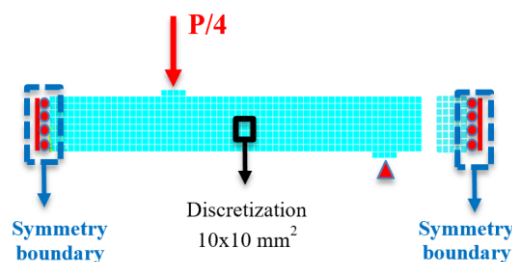


Figure 5.4 A quarter typical FE model for numerical program by using ANSYS 15.0

### 5.3.1.1 Element types

SOLID65, LINK180 and SOLID45 are used as the ANSYS 15.0 elements for nonlinear 3D modelling of concrete materials, reinforcement and elastic steel support, respectively. The SOLID65 element is capable of modelling of concrete cracking in tension and crushing in compression. The SOLID65 element is also defined by eight nodes, and each node has three degrees of freedom that are the translations in the nodal x, y, and z directions (Linh et al. 2017). However, LINK180 is a uniaxial tension-compression element with three degrees of freedom at each node that are the translations in the nodal x, y, and z directions (Linh et al. 2017). In addition to SOLID45, which is applied to model the supporting and loading plates, the software that is used for the three-dimensional modelling of solid structures and the definition of the SOLID45 element is similar to that of the SOLID65 element except for the capability of cracking in tension and crushing in compression (Hawileh 2015, Linh et al. 2017). The perfect bond behavior between reinforcement and concrete is assumed in the FE models.

### 5.3.1.2 Material models

Various constitutive models have been employed in FE simulations of hybrid FRP-steel RC beams to describe the behavior of concrete under a wide range of complex stress and strain histories. These models included nonlinear elastic models and plasticity-based models whether perfect plasticity models or elastic-plastic models (Godat et al. 2012). In this study, the model of Hognestad et al. (1955) is adopted to simulate the nonlinear response of concrete in compression. Equation (5.1) and Figure 5.5(a) show more details of the Hognestad et al. (1955) parabola.

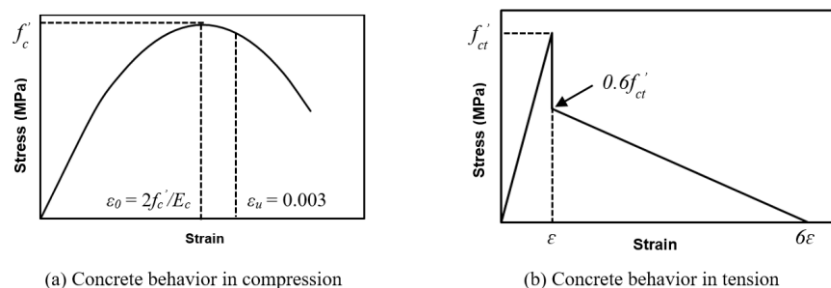


Figure 5.5 Models of concrete in compression and tension

$$f_c = f_c' \left[ 2 \left( \frac{\varepsilon}{\varepsilon_0} \right) - \left( \frac{\varepsilon}{\varepsilon_0} \right)^2 \right] \quad (5.1)$$

where

$f_c$  is the compressive stress of the concrete (MPa) corresponding to the specified strain,  $\varepsilon$ ,

$f_c'$  is the concrete compressive strength (MPa),

$\varepsilon_0 = \frac{2f_c'}{E_c}$ , and  $E_c$  is the elastic modulus of the concrete (MPa).

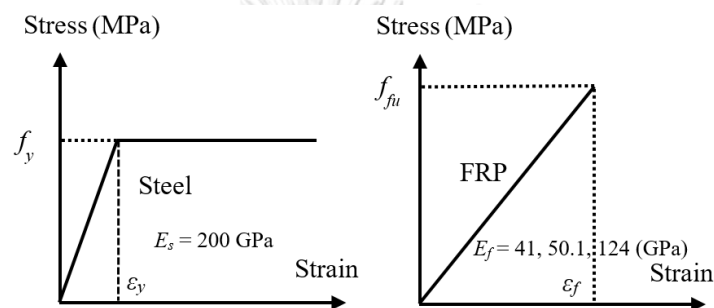


Figure 5.6 Stress-strain relationships of steel and FRP reinforcement

Linh et al. (2017) showed the concrete behavior in tension according to the model of William and Warnke, which was recommended by the ANSYS software. Figure 5.5(b) shows the stress-strain relationship of concrete under tension. At first, the linear elasticity to the concrete tensile strength is used for concrete behavior in tension. Then, a steep drop in the concrete tensile stress by 40% is the stress relaxation in tension. The rest of model is represented as the curve that descends linearly to zero tensile stress at a strain value six times larger than strain value at the concrete tensile strength (Hawileh 2015). On the other hand, the steel reinforcement is described as the elastic fully plastic model based on the von Mises yield criterion, while the FRP bars are simulated as elastic-brittle materials until rupture. Figure 5.6 shows the stress-strain relationships of steel and FRP reinforcement that are applied in the FE simulations. Moreover, the mechanical properties of concrete, steel, and FRP reinforcement of all the investigated beams taken from the above three past studies shown in Table 5.2.

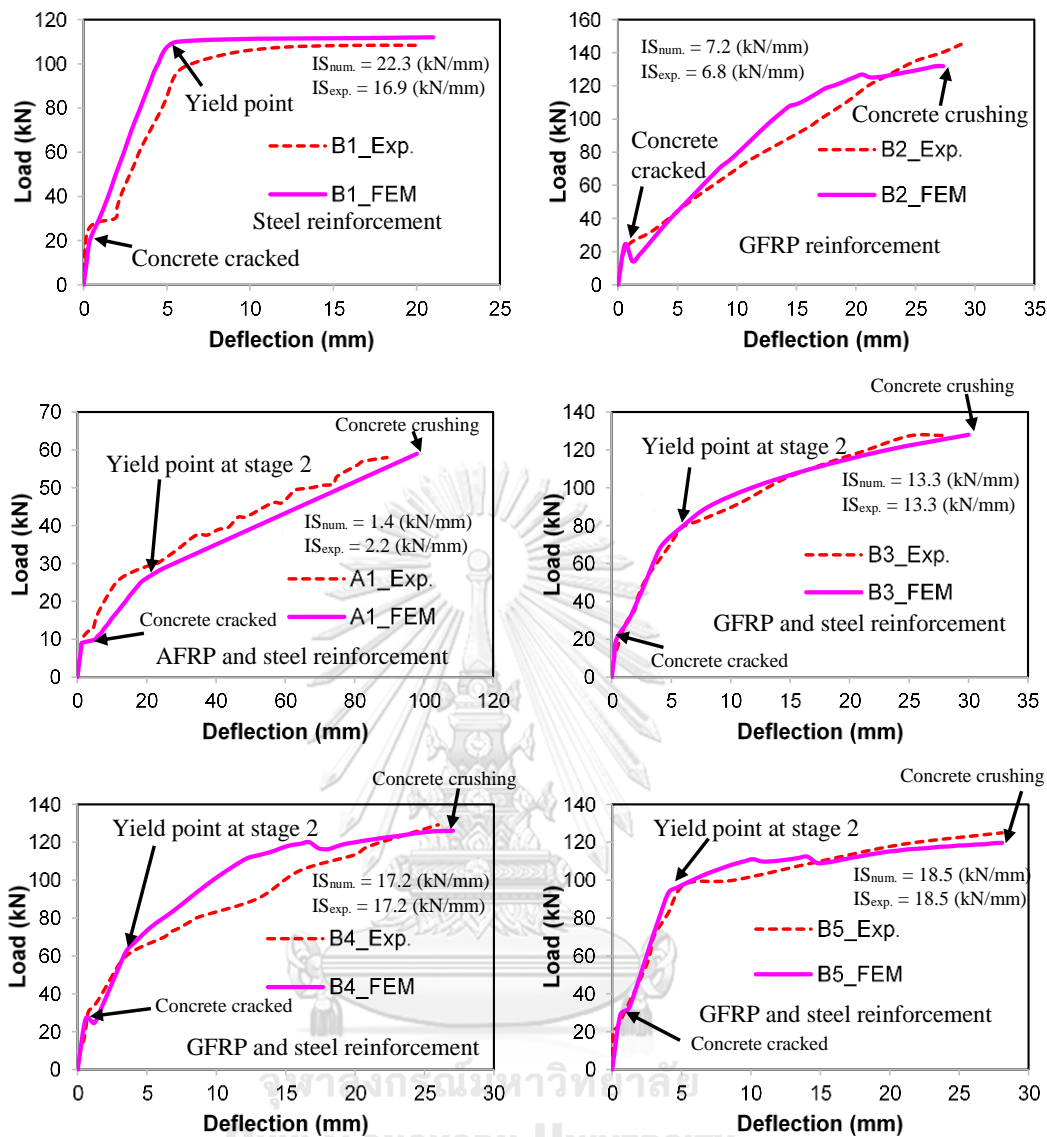


Figure 5.7 Comparison of load-midspan deflection relationship between the tested and FE results: the first two specimens are steel and FRP RC beams, respectively, and the remaining specimens are hybrid beams



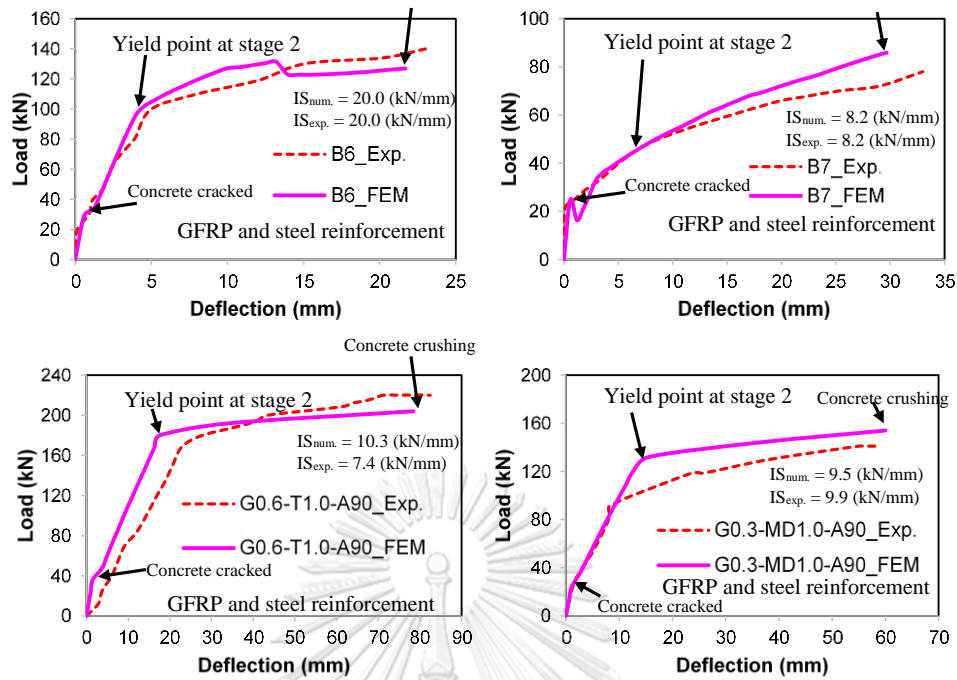


Fig. 5.7 (continued)

### 5.3.2 Results and discussion

To verify the reliability of the FE method, the concrete beams reinforced by steel, FRP, and steel-FRP tension reinforcements in Section 5.2 were simulated, and the simulation results are investigated. The failure definition of beam specimens in the FE analysis is, after steel yielding, either the stress in FRP reinforcement reaching their rupture strength or the concrete compressive strain exceeding 0.003. The structural performances of the hybrid FRP-steel RC beams in terms of load-deflection response and failure modes of the FE models are compared with the results obtained from the corresponding experimental data. In addition, the stress of reinforcement and crack propagation at the load steps of a representative beam B3 are also described.

Figure 5.7 shows the load-midspan deflection curves of experimental and simulated results for the ten beam specimens with the one steel RC beam, one pure FRP RC beam, and eight hybrid FRP-steel RC beams. It is explicit that the FE results attain the good appraisal in the comparison with the tested data, and a maximum

deviation less than 10% not only in the load-carrying capacity but also in the displacement is easily found from Fig. 5.7 and Table 5.3. On the other hand, Fig. 5.8 and Fig. 5.9 show the stress distribution and cracking pattern in the hybrid FRP-steel RC beam (B3) as an example. In general, the load-displacement curves from the FE analysis are slightly stiffer than the load-displacement curves from the experimental results. One of the reasons is the perfect bond assumption between reinforcement and concrete in the FE model. The effects of the concrete shrinkage, which may cause cracking, are not considered in the simulation, which is possibly another cause of this overestimated stiffness. On the other hand, by using FRP bars, the load-carrying capacity of the hybrid FRP-steel RC beam increases because the FRP strength is higher than that of steel, and the overall beam behavior changes to be more brittle due to the lack of plasticity of FRP. As shown in Table 5.3, the simulated beams fail in the concrete crushing after steel yielding, and this failure mode is also indicated in the experimental program in the literature. Evidence for this statement is shown in Fig. 5.8(a), in which the stress of the FRP bar in the beam B3 is less than the rupture values. Similarly, at the ultimate load, the steel reinforcement yields (Fig. 5.8(b)) and after the diagonal cracking zone is formed (Fig. 5.8(d)), the concrete is crushed (Figs. 5.8(c), (d) and Fig. 5.9). All beams in this investigation are designed to fail upon the concrete crushing; therefore, the strength in the FRP bars is reserved, and plastic deformation of the concrete is allowed. As seen in the experimental and numerical comparison (Fig. 5.7), since the load applied to the beam after steel yielding is all taken up by the FRP reinforcement and the concrete, the slopes of the curves before and after steel yielding of the hybrid FRP-steel RC beams change more gradually.

Furthermore, the crack propagation at the applied load stages and the general response of the concrete beams with the hybrid use of FRP and steel reinforcement are exhibited in Fig. 5.9 and Fig. 5.10, respectively. Figure 5.9 shows the zones where specific cracking takes place, which are represented by a circle that appears when a principal tensile stress exceeds the ultimate tensile strength of the concrete. In stage 1, tensile concrete is cracked, and the steel and FRP reinforcement are beginning to activate under the increase in the applied load (as shown in Fig. 5.7). Then, the

concrete cracking zone propagates vertically and then horizontally to the two ends of the beams. As demonstrated in Fig. 5.10, until the steel reinforcement yields, FRP reinforcement works slightly. This is the behavior of hybrid FRP-steel RC beams at the end of stage 2, and the yielding point of each analyzed specimen is also presented in Fig. 5.7. In stage 3, in which the steel reinforcement yields, FRP is significantly activated, and concrete is crushed in the compression zone, resulting in the failure of the hybrid FRP-steel RC beam (as indicated in Fig. 5.7). In addition, from Fig. 5.11, the FE investigation of the strain distribution through the depth at the middle section of beams B5, B6 and B7 demonstrates a good agreement with the strain distribution through the depth at corresponding section of those specimens measured in the experiment. Obtained results from the comparison imply that the assumption of the plane cross section was still effective for concrete beams with hybrid use of steel and FRP tension reinforcement, because the strain distribution in concrete and longitudinal reinforcement were nearly proportional to the distance from the neutral axis.

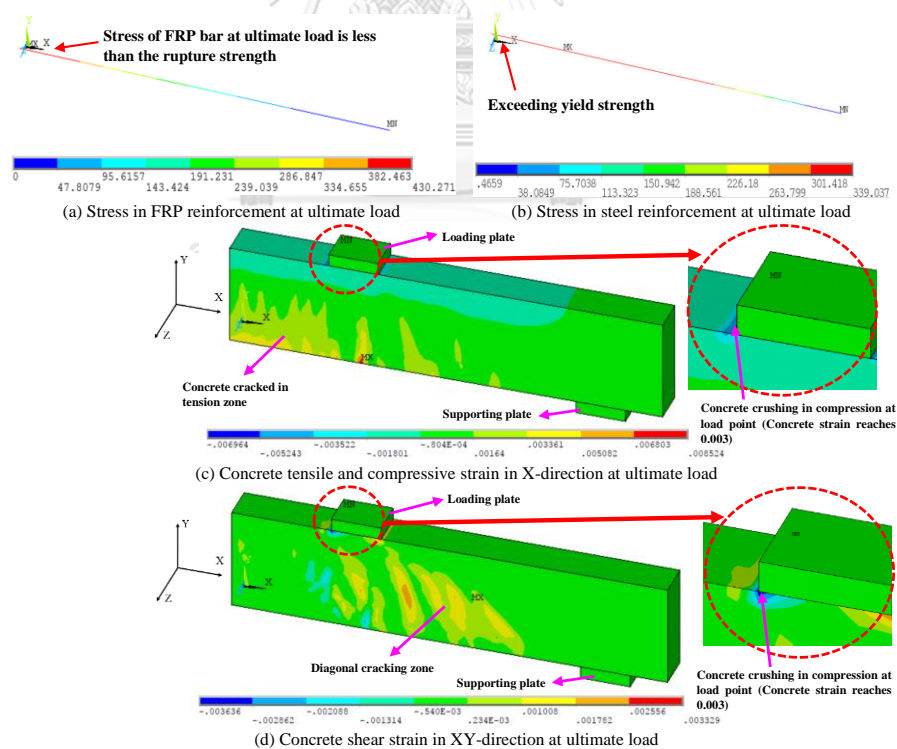


Figure 5.8 Stress in FRP bar, stress of steel reinforcement, and concrete strain at ultimate load of the representative hybrid beam B3

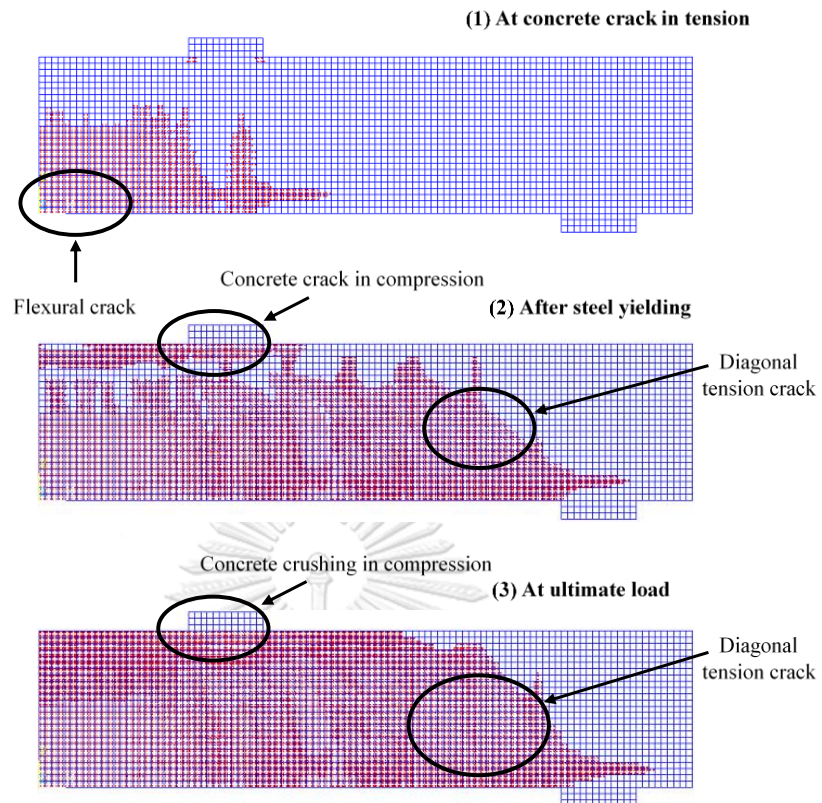


Figure 5.9 Crack propagation under the load stages of the representative hybrid FRP-steel RC beam B3

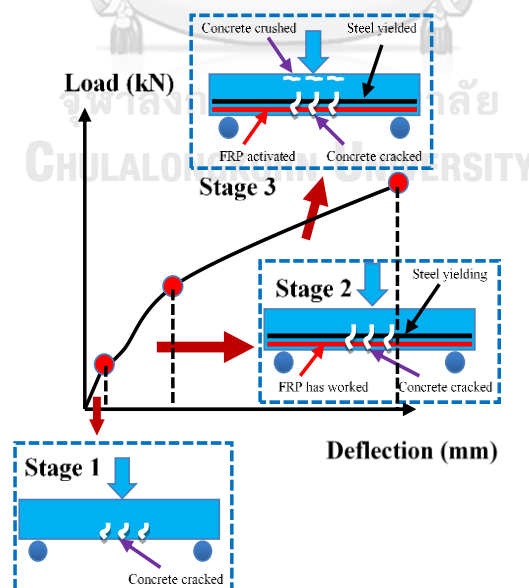


Figure 5.10 General behavior of hybrid beams

Table 5.3 Experimental and numerical results on load carrying capacity, absorption energy and failure mode

Authors	Beam ID	$P_{exp.}$ (kN)	$P_{num.}$ (kN)	Difference in load (%)	$\rho_r =$ $A_p/A_s$	Failure mode	
		(Absorption energy (kNmm))	(Absorption energy (kNmm))			Experiment	Simulation
Aiello and Ombres (2002)	A1	58 (3515.0)	59 (3658.6)	1.72	0.8789	SY-CC*	SY-CC
	B1	108 (1815.9)	112 (2075.6)	3.70	-	SY-CC	SY-CC
	B2	145 (2520.9)	132 (2449.1)	8.97	-	CC	CC
Qu <i>et al.</i> (2009)	B3	127 (2669.4)	128 (2937.3)	0.79	1.1201	SY-CC	SY-CC
	B4	129 (2330.8)	126 (2602.0)	2.33	1.9751	SY-CC	SY-CC
	B5	125 (2864.8)	120 (2888.4)	4.00	0.3525	SY-CC	SY-CC
	B6	140 (2512.3)	127 (2365.3)	9.29	0.6301	SY-CC	SY-CC
	B7	78 (1892.4)	85 (1777.5)	8.97	1.2535	SY-CC	SY-CC
Lau and Pam (2010)	G0.6-T1.0- A90	220 (13920.6)	204 (13575.4)	7.27	0.5776	SY-CC	SY-CC
	G0.3- MD1.0- A90	141 (6505.0)	154 (7608.9)	9.22	0.2888	SY-CC	SY-CC

\*SY and CC: The steel yielding and concrete crushing, respectively

CHULALONGKORN UNIVERSITY

To further validate the simulated results with the tested data, consider the analyzed beams in terms of the absorption energy, which is defined as the area under the load-displacement diagrams and is shown in Table 5.3. The energy values computed by the numerical results are close to the absorption energy values calculated from the experimental data. In addition, it is also obvious from Fig. 5.7 that the initial stiffness (IS), which is estimated by the ratio of load to deflection at the yield point, of the investigated beams computed from experimental data is close to the values of the initial stiffness calculated from the numerical results. Observing the trend of the values of the initial stiffness in Fig. 5.7, the initial stiffness of the specimens is governed by the reinforcement ratio of  $A_p/A_s$ . The lower hybrid

reinforcement ratios  $A_f/A_s$  result in the higher initial rigidity, and the beam reinforced with single steel tension bars provides the highest stiffness. Moreover, the trend of the absorption energy values presented in Table 5.3 implies that the ductility of the beams reinforced by steel and FRP tension bars is also decided by the reinforcement ratio  $A_f/A_s$ . The use of the low ratio of FRP to steel ( $A_f/A_s$ ) results in the higher absorption energy, therefore the beams with small hybrid reinforcement ratio offer the enhancement of the ductility and initial rigidity of the hybrid FRP-steel beams in the comparison with the beams reinforced by FRP bars. However, specific reinforcement ratios  $A_f/A_s$  used to show the feasibility of the hybrid FRP-steel RC beams compared with the steel RC beams could not be proposed in this section due to the lack of analytical data. Thus, to obtain the deep understanding on the effect of reinforcement ratio  $A_f/A_s$  on the structural response and the ductility of concrete beams reinforced with FRP and steel tension bars, the parametric study for this ratio should be carried out.

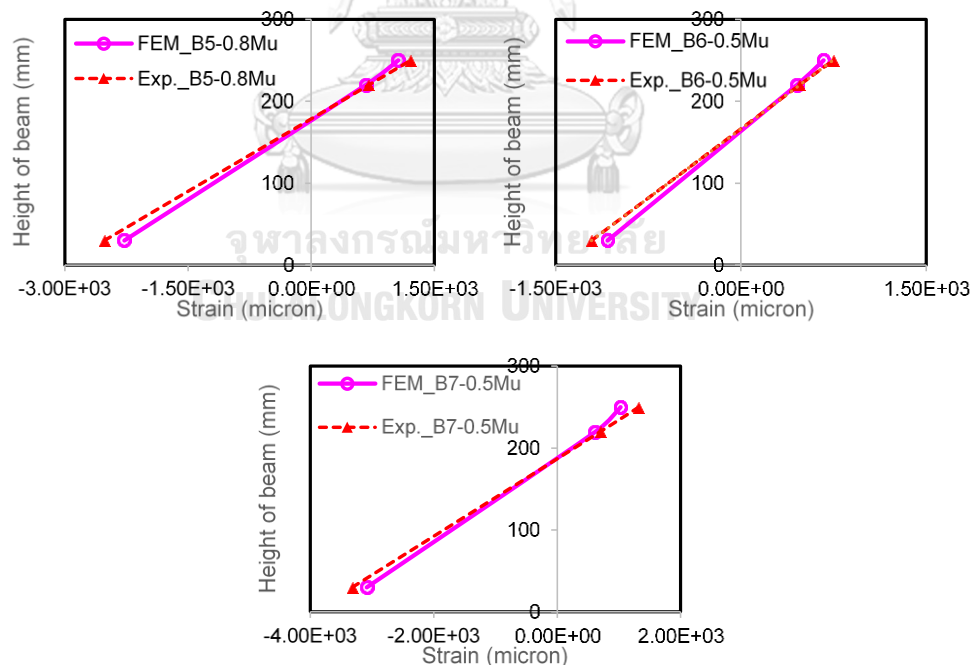


Figure 5.11 Comparison between tested and simulated results in strain distribution

In conclusion, the FE method is an effective tool to accurately predict various features, including the load-deflection relationship, stress evolution in FRP and steel reinforcement, failure mode, strain distribution and crack propagation of concrete beams reinforced with both steel and FRP tension reinforcements. In addition, the stiffness of the concrete beams reinforced with FRP-steel bars is well assessed through the FE simulation. Moreover, the ductility evaluation of the hybrid FRP-steel RC beams by means of absorption energy is also feasible through the FE simulation.

#### 5.4 Parametric study by means of the finite element (FE) analysis

The reliability of FE simulations for the hybrid FRP-steel RC beams has been confirmed in Section 5.3. Therefore, the extensive FE model specimens with various parameters have been prepared making beam specimen B4 the reference specimen. The objective of this Section is to extend and enhance the discussion on how to improve the member ductility by providing optimum parameters.

##### 5.4.1 Design of parametric investigation

The investigated parameters are the reinforcement ratios together with the concrete compressive strength and the FRP types, and the arrangement of the tension reinforcement. To consider the effect of the reinforcement arrangement, the FE models B4\_Diff. level with the FRP bars in the outer layer of two layers of tension reinforcement are created to compare with the original B4\_Same level (FRP bars in one layer of reinforcement) evaluated in Section 5.3. For the FE models of the beam B4 with different levels, the vertical spacing from the center of FRP bars to the center of the steel bars is changed with the values of 10 mm, 20 mm and 30 mm. To consider the safety requirement, the four beams with the different gaps ( $a = 0, 10, 20, 30$  mm) between FRP and steel bars are designed with the same flexural strength of 140 kN, as shown in Table 5.4 and Fig. 5.12(a).

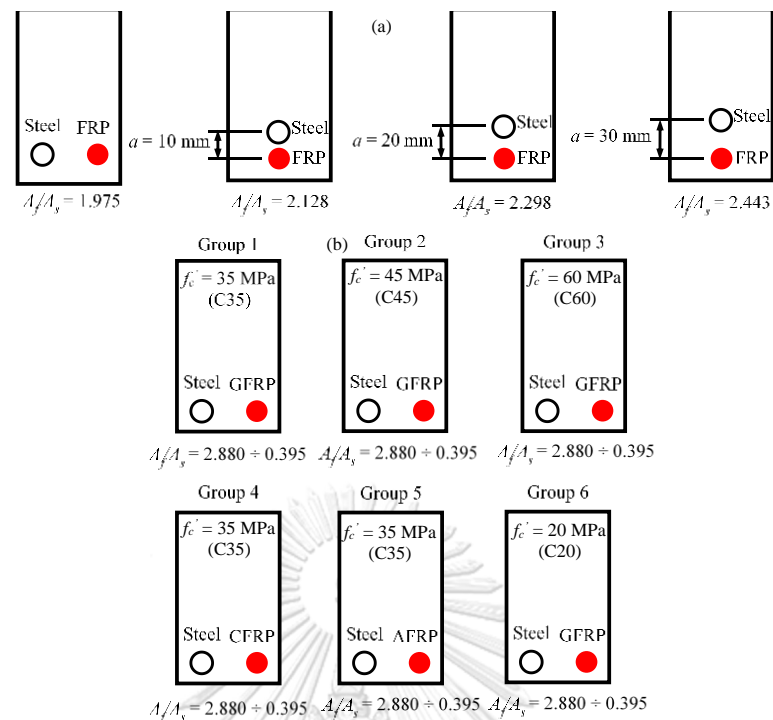


Figure 5.12 (a) Reinforcement arrangement cases, and (b) cases of reinforcement ratios among concrete compressive strength and FRP types (each group has a steel RC beam with the same flexural capacity design)

On the other hand, the designed beams for the parametric study on the influences of the reinforcement ratios together with the concrete compressive strength and the FRP types are described in Table 5.4 and Fig. 5.12(b). The load-carrying capacities by bending theory of the beams in each group are similar, and the values of 140 kN, 160 kN, 190 kN, 150 kN, 145 kN, and 110 kN are computed for the flexural capacities of the beam specimens in the groups 1, 2, 3, 4, 5, and 6 respectively. Furthermore, to investigate the effect of FRP types on the flexural performance of hybrid FRP-steel beams, the three beam specimens B4\_G1\_R8 (proposed FRP), B4\_G4\_R8 (CFRP) and B4\_G5\_R8 (AFRP) are designed for group 1, group 4 and group 5 with the same flexural strength as the beam B4\_G1\_R2 (GFRP) in group 1. Groups 1-3 and 6 are designed to investigate the effects of the hybrid reinforcement ratio for four cases of the concrete compressive strength. According to the ACI code (ACI 211.1-91), the concrete compressive strengths are selected with



practical values of 20 MPa, 35 MPa, 45 MPa and 60 MPa. Groups 1, 4, 5 are employed to investigate the effects of the hybrid reinforcement ratio for three types of FRP reinforcement. In addition, the failure mode of all beams in Table 5.4 is the concrete crushing in which the compressive strain exceeds 0.003, after steel yields.

#### 5.4.2 Effect of reinforcement ratios among concrete compressive strength and FRP types

In Figs. 5.13(a), (b), (c), (d) and Figs. 5.14(a), (b), there is a clear correlation between the load-deflection performance and the reinforcement ratio. In general, it is obvious from the aforementioned figures and Table 5.4 that the mechanical performances of the ductility, absorption energy and initial stiffness of the reference steel RC beams are better than those of the hybrid FRP-steel RC beams. In the hybrid FRP-steel beams, FRP tension reinforcement is employed to take up the flexural strength while the steel reinforcement is mainly responsible for improving the ductility requirement. As displayed in Table 5.4 and drawn in Fig. 5.17, the values of absorption energy of the simulated beams generally increase as the hybrid reinforcement ratios ( $A_f/A_s$ ) decrease and the concrete beams reinforced with single steel tension bars provide the highest absorption energy values in each group. However, in several cases, the absorption energy values of the beams with a high hybrid reinforcement ratio are greater than those of the specimens with a low hybrid reinforcement ratio, implying that the fracture energy was affected by not only the hybrid reinforcement ratio but also the mechanical properties of the concrete and FRP bars. By observing the values of energy in each beam group in Table 5.4, the minimum absorption energy of the hybrid FRP-steel RC beams in each group is found in the beam with the hybrid reinforcement ratio of 2.880, which is approximately 47-76% of absorption energy of the corresponding reference beam.

From Table 5.4, the conditions of the energy of the hybrid FRP-steel beams achieve the 80% of the absorption energy of the steel RC beams with the same flexural strength as follows. In the case of the beams reinforced by FRP and steel tension bars with concrete compressive strength of 35 MPa, the hybrid reinforcement

ratios ( $A_f/A_s$ ) are respectively no greater than 0.641, 0.395 and 0.641 for GFRP, CFRP and AFRP types. Due to the very high elastic modulus of CFRP, the displacement and the ultimate load of the beams with CFRP and steel bars are respectively lower and greater than those with GFRP/AFRP (low elastic modulus) and steel bars. Additionally, the steel reinforcement plays an important role in the ductility displacement of the hybrid FRP-steel RC beams. Therefore, to obtain the good ductility, the reinforcement ratio of CFRP to steel in the hybrid CFRP-steel RC beams is lower than the reinforcement ratio of the beams with GFRP/AFRP and steel tension bars.

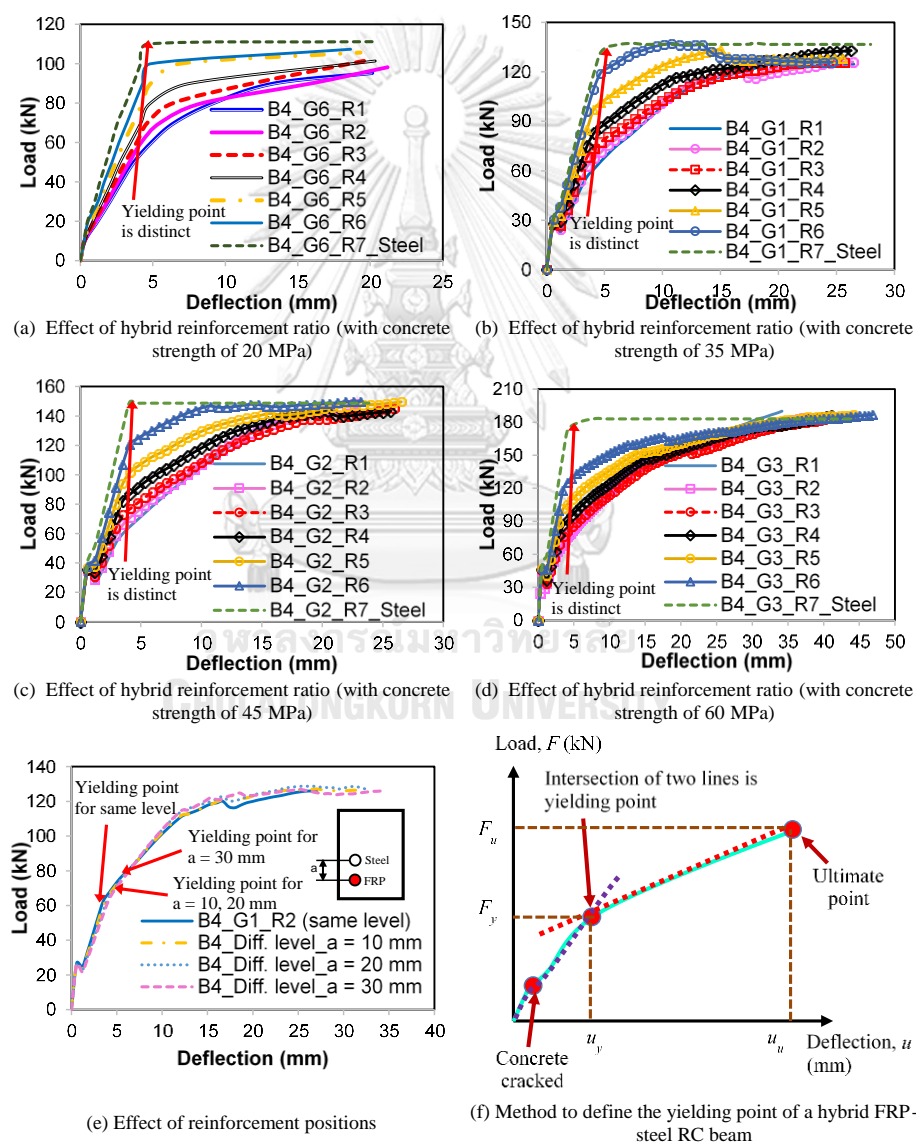


Figure 5.13 Effect of hybrid reinforcement ratio with different concrete compressive strengths and effect of reinforcement arrangement

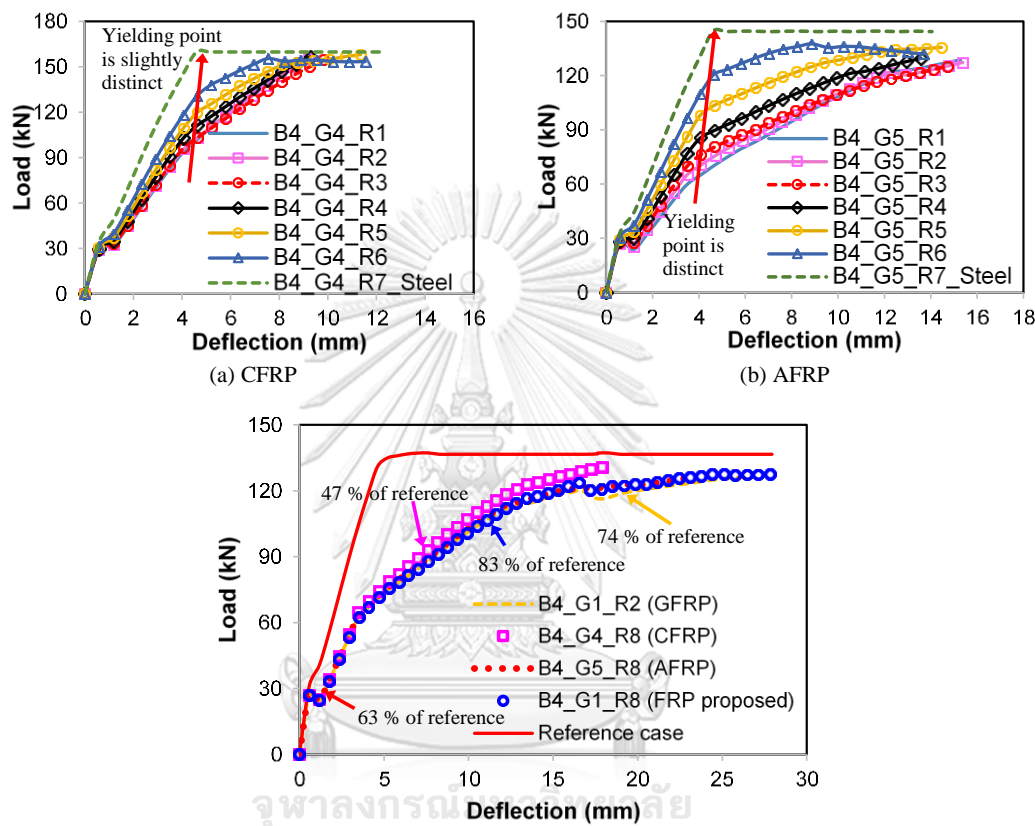
In the case of the beams reinforced with GFRP and steel tension bars, the hybrid reinforcement ratios ( $A_f/A_s$ ) that are no greater than 1.000, 0.641, 1.000 and 0.641 for the corresponding concrete strength of 20 MPa, 35 MPa, 45 MPa and 60 MPa should be provided to achieve 80% of the absorption energy of the corresponding steel RC beams. Under the contribution of concrete, as observed from Figs. 5.13(a), (b), (c) and Table 5.4, with the higher concrete compressive strength, the yielding load and the deformation are greater. Together with the increase in concrete strength, the use of a low hybrid reinforcement ratio makes the yielding load of the beams achieve high level. Therefore, the absorption energy of the beams with high concrete strength and low hybrid reinforcement ratio is high, and the ductility of those beams is improved.

The findings described above indicate that together with reinforcement ratio ( $A_f/A_s$ ), the concrete strength and the FRP types affect the ductility of beams with hybrid use of steel and FRP reinforcement. However, the lower hybrid reinforcement ratios  $A_f/A_s$  result in the higher initial rigidity, which is clearly shown in Figs. 5.13-5.14 and is rather explicit in the cases using the GFRP and AFRP bars for the partial tension reinforcement. Due to the very high elastic modulus of carbon fiber-reinforced polymer (CFRP) bars, the initial stiffness of the hybrid CFRP-steel RC beams is clearly indistinct by reducing the reinforcement ratio  $A_f/A_s$ . Generally, with a higher ratio of  $A_f/A_s$ , the load-carrying capacity of the hybrid FRP-steel RC beams can be enhanced as well as the FRP reinforcement tending to suffer higher tensile forces after the steel yielded. From Figs. 5.13(a)-(c) and Figs. 5.14(a)-(b), the yielding point, which is defined in Fig. 5.13(f) and revealed in Tables 5.4 and 5.5, of the simulated beams is distinctly defined by decreasing the hybrid reinforcement ratio  $A_f/A_s$ ; therefore, the yielding load is relatively smaller than the ultimate load of the beams with the low ratio of FRP to steel tension bars, increasing the ductility of those specimens.

#### 5.4.3 Effect of reinforcement arrangement

The behavior of the four concrete beams reinforced with the different positions of FRP and steel bars is determined in Fig. 5.13(e). Clearly, the responses in terms of the service conditions, before 60% of the ultimate load, of the four specimens

B4\_G1\_R2 (same level) and B4\_Diff. level are clearly similar. However, the slope of load-deflection curves of those beams is changed at the high load level. Specifically, the initial rigidity of specimen B4\_G1\_R2 (same level) is slightly higher than that of specimens B4\_Diff. level\_a = 10, 20, and 30 mm.



(c) A comparison of effect of FRP types,  $E_f$ (GFRP) = 41 GPa,  $E_f$ (proposed FRP) = 10.25 GPa,  $E_f$ (CFRP) = 124 GPa and  $E_f$ (AFRP) = 50.1 GPa

Figure 5.14 Effect of reinforcement ratio together with FRP types

Furthermore, Table 5.5 shows that the load-carrying capacity of beams reinforced by the different levels of tension bars is almost the same as that of the concrete member with the same level of GFRP and steel reinforcement. In the FE simulation, however, the maximum deflection of the hybrid beams with the two layers of bars is increased by 15.78%, 21.63%, and 27.17% with the increase in the gap between the steel and FRP reinforcement in comparison with the reference specimen, B4\_G1\_R2 (same level). Under the condition of the same flexural strength and the same failure

mode of concrete crushing after steel yields, the beams reinforced with larger gap between FRP and steel bars result in the greater effective depth to FRP reinforcement. Hence, the tensile force carrying capacity of the FRP bars is small for the specimens with larger FRP to steel reinforcement distances, and the maximum deflection of those specimens is therefore increased.

Since the ultimate deflection increases as the gap between the FRP and steel bars increases, the absorption energy of the hybrid FRP-steel beams with larger gap of FRP to steel bars is enhanced, as shown in the last column of Table 5.5. Therefore, Fig. 5.13(e) indicates that the larger gap between the steel and FRP reinforcement shows an improvement in ductility for the hybrid beams rather than the smaller spacing between steel and FRP bars. Moreover, the hybrid beams with greater spacing of FRP to steel bars reveal that the yielding load of steel reinforcement, which is indicated in Fig. 5.13(e) and Table 5.5, was relatively small compared to the ultimate load, increasing the ductility of those beams that were also improved in the comparison with the beams reinforced by the smaller gap between FRP and steel bars. From the aforementioned discussions, comparing the hybrid beams with the same level of FRP and steel reinforcement, the strength, rigidity and ductility of the hybrid FRP-steel RC beams can be compensated by providing more FRP and placing the steel and FRP bars at the different levels in the tension zone with the large distance between FRP and steel reinforcement. Moreover, the corrosion of steel reinforcement is mitigated by arranging the different level of reinforcement in which FRP bars are placed in the outer layer and steel bars are laid in the inner layer.

#### 5.4.4 Effect of FRP types

For the effects of the FRP type on the load-deflection response, ultimately applied load and midspan deflection results of the simulated hybrid beams are shown in Fig. 5.14(c) and Table 5.5. The hybrid reinforcement ratios ( $A_f/A_s$ ) of the investigated specimens B4\_G1\_R2 (group 1), B4\_G1\_R8 (group 1), B4\_G4\_R8 (group 4) and B4\_G5\_R8 (group 5) of Table 5.4 are 1.975, 7.990, 0.750 and 1.688, respectively. Moreover, those analyzed specimens contained the same steel reinforcement

amount,  $A_s = 201.2 \text{ mm}^2$ . The FRP-steel RC beam B4\_G1\_R8 employs FRP bars whose rupture strain is four times that of the GFRP and whose elastic modulus is one-fourth that of the GFRP. Clearly, the initial response of the three specimens reinforced with the GFRP, CFRP and AFRP bars is relatively similar. However, the slope of load-deflection curves of those beams is changed after the cracking of the concrete. Specifically, the stiffness of the specimen reinforced by CFRP-steel bars is greater than the stiffness of the beams reinforced with AFRP/GFRP and steel rods, due to the higher elastic modulus of CFRP bars. In Fig. 5.14(c), as expected, the B4\_G4\_R8 (CFRP) and B4\_G5\_R8 (AFRP) models achieve the similar load-carrying capacities to the control beam B4\_G1\_R2 (GFRP) with values obtained in range from 126 kN to 131 kN of failure load. However, the maximum deflections of the hybrid CFRP-steel and AFRP-steel RC beams are dropped by 33.83% and 14.97% in the comparison with the beam reinforced by GFRP-steel bars. Under the same flexural strength and the same failure mode of concrete crushing of the investigated specimens, the aforementioned finding may be mainly due to the lower elastic modulus of GFRP, which results in a greater deformation, compared to those of AFRP and CFRP.

By using the same ductility definition as the case of the effect of reinforcement arrangement, a lack of ductility is easily recognized in the concrete beams reinforced with CFRP and steel tension bars since the energy absorption of those beams is lower than the energy absorption of the concrete beams with hybrid use of AFRP/GFRP and steel reinforcement (see the last column of Table 5.5 for the values of energy absorption). Additionally, the high elastic modulus and the low fracturing strain of CFRP rods make the hybrid CFRP-steel RC members stiff and brittle; therefore, the beams reach the peak load at a low displacement, then fail immediately by concrete crushing. The contribution of the elastic moduli of CFRP bars is significant in the load-carrying capacity and rigidity of the hybrid beams. However, this effect causes a negative influence on the ductility consideration of the hybrid members. With the highest value of the absorption energy, the concrete beams reinforced by GFRP and steel bars improve the ductility since the lower elastic modulus and the higher fracturing strain of GFRP bars allow the contribution of steel reinforcement on the ductility of the hybrid GFRP-steel beam to be heavily

utilized. By comparison to the steel RC beams with the same flexural capacity, the concrete beam reinforced by GFRP and steel bars can achieve 74% of the absorption energy of the steel RC beams. Furthermore, the absorption energy of the hybrid FRP-steel RC beam B4\_G1\_R8, in which the mechanical property of reinforced FRP bars is proposed above, can reach 83% of the absorption energy of the reference beam reinforced with single steel bars under the same flexural strength. Therefore, the property of the FRP bars employed in specimen B4\_G1\_R8 with 10.25 GPa of Young's modulus (one-fourth of the GFRP elastic modulus) and 7.36% of the rupturing strain (four times the GFRP fracturing strain) can be a better option than GFRP for practical use.

In conclusion, the strength and stiffness of FRP bars can be compensated by providing more FRP reinforcement. However, the low fracturing strain, which is a weak point of carbon and aramid fibers, cannot be substituted by any. Thus, the beams reinforced with FRP, such as GFRP which has a low elastic moduli and high rupturing strain, and steel bars imply a better ductility than the beams with hybrid CFRP/AFRP and steel reinforcement. In addition, a Young's modulus of 10.25 GPa and a fracturing strain of 7.36% is proposed for the property of FRP tension reinforcement in the concrete beams with hybrid use of FRP and steel bars to achieve an absorption energy close to that of the reference steel RC beam under the same load carrying capacity.



#### 5.4.5 Ductility-related indices

Aside from the ductility corresponding to the area under the load-displacement curves, as explained above, the current study uses the ductility factor defined by the ratio of ultimate displacement to yielding deflection. This work also proposes a ductility index to discuss the ductility measurements of the concrete beams with the combination of FRP and steel tension reinforcement.

Figure 5.10 indicates that the behavior of concrete beams reinforced by FRP-steel bars was divided into the three stages. To consider the ductility of the beams, stage 2 and stage 3 were carefully investigated. Based on the consideration of the post-

yield stiffness of the beams, which was also adopted in the study of Arafa et al. (2015) to assess the ductility behavior of the RC members, this research introduces a simple ductility index to evaluate the ductility of hybrid FRP-steel RC beams. Since the post-yield stiffness of a hybrid FRP-steel RC beam is almost decided by FRP reinforcement; therefore, the magnitude of the post-yield rigidity to whole stiffness ratio  $[(\Delta u/u_u)/(\Delta F/F_u)]$  is correlated with the ductility of this beam. The  $\Delta u = u_u - u_y$  (mm),  $\Delta F = F_u - F_y$  (kN), and  $F_u, F_y, u_u, u_y$  correspond to the applied loads and deflections at the ultimate and steel yielding. As a ductility definition, the ductility of a beam is enhanced when the ductility index computed by  $(\Delta u/u_u)/(\Delta F/F_u)$  increases.

Table 5.6 Absorption energy, ductility factor and ductility index of the experimental results

Authors	Beam ID	Absorption energy (kNmm)	Ductility factor, $u_u/u_y$	Ductility index $(\Delta u/u_u)/(\Delta F/F_u)$
Aiello and Ombres (2002)	A1	3515.0	5.92	1.56
	A2	3401.4	5.08	1.70
	A3	9575.8	4.08	2.29
Qu et al. (2009)	B1	1815.9	3.08	8.76
	B2	2520.9	-	-
	B3	2669.4	4.78	2.15
	B4	2330.8	8.42	1.73
	B5	2864.8	5.87	2.98
	B6	2512.3	4.82	2.80
	B7	1892.4	11.00	1.65
	B8	1777.8	1.61	0.53
Lau and Pam (2010)	G0.6-T1.0-A90	13920.6	4.19	1.89
	G1.0-T0.7-A90	19025.4	3.86	1.90
	G0.3-MD1.0-A90	6505.0	7.28	1.99

Table 5.6 shows the results of the ductility of the hybrid FRP-steel RC beams in the literature defined according to the methods of conventional steel RC beams



(ductility factor,  $u_u/u_y$ ) and the index proposed in the present study. As defined in each index meaning, Table 5.6 shows that the absorption energy of the tested beams is enhanced when the ductility index increases. This trend is observed in the studies of Qu et al. (2009) and of Lau and Pam (2010). Table 5.6 also implies that beam B8 is the most brittle because of the smallest values of ductility factor,  $u_u/u_y$ , absorption energy and ductility index  $(\Delta u/u_u)/(\Delta F/F_u)$ . Beam B8 therefore fails immediately after steel yielding. For the beams A1, A2, and A3, the ductility index provides the same ranking with the calculated absorption energy. Clearly, beam A3 has the largest values of the fracture energy and the ductility index,  $(\Delta u/u_u)/(\Delta F/F_u)$ ; thus, the most ductile beam is A3. However, the ductility evaluation of the tested specimens by adopting the ductility index and absorption energy in this study are different from that using the ductility factor defined as the conventional steel RC beams. These above findings are in complete agreement with the results obtained by Pang et al. (2015).

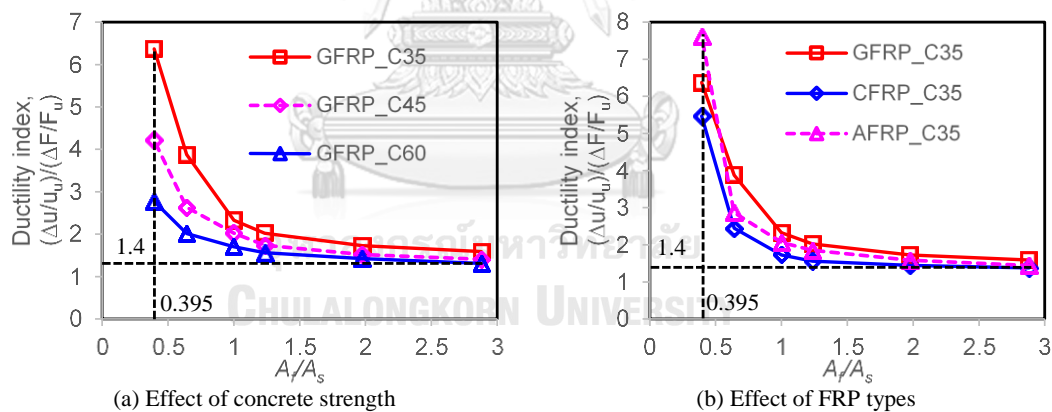


Figure 5.15 Relationship of reinforcement ratio and ductility index in the beams of parametric study

Additionally, the description of mechanical performance of hybrid FRP-steel RC beams in comparison with steel RC beam is carried out by comparing the three indices: ductility factor, ductility index and absorption energy. The simulated results of the parametric study with the beams designed in Table 5.4 are employed. Figures

5.15, 5.16 and 5.17 show the relationships between ductility indices, FRP types and concrete compressive strength varying among hybrid reinforcement ratios of the analyzed beams. Moreover, the exponential function regression is applied to draw the trend lines of those relationships. From Figs. 5.15 and 5.17, under the same flexural capacity in each beam group, it is similar to the trend of absorption energy defined in the previous sections, in which the ductility index values decreased as the hybrid reinforcement ratios  $A_f/A_s$  increased.

The ductility index of the steel RC beams is much higher than that of the hybrid FRP-steel members since the post-yield response of those reference specimens is nearly horizontal, implying that with the same load carrying capacity, a hybrid FRP-steel beam could be ductile if its post-yield stiffness is close to that of the corresponding steel RC beam. This finding can be obtained through the beams resulting in high yielding load and large ultimate displacement, in which the corresponding absorption energy of those specimens is high. In the contrast to the aforementioned observations, the ductility defined by the ductility factor of the hybrid FRP-steel RC beams is slightly enhanced as the hybrid reinforcement ratio increases. Moreover, by using the ductility factor and absorption energy, Fig. 5.16(a) and Fig. 5.17(a) indicate that the ductility indices are reduced by decreasing the concrete compressive strength. This finding is completely opposite to the values defined by the ductility index (as seen in Fig. 5.15(a)). From Figs. 5.15(b), 5.16(b) and 5.17(b), the results computed by the three ductility indices of the GFRP-steel RC beam are generally greater than those of the AFRP-steel and CFRP-steel RC beams.

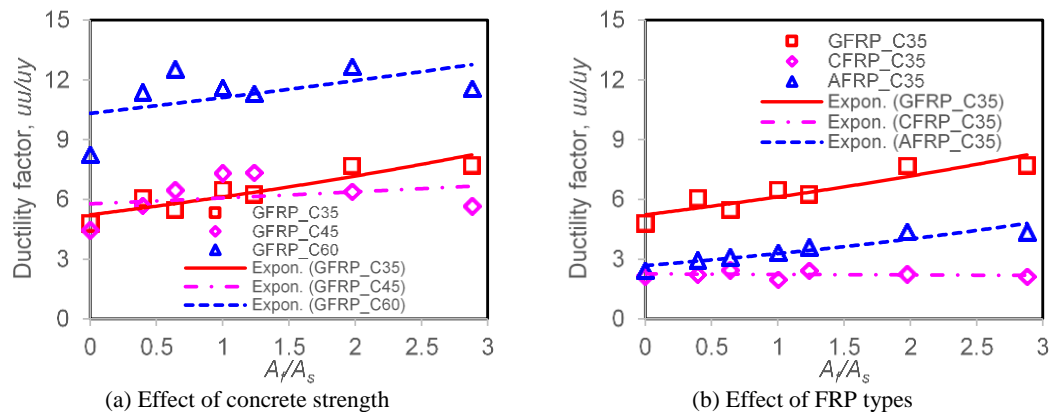


Figure 5.16 Relationship of reinforcement ratio and ductility factor in the beams of parametric study

Based on the observations from Fig. 5.15 and Fig. 5.17, the practical feasibility of the hybrid FRP-steel RC beams through the requirement of the ductility index, which requires the 80% of the absorption energy of the steel reference beams, is expressed as follows. The hybrid FRP-steel RC beams with concrete compressive strength of 33.1 MPa should hold the ductility index  $(\Delta u/u_u)/(\Delta F/F_u)$  to no less than 3.88, 5.47 and 2.87 for the GFRP, CFRP and AFRP types, respectively. To provide these ductility index values sufficiently, the hybrid reinforcement ratio  $A_f/A_s$  is required to be not larger than 0.641 for the beams with GFRP/AFRP-steel cases and that ratio is also recommended to be no greater than 0.395 for the specimens reinforced with CFRP-steel bars. In the case of the beams reinforced with GFRP and steel tension bars, the ductility indices  $(\Delta u/u_u)/(\Delta F/F_u)$  that are no less than 3.88, 2.03 and 2.01 should be ensured for the corresponding concrete strengths of 35 MPa, 45 MPa and 60 MPa. To satisfy these ductility requirements, the hybrid reinforcement ratio  $A_f/A_s$  should be controlled to be no greater than 0.641 for concrete strength ranging from 35 to 60.0 MPa. On the other hand, the minimum ductility index of 1.40 corresponding to 47% of the steel RC beam absorption energy can be achieved for a concrete compressive strength ranging from 35 to 60 MPa, the FRP types with the elastic moduli from 41 to 124 GPa and the hybrid reinforcement ratio from 0.395 to 2.880.

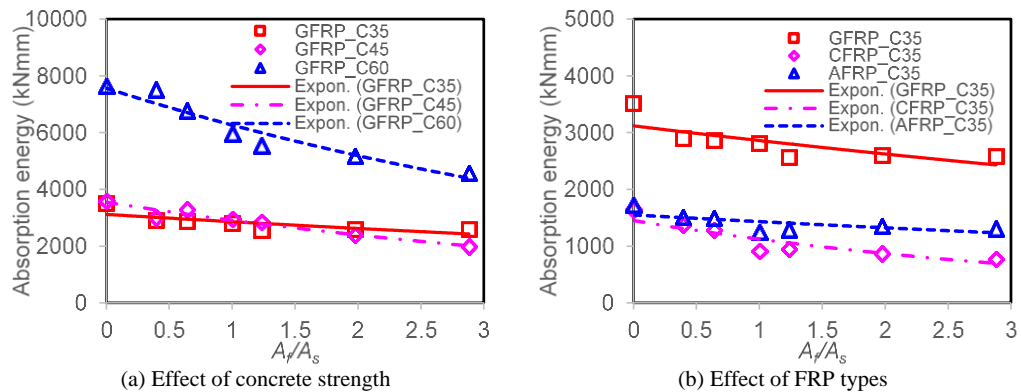


Figure 5.17 Relationship of reinforcement ratio and absorption energy in the beams of parametric study

Table 5.4 Details of the parametric study on reinforcement ratios, concrete compressive strength and types of FRP, and simulated absorption energy and yielding load

Group	Beam ID	$A_s$ (mm <sup>2</sup> )	$A_f$ (mm <sup>2</sup> ) $\rho_r = \frac{A_f}{A_s}$	$E_f$ (MPa)	$f_f$ (MPa)	$f_c'$ (MPa)	Absorption energy (kNmm)	Yielding load (kN)	
Group 1	B4_G1_R1	157.0 (2d10)	452.4 (4d12)	2.880	41000	755	35	2585.0	57
	B4_G1_R2	201.2 (4d8)	395.9 (2d16)	1.975	41000	755	35	2602.0	63
	B4_Diff. level_a = 10 mm	201.2 (4d8)	427.6 (2d16.5)	2.128	41000	755	35	3279.4	66
	B4_Diff. level_a = 20 mm	201.2 (4d8)	461.8 (4d14)	2.298	41000	755	35	3469.4	65
	B4_Diff. level_a = 30 mm	201.2 (4d8)	490.8 (1d25)	2.443	41000	755	35	3627.6	68
	B4_G1_R3	251.5 (5d8)	314.2 (4d10)	1.235	41000	755	35	2569.5	73
	B4_G1_R4	301.8 (6d8)	307.9 (2d14)	1.000	41000	755	35	2807.2	83
	B4_G1_R5	402.2 (2d16)	254.5 (2d12.7)	0.641	41000	755	35	2870.3	101

	B4_G1_R6	503.0 (10d8)	201.2 (4d8)	0.395	41000	755	35	2899.9	109
	B4_G1_R7_Steel	628.4 (2d20)	-	-	-	-	35	3515.5	136
	B4_G1_R8	201.2 (4d8)	1587.6 (3d26)	7.900	10250	755	35	2949.3	63
	B4_G2_R1	157.0	452.4	2.880	41000	755	45	1987.8	60
	B4_G2_R2	201.2	395.9	1.975	41000	755	45	2389.0	66
	B4_G2_R3	251.5	314.2	1.235	41000	755	45	2851.7	73
Group 2	B4_G2_R4	301.8	307.9	1.000	41000	755	45	2961.0	82
	B4_G2_R5	402.2	254.5	0.641	41000	755	45	3280.7	102
	B4_G2_R6	503.0	201.2	0.395	41000	755	45	3015.2	121
	B4_G2_R7_Steel	760.2	-	-	-	-	45	3590.1	149
	B4_G3_R1	157.0	452.4	2.880	41000	755	60	4588.4	58
	B4_G3_R2	201.2	395.9	1.975	41000	755	60	5173.2	65
	B4_G3_R3	251.5	314.2	1.235	41000	755	60	5545.2	76
Group 3	B4_G3_R4	301.8	307.9	1.000	41000	755	60	5965.9	86
	B4_G3_R5	402.2	254.5	0.641	41000	755	60	6780.6	101
	B4_G3_R6	503.0	201.2	0.395	41000	755	60	7529.1	125
	B4_G3_R7_Steel	804.4	-	-	-	-	60	7645.4	179
	B4_G4_R1	157.0	452.4	2.880	124000	1700	35	775.0	94
	B4_G4_R2	201.2	395.9	1.975	124000	1700	35	865.6	96
	B4_G4_R3	251.5	314.2	1.235	124000	1700	35	951.1	96
Group 4	B4_G4_R4	301.8	307.9	1.000	124000	1700	35	915.6	111
	B4_G4_R5	402.2	254.5	0.641	124000	1700	35	1282.6	120
	B4_G4_R6	503.0	201.2	0.395	124000	1700	35	1369.4	138
	B4_G4_R7_Steel	981.8	-	-	-	-	35	1645.7	160
	B4_G4_R8	201.2	150.8	0.750	124000	1700	35	1657.5	64
	B4_G5_R1	157.0	452.4	2.880	50100	1366	35	1313.9	60
	B4_G5_R2	201.2	395.9	1.975	50100	1366	35	1354.2	65
	B4_G5_R3	251.5	314.2	1.235	50100	1366	35	1294.9	76
Group 5	B4_G5_R4	301.8	307.9	1.000	50100	1366	35	1252.4	86
	B4_G5_R5	402.2	254.5	0.641	50100	1366	35	1497.9	104
	B4_G5_R6	503.0	201.2	0.395	50100	1366	35	1511.0	120

	B4_G5_R7_Steel	760.2	-	-	-	-	35	1728.9	145
	B4_G5_R8	201.2	339.3	1.688	50100	1366	35	2214.0	63
	B4_G6_R1	157.0	452.4	2.880	41000	755	20	1456.9	46
	B4_G6_R2	201.2	395.9	1.975	41000	755	20	1576.3	60
	B4_G6_R3	251.5	314.2	1.235	41000	755	20	1552.2	69
Group 6	B4_G6_R4	301.8	307.9	1.000	41000	755	20	1664.8	76
	B4_G6_R5	402.2	254.5	0.641	41000	755	20	1707.8	85
	B4_G6_R6	503.0	201.2	0.395	41000	755	20	1692.7	97
	B4_G6_R7_Steel	760.2	-	-	-	-	20	2000.9	108

Table 5.5 Effects of reinforcement arrangement and types of FRP reinforcement

Parameter	Specimen	$A_s$ (mm <sup>2</sup> )	$A_f$ (mm <sup>2</sup> )	$\rho_f = A_f/A_s$	Designed ultimate load (kN)	FEM ultimate load (kN)	Difference in load (%)
FRP types	B4_G1_R2 (GFRP)	201.2	395.9	1.975	140	127	NA
	B4_G4_R8 (CFRP)	201.2	150.8	0.750	140	131	3.14
	B4_G5_R8 (AFRP)	201.2	339.3	1.688	140	126	0.79
	B4_G1_R8 (FRP proposed)	201.2	1587.6	7.900	140	127	0.00
	B4_G1_R2 (same level)	201.2	395.9	1.975	140	127	NA
Reinforcement arrangement	B4_Diff. level_a = 10 mm	201.2	427.7	2.128	140	127	0.00
	B4_Diff. level_a = 20 mm	201.2	461.8	2.298	140	126	0.79
	B4_Diff. level_a = 30 mm	201.2	490.8	2.443	140	126	0.79

Table 5.5 (continued)

Parameter	Specimen	Ultimate deflection (mm)	Difference in deflection (%)	Yielding load (kN)	Absorption energy (kNmm)
FRP types	B4_G1_R2 (GFRP)	27.05	NA	63	2602.0
	B4_G4_R8 (CFRP)	17.90	33.83	64	1657.5
	B4_G5_R8 (AFRP)	23.00	14.97	63	2214.0
	B4_G1_R8 (FRP proposed)	27.84	2.92	63	2949.3
Reinforcement arrangement	B4_G1_R2 (same level)	27.05	NA	63	2602.0
	B4_Diff. level_a = 10 mm	31.59	15.78	66	3279.4
	B4_Diff. level_a = 20 mm	32.90	21.63	65	3469.4
	B4_Diff. level_a = 30 mm	34.40	27.17	68	3627.6

## 5.5 Conclusions

The reliability of the FE modelling is validated through comparing the simulated results to the experimental data for the beams tested in the previous studies. Additionally, an extensive parametric study is also carried out by means of the FE program to analyze the ductility of the hybrid FRP-steel RC beams by providing optimum experimental parameters. From the numerical investigation, the following conclusions can be drawn.

Based on the FE simulation results of the available data, the FE models can predict the load-deflection relationships of the hybrid FRP-steel RC beams well with a maximum deviation less than 10% in the load-carrying capacity and the displacement. The stiffness of the beams simulated by the FE method is higher than those of the experimental results mainly due to the perfect bond assumption between the reinforcement and concrete. In addition, the FE tool also simulates the failure mode of concrete crushing after steel yielding of the hybrid FRP-steel RC beams well. On the other hand, the FE results indicate the difference on the role of FRP and steel reinforcement in a hybrid RC beam. In fact, the FRP bars are mainly responsible for the ultimate strength of the hybrid RC beam, while the ductility performance of that specimen is almost concentrated on the steel reinforcement.

Therefore, the ductility defined by absorption energy of the FRP-steel RC beam could be enhanced if the hybrid reinforcement ratio  $A_f/A_s$  is small.

Generally, the use of the high strength concrete and the low hybrid reinforcement ratio  $A_f/A_s$  offers the enhancement on the ductility defined by the absorption energy of the hybrid FRP-steel beams. In addition, the beams reinforced with the larger gap between FRP and steel bars in the tension zone provide a better ductility in the comparison with the hybrid beams with the smaller spacing between FRP and steel reinforcement. In addition, the ductility defined through the fracture energy of the hybrid FRP-steel RC beams is improved when the FRP bars with low elastic modulus and high rupturing strain (such as GFRP) are employed. Indeed, based on the simulated results, the FRP property with 10.25 GPa of Young's modulus (one-fourth that of GFRP) and 7.36% of rupturing strain (four times that of GFRP) can achieve over 80% of the absorption energy of the reference steel RC beams.

A simple and reliable ductility index is proposed to evaluate the ductility of concrete beams reinforced with steel and FRP bars. This ductility index displays a similar observation of the absorption energy concept in the ductility performance. Similar to the results obtained from the absorption energy, the ductility index values decrease as the hybrid reinforcement ratios  $A_f/A_s$  increase. Under the same flexural capacity condition, the absorption energy of the hybrid FRP-steel RC beams can achieve 80% of that of the steel reference beams when the following requirements on the ductility index are sufficiently offered. For the hybrid beams with concrete strength of 35 MPa, the ductility index values are no less than 3.88, 5.47 and 2.87 for the GFRP, CFRP and AFRP types, and the corresponding hybrid reinforcement ratios are no greater than 0.641 (for the GFRP and AFRP cases) and 0.395 (for the CFRP case). In addition, the ductility indices  $(\Delta u/u_u)/(\Delta F/F_u)$  that are no less than 3.88, 2.03 and 2.01 for the corresponding concrete strength of 35 MPa, 45 MPa and 60 MPa should be ensured for the concrete beams reinforced by GFRP and steel bars, attained when the hybrid reinforcement ratio of FRP to steel bars is less than or equal to 0.641. On the other hand, the minimum ductility index of 1.40 of the beams analyzed in this work can be achieved by at least 47% of the absorption energy of the corresponding steel RC beams.



## Chapter 6 GENERAL CONCLUSIONS AND FUTURE DEVELOPMENTS

### 6.1 General conclusions

At first objective, the present research deals with the reinforced concrete beams strengthened in shear by ETS steel or FRP bars, which are embedded into pre-drilled holes through the section of the members. This study also deals with the concrete beams reinforced in shear with hybrid inclination of the transverse steel. An experimental program to study the mechanical responses of concrete beams retrofitted by ETS steel/GFRP bars was carried out. The overall behaviors of the tested members such as load-deflection relationship, crack pattern, cracking failure and strain of shear reinforcement are investigated. Additionally, the comparisons between the tested results and the data in the previous studies are conducted to analyze the effectiveness of the ETS strengthening system inserted the mechanical anchorage. On the other hand, the efficiency of ETS FRP in terms of combined usage of steel and FRP is assessed through the truss analogy theory. The average strain equation of the ETS FRP reinforcement in the existing shear resisting methods is also developed.

In addition, an experimental program to investigate the bond behavior between ETS steel/GFRP bars and concrete was carried out. The various effects such as the anchorage presence, the ETS type, the anchorage length, the ETS bar diameter and the embedment length on the bonding performance of ETS bars to concrete are examined. Based on Dai et al.'s method, the bond model is developed for analytically deriving the bond response between ETS FRP bars and concrete. On the other hand, a FE program is developed to simulate the structural response of concrete beams strengthened by ETS steel and GFRP bars. Based on the results of the analyses, general conclusions are summarized as follows:

(1) The results attained from the experiment indicate that the contribution in shear resistance of ETS bars inserted anchorage is significantly higher than that of the ETS strengthened beams without anchorage. Furthermore, due to the close shape

configuration of vertical stirrups reinforced in the beams, the shear resistance of ETS vertical bars is less than that of the ordinary shear reinforcement. However, the shear contribution of ETS diagonal system is slightly higher than the contribution of internal diagonal-vertical reinforcement in shear since the ETS diagonal bars offered the longer bond length compared to the non-close configuration of hybrid shear diagonal reinforcement, providing a short bond length and a poor anchorage. On the other hand, the truss analogy theory can predict well the shear resistance of the internal steel reinforcement, however, this model cannot predict well the shear contribution of the low percentage of ETS reinforcement due to the beams with the low ratio of ETS strengthened bars (provided a low bonding performance) failed by the debonding instead of the yielding of ETS reinforcement.

(2) Concrete beams strengthened by the ETS bars inclined at  $45^{\circ}$  provide the higher shear strengthening efficiency in the comparison with those retrofitted by the vertical ETS bars. Besides, the displacement at ultimate load of the beams retrofitted by ETS GFRP rods is feasible compared to that of the ETS steel retrofitted beams. Moreover, by applying the mechanical anchorage at the tension ends of the ETS strengthening system, all investigated beams were failed in shear due to the significant and wider shear cracks in shear cracking zone of the members. The rupture of the ETS bars and the debonding and leaving of the ETS bars to concrete and to the mechanical anchorage were not occurred. As another effectiveness of the anchorage insert at the ends of the ETS bars, the activation of the ETS system and the existing steel stirrups is simultaneous in the shear resistance since the shear transfer mechanism of concrete-adhesive-ETS bars were improved. This fact may utilize all of capacity of the ETS strengthening tool.

(3) The beam strengthened with ETS GFRP system with anchorage provided an encouraging anchorage and confinement to the retrofitted bars, leading the ETS system is drastically triggered; therefore the shear contribution of the ETS GFRP vertical one is higher than that of the ETS CFRP vertical one without anchorage. When the bond length is improved by the inclination arrangement of ETS bars, the contribution of ETS CFRP diagonal reinforcement in shear is greater than that of ETS GFRP diagonal rods. Besides, as observed from the experimentation, the shear failure

modes of the beams, which is retrofitted with ETS GFRP bars installed mechanical anchorage, intended to convert into the flexural failures by crushing concrete at the load points, and this might improve the ductility of the ETS strengthened members.

(4) The presence of stirrups reduced the resistance of ETS strengthened bars in shear. With low percentage transverse steel compared to the percentage of ETS reinforcement, the detrimental effect induced by presence of existing stirrups did not occur in the specimens strengthened by ETS bars with mechanical anchorage insert. Furthermore, the shear contribution of strengthening system adopting the ETS method always offered higher values than that of the NSM retrofitted bars, since the good anchorage and confinement of the concrete core to ETS bars that made the shear transfer mechanism of concrete-adhesive-ETS bars significantly enhanced and triggered, resulting in the contribution of ETS bars in shear drastically improved.

(5) For the concrete beams retrofitted with the ETS method and failed with no debonding effects of the strengthening system to concrete, to predict the shear contribution of the strengthening system, the original Ueda et al.'s model can be employed for the ETS steel cases, and the ACI and JSCE model with the developed average strain equation can be used for the ETS FRP cases with/with no mechanical anchorage attachment.

(6) From the pullout test analysis, before the mechanical anchorage being activated, the initial response of the specimen embedded by ETS bars with anchorage attachment is completely similar to the corresponding specimen embedded by ETS bars without anchorage. The specimen with mechanical anchorage presence results in the significantly higher maximum pullout force than that obtained by the test of the specimen without anchorage since the use of anchorage enhanced drastically the tension capacity of rod at the bar end. For the effect of embedment length, the ultimate pullout forces of the tested specimens are similar since the failure mode is the GFRP bar rupture. In addition, the specimen with ETS GFRP bar diameter of 10 mm offered the lower ultimate pullout force and smaller maximum slip in the comparison with those of the specimen with ETS GFRP bar diameter of 8 mm. This fact can be due to the bigger ETS bar size induced the poorer adhesive resin injection, while with the smaller ETS bar size the adhesive resin is filled up more properly. For the effect of ETS

types, the tested results reveal that the concrete block embedded by ETS steel bar exhibited higher pullout force and smaller slip in the comparison with the member retrofitted with ETS GFRP rod since the high Young's modulus of steel of 200 GPa, the low yielding strain of steel of 2000 micron. Moreover, the specimens with the longer anchorage length (four and six anchoring nuts) resulted in the greater pullout force than that of the specimen with the short anchorage length (two anchoring nuts). The failure mode of the specimen with short anchored ETS bar failed by pullout of ETS bar leaving the nuts in concrete, meaning the two nuts are not enough to assure the full tension capacity of ETS GFRP bar.

(7) By developing the bond model based on Dai et al.'s method, the good agreement is obtained in the comparison between the analytical maximum pullout forces and the experimental maximum pullout loads. The results computed by the developed ETS bond model fitted well with the tested data, especially in the ascending branch of the curves, in terms of the bond stress and slip relationship. Besides, the interfacial fracture energy ( $G_f$ ) and ductility index ( $B$ ) are important factors affecting the ETS bond response. The application of developed bond model for the ETS bars in the simulation indicated that the FE modelling is an effective tool to accurately predict various features, including the load-midspan deflection, stress of FRP and steel reinforcement, failure mode and crack propagation of concrete beams reinforced in shear by ordinary vertical and diagonal steel reinforcement, and strengthened by ETS steel/GFRP bars.

At second objective, this study deals with the concrete beams reinforced by hybrid FRP and steel tension bars. This research gains insight into the mechanical performance and the ductility of concrete beams reinforced by FRP and steel tension bars. The reliability of the FE modelling is validated through comparing the simulated results to the experimental data for the beams tested in the previous studies. Additionally, an extensive parametric study is also carried out by means of the FE program to analyze the ductility of the hybrid FRP-steel RC beams by providing optimum experimental parameters. From the numerical investigation, the following general conclusions can be drawn as follows:

(1) The FE models can predict the load-deflection relationships of the hybrid FRP-steel RC beams well with a maximum deviation less than 10% in the load-carrying capacity and the displacement. The stiffness of the beams simulated by the FE method is higher than those of the experimental results mainly due to the perfect bond assumption between the reinforcement and concrete. In addition, the FE tool also simulates the failure mode of concrete crushing after steel yielding of the hybrid FRP-steel RC beams well. On the other hand, the FE results also indicate that the FRP bars are mainly responsible for the ultimate strength, while the steel reinforcement is most responsible for the ductility performance of hybrid RC beams. Therefore, the stiffness and ductility defined by absorption energy of the FRP-steel RC beam would be enhanced if the hybrid reinforcement ratio  $A_f/A_s$  was small.

(2) From the parametric study, generally, the use of the high strength concrete and the low hybrid reinforcement ratio  $A_f/A_s$  offers the enhancement on the ductility defined by the absorption energy of the hybrid FRP-steel beams. In addition, the beams reinforced with the larger gap between FRP and steel bars in the tension zone provide a better ductility in the comparison with the hybrid beams with the smaller spacing between FRP and steel reinforcement. The ductility defined through the fracture energy of the hybrid FRP-steel RC beams is improved when the FRP bars with low elastic modulus and high rupturing strain (such as GFRP) are employed. Indeed, based on the simulated results, the FRP property with 10.25 GPa of Young's modulus (one-fourth that of GFRP) and 7.36% of rupturing strain (four times that of GFRP) can achieve over 80% of the absorption energy of the reference steel RC beams.

(3) The ductility index proposed in this study displays a similar observation of the absorption energy concept in the ductility performance. The ductility index values decrease as the hybrid reinforcement ratios  $A_f/A_s$  increase. Under the same flexural capacity condition, the absorption energy of the hybrid FRP-steel RC beams can achieve 80% of that of the steel reference beams when the following requirements on the ductility index are sufficiently offered. For the hybrid beams with concrete strength of 35 MPa, the ductility index values are no less than 3.88, 5.47 and 2.87 for the GFRP, CFRP and AFRP types, and the corresponding hybrid

reinforcement ratios are no greater than 0.641 (for the GFRP and AFRP cases) and 0.395 (for the CFRP case). In addition, the ductility indices  $(\Delta u/u_u)/(\Delta F/F_u)$  that are no less than 3.88, 2.03 and 2.01 for the corresponding concrete strength of 35 MPa, 45 MPa and 60 MPa should be ensured for the concrete beams reinforced by GFRP and steel bars, attained when the hybrid reinforcement ratio of FRP to steel bars is less than or equal to 0.641. On the other hand, the minimum ductility index of 1.40 of the beams analyzed in this work can be achieved by at least 47% of the absorption energy of the corresponding steel RC beams.

## 6.2 Future developments

Together with the findings obtained in this study, the future developments are needed to extend and apply the shear strengthening method using ETS technique and the concrete beams reinforced with hybrid FRP-steel tension bars for the practical use. The important points of the future developments are shown as follows:

(1) More experimental program of concrete beams retrofitted in shear using ETS technique is expected to investigate the effects of concrete compressive strength, size of section, shear span length, bar diameter, bar type and bar surface on the shear strengthening effectiveness.

(2) The steel anchoring nuts in this study can be replaced by the FRP anchorage to meet the durability requirement of the strengthened structures. In addition, further investigations on the influences of the mechanical anchorage such as the anchorage length and the anchorage detailing on the strengthening performances should be carried out.

(3) Hybrid method of ETS and EB/NSM for strengthening in both shear and flexure is desired to improve the retrofitting efficiency of the structures in the practical use.

(4) More pullout test of bonding between ETS bars and concrete under various influences such as failure criteria, ETS bar type and anchorage detailing is needed to

offer the good bond model for analyzing well the bond behavior of ETS bars to concrete.

(5) Although there are numerous experiments and this study provides a large range of ductility assessment, the further investigations on the effects of the span length, the size of section and the anchorage length of reinforcement on the performances of the concrete beams reinforced by FRP and steel tension bars are expected.



## REFERENCES



จุฬาลงกรณ์มหาวิทยาลัย  
**CHULALONGKORN UNIVERSITY**



## REFERENCES

- ACI 211.1-91, (2002). "Standard practice for selecting proportions for normal, heavyweight, and mass concrete." Detroit: American Concrete Institute; USA.
- ACI 440.1R-06, (2006). "Guide for the design and construction of structural concrete reinforced with FRP bars." Detroit: American Concrete Institute; USA.
- ACI 440R-96, (1996b). "State of the art report on fiber reinforced plastic reinforcement for concrete structures." Detroit: American Concrete Institute; USA.
- Aiello, M. A. and Ombres, L., (2002). "Structural performances of concrete beams with hybrid (Fiber-Reinforced Polymer-Steel) reinforcements." *Journal of Composites for Construction*, 6(2), 133-140.
- Akter, M. H., Jummat, M. Z. and Islam, A. B. M. S. (2015). "Side Near Surface Mounted (SNSM) technique for flexural enhancement of RC beams." *Materials & Design*, **83**, 587–597.
- Ali, A., Abdalla, J., Hawileh, R. and Galal, K. (2014). "CFRP mechanical anchorage for externally strengthened RC beams under flexure." *Physics Procedia*, **55**, 10-16.
- ANSYS – Release Version 15.0, (2013). "A finite element computer software and user manual for nonlinear structural analysis." Canonsburg, USA.
- Arafa, M. A. I., Zhishen W., Mohamed F. M. F. and Doaa K., (2015). " Experimental study on cyclic response of concrete bridge columns reinforced by steel and basalt FRP reinforcements." *Journal of Composites for Construction*, 20(3), 1-19.
- Barros, J. A. O. and DalFre, G. M. (2013), "Assessment of the effectiveness of the embedded through-section technique for the shear strengthening of reinforced concrete beams." *Strains*, 49, 75-93.
- Bencardino, F., Condello, A. and Ombres L., (2016). "Numerical and analytical modelling of concrete beams with steel, FRP and hybrid FRP-steel reinforcements." *Composite Structures*, 140, 53-65.
- Bischoff, P. H., (2007). "Deflection calculation of FRP reinforced concrete beams based on modifications to the existing Branson equation." *Journal of Composites for Construction*, 11(1), 4-14.

- Branson, D. E. (1977), *Deformation of Concrete Structures*, McGraw-Hill, New York, USA.
- Breveglieri, M., Aprile, A. and Barros, J. A. O. (2014), "Shear strengthening of reinforced concrete beams strengthened using embedded through-section steel bars." *Engineering Structures*, 81, 76-87.
- Breveglieri, M., Aprile, A. and Barros, J. A. O. (2015), "Embedded Through-Section shear strengthening technique using steel and CFRP bars in RC beams of different percentage of existing stirrups." *Composite Structures*, 126, 101-113.
- Breveglieri, M., Aprile, A. and Barros, J. A. O. (2016), "RC beams strengthened in shear using the Embedded Through-Section technique: Experimental results and analytical formulation." *Composites Part B: Engineering*, 89, 266-281.
- Burke, P. J., Bisby, L. A. and Green, M. F. (2013). "Effects of elevated temperature on near surface mounted and externally bonded FRP strengthening systems for concrete." *Cement and Concrete Composites*, 35(1), 190-199.
- Chaallal, O., Mofidi, A., Benmokrane, B. and Neale, K. W. (2011), "Embedded through-section FRP rod method for shear strengthening of RC beams: performance and comparison with existing techniques." *Journal of Composites for Construction*, 15(3), 374-383.
- Comite Euro-International du Beton (CEB-FIP), CEB-FIP model code, 2010. "*Bulletin D'Information No. 213/214 (Concrete Structures)*", Lausanne, Switzerland.
- Dalgre, G. M., Barros, J. and Machado, D. (2011), "Embedded through-section bars for the shear strengthening of RC beams", see URL also [https://repositorium.sdum.uminho.pt/bitstream/1822/21563/1/IC\\_117.pdf](https://repositorium.sdum.uminho.pt/bitstream/1822/21563/1/IC_117.pdf)
- Dai, J. G., Sato, Y., and Ueda, T. (2005). "Development of the nonlinear bond stress-slip model of fiber reinforced plastics sheet-concrete interfaces with a simple method." *Journal of Composites for Construction*, 9(1), 52-62.
- Dias, S. and Barros, J. (2008), "Shear strengthening of T cross section reinforced concrete beams by near-surface mounted technique." *Journal of Composites for Construction*, 12(3), 374-383.
- Faza, S. S. and GangaRao, H. V. S., (1993). "Theoretical and experimental correlation of behaviour of concrete beams reinforced with fiber plastic rebars", *Fiber*

- Reinforced Plastic Reinforcement for Concrete Structures*, SP-138, American Concrete Institute, Detroit, 599-614.
- Firino, J. P., Correia, J. R., Pitta, D., Tiago, C. and Arruda, M. R. T. (2015). "Experimental characterization of the bond between externally bonded reinforcement (EBR) CFRP strips and concrete at elevated temperatures." *Cement and Concrete Composites*, 60, 44-54.
- Godat, A., Chaallal, O. and Neale, K. W. (2013). "Nonlinear finite element models for the embedded through-section FRP shear-strengthening method." *Computers & Structures*, 119, 12-22.
- Godat, A., Labossière, P., Neale, K. W. and Chaallal, O., (2012). "Behavior of RC members strengthened in shear with EB FRP: Assessment of models and FE simulation approaches." *Computures & Structures*, 92-93, 269-282.
- Ge, W., Zhang, J., Cao, D. and Tu, Y., (2015). "Flexural behaviors of hybrid concrete beams reinforced with BFRP bars and steel bars." *Construction and Building Materials*, 87, 28-37.
- Hawileh, R. A., (2015). "Finite element modelling of reinforced concrete beams with a hybrid combination of steel and aramid reinforcement." *Materials & Design*, 65, 831-839.
- Hawileh, R. A., Rasheed, H. A., Abdalla, J. A. and Al-Tamimi, A. K. (2014). "Behavior of reinforced concrete beams strengthened with externally bonded hybrid fiber reinforced polymer systems." *Materials & Design*, 53, 972-982.
- Hognestad, E., Hanson, N. W. and McHenry D., (1955), "Concrete stress distribution in ultimate strength design." *ACI Journal Proceedings*, 52(12), 455-479.
- Hong, K. N., Cho, C. G., Lee, S. H. and Park, Y. (2014). "Flexural behavior of RC members using externally bonded aluminum-glass fiber composite beams." *Polymers*, 6(3), 667-685.
- Japan Society of Civil Engineers (JSCE), 1997. "*Recommendations for design and construction of concrete structures using continuous fiber reinforcing materials*", vol. C. Concrete E.; 325. Japan:
- Kara, I. F., Ashour, A. F. and Köroğlu, M. A., (2015). "Flexural behavior of hybrid FRP/steel reinforced concrete beams." *Composite Structures*, 129, 111-121.

- Kara, I. F., (2016). "Flexural performance of FRP-reinforced concrete encased steel composite beams." *Structural Engineering and Mechanics*, 59(4), 775-793.
- Lau, D. and Pam, H. J., (2010). "Experimental study of hybrid FRP reinforced concrete beams." *Engineering Structures*, 32(12), 3857-3865.
- Linh, V. H. B., Boonchai, S. and Ueda, T., (2017). "Mechanical performances of concrete beams with hybrid usage of steel and FRP tension reinforcement." *Computers and Concrete*, 20(4), 391-407.
- Lorenzis, D. L., Nanni, A. and Tegola, A. L. (2000). Strengthening of RC structures with near surface mounted FRP rods. International Meeting on Composite Materials, PLAST 2000, Milan, Italy, May 9-11.
- Mofidi, O. C., Brahim, B. and Kenneth, N. (2012), "Experimental tests and design model for RC beams strengthened in shear using the embedded through-section FRP method." *Journal of Composites for Construction*, 16(5), 540-550.
- Oller, E., Marí, A., Bairán, J. A. and Cladera, A., (2015). "Shear design of reinforced concrete beams with FRP longitudinal and transverse reinforcement." *Composites Part B: Engineering*, 74, 104-122.
- Pang, L., Qu, P., Zhu, P. and Xu, J., (2015). "Design propositions for hybrid FRP-steel reinforced concrete beams." *Journal of Composites for Construction*, 20(4), 1-9.
- Panigrahi, A. K., Biswal, K. C. and Barik, M. R. (2014). "Strengthening of shear deficient RC T-beams with externally bonded GFRP sheets." *Construction and Building Materials*, 57, 81-91.
- Qin, R., Zhou, A. and Lau, D., (2017). "Effect of reinforcement ratio on the flexural performance of hybrid FRP reinforced concrete beams." *Composites Part B: Engineering*, 108, 200-209.
- Qu, W., Zhang, X. and Huang, H., (2009). "Flexural behavior of concrete beams reinforced with hybrid (GFRP and steel) bars." *Journal of Composites for Construction*, 13(5), 350-359.
- Rahal, K. N. and Rumaih, H. A. (2011). "Tests on reinforced concrete beams strengthened in shear using near surface mounted CFRP and steel bars." *Engineering Structures*, 33(1), 53-62.

- Rizkalla, R. E. H. and Raafat, E. H. (2004). "Near-Surface-Mounted Fiber-Reinforced Polymer Reinforcements for Flexural Strengthening of Concrete Structures." *ACI Structural Journal*, 101(5), 717-726.
- Sato, Y., Ueda, T. and Kakuta, Y. (1994), "Qualitative evaluation of shear resisting behavior of concrete beams reinforced with FRP rods by finite element analysis", *Proceeding of JSCE*, JSCE, Tokyo, 193-209.
- Tan, K. H., (1997). "Behavior of hybrid FRP-steel reinforced concrete beams", *Proceeding 3rd International Symposium on Non-Metallic (FRP) Reinforcement for Concrete Structures (FRPRCS-3)*, Japan Concrete Institute, Tokyo, 487-494.
- TIS 24-2548, (2003). "Steel bars for reinforced concrete: deformed bars." Thai Industrial Standards Institute (TISI), Thailand.
- Ueda, T., Sato, Y. and Kakuta, Y. (1996), "Shear strength of reinforced and prestressed concrete beams with shear reinforcement", *Proceeding of JSCE*, JSCE, Tokyo, 233-247.
- Valerio, P., Ibell, T. J. and Darby, A. P. (2009), "Deep embedment of FRP for concrete shear strengthening", *Proceedings of the ICE - Structures and Buildings*, 162(5), 311-321.
- Yoo, D. Y. and Banthia, N., (2015). "Numerical simulation on structural behavior of UHPFRC beams with steel and GFRP bars." *Computers and Concrete*, 16(5), 759-774.
- Yoo, D. Y., Banthia, N. and Yoon, Y. S., (2016). "Flexural behavior of ultra-high-performance fiber-reinforced concrete beams reinforced with GFRP and steel rebars." *Engineering Structures*, 111, 246-262.
- Zhang, D., Ueda, T. and Furuuchi, H., (2012). "A design proposal for concrete cover separation in beams strengthened by various externally bonded tension reinforcements." *Journal of Advanced Concrete Technology*, 10, 285-300.
- Zhang, D., Wang, Q. and Dong, J., (2016). "Simulation study on CFRP strengthened reinforced concrete beam under four-point bending." *Computers and Concrete*, 17(3), 407-421.

Zhang, S. S. and Teng, J. G. (2013). "Interaction forces in RC beams strengthened with near-surface mounted rectangular bars and strips." *Composites Part B: Engineering*, 45(1), 697-709.



## VITA

**NAME** Linh Van Hong Bui

**DATE OF BIRTH** 29 April 1992

**PLACE OF BIRTH** Quang Ngai, Viet Nam

**INSTITUTIONS ATTENDED** Ho Chi Minh City University of Technology, Chulalongkorn University and Hokkaido University

**HOME ADDRESS** Nghia Dong Ward, Quang Ngai City, Vietnam

**PUBLICATION**

Linh, V.H.B., Boonchai, S. and Ueda, T., (2018). "Ductility of concrete beams reinforced with both FRP and steel tension bars." *The Journal of Advanced Concrete Technology*, 16 (11), 531-548 (ISI, Q1, IF = 1.134).

Linh, V.H.B., Boonchai, S., Ueda, T. and Pitcha, J., (2018). "Bond behavior between embedded through-section bars and concrete." *International Journal on Advanced Science, Engineering and Information Technology*, 8(4), 1008-1014 (Scopus, Q2).

Linh, V.H.B., Boonchai, S. and Ueda, T., (2017). "Mechanical performances of concrete beams with hybrid usage of steel and FRP tension reinforcement." *Computers and Concrete*, 20(4), 391-407 (ISI, Q2, IF = 1.67).

Linh, V.H.B., Boonchai, S. and Ueda, T., (2018). Bond response of ETS GFRP bars to concrete. *The 20th Int'l Summer Symposium in 2018*, 29-30 August 2018, Hokkaido, Japan.

Linh, V.H.B., Boonchai, S. and Ueda, T., (2017). Mechanical performances of concrete beams strengthened by ETS bars. *The 30th KKHTCNN Symposium on Civil Engineering*, 02-04 November 2017, Taipei, Taiwan.



จุฬาลงกรณ์มหาวิทยาลัย  
**CHULALONGKORN UNIVERSITY**